Rigid plastic modeling of RC beams under Impact loading

By

Asad Ullah

MS-2018-00000-277287

Supervisor

Dr. Azam Khan

NUST INSTITUTE OF CIVIL ENGINEERING

SCHOOL OF CIVIL AND ENVIRONMENTAL ENGINEERING

NATIONAL UNIVERSITY OF SCIENCES AND TECHNOLOGY

H-12, ISLAMABAD

2021

This is to certify that thesis titled

Rigid plastic modeling of RC beams under Impact loading

Submitted by

Asad Ullah

Fall 2016-MS Structural Engineering

00000-277287

Has been accepted towards the partial fulfillment

of

the requirement for the award of the degree of

Master of Science in Structural Engineering

Thesis Supervisor

Dr. Azam Khan

Assistant Professor

NUST Institute of Civil Engineering (NICE)

National University of Sciences and Technology (NUST),

Islamabad, Pakistan.

THESIS ACCEPTANCE CERTIFICATE

It is certified that the final copy of MS thesis written by **Mr. Asad Ullah**, Registration No. **00000-277287**, of **NUST INSTITUTE OF CIVIL ENGINEERING (NICE)** has been vetted by the undersigned, found complete in all respect as per NUST Statutes/Regulations, is free of plagiarism, errors, and mistakes and is accepted as partial fulfillment for the award of MS degree in Structural Engineering.

Signature: _____

Name of Supervisor: **Dr. Azam Khan**

Date: _____

Signature (HOD): _____

Date: _____

Signature (Dean/Principal): _____

Date: _____

DECLARATION

I certify that this research work titled "*Rigid plastic modeling of RC beams under impact loading"* is my own work. The work has not been presented elsewhere for assessment. The material that has been used from other sources has been properly acknowledged/referred.

Signature of Student

Asad Ullah
00000-277287

PLAGIARISM CERTIFICATE (Turnitin Report)

This thesis has been checked for Plagiarism. Turnitin report endorsed by Supervisor is attached.

Signature of Student

Asad Ullah
00000-277287

Signature of Supervisor

Rigid plastic modeling of RC beams under impact loading

by

Asad Ullah

This is to certify that we have examined the above MS thesis and found that it is complete and satisfactory in all respects and that any, and all revisions required by the thesis examination committee have been made.

Dr. Azam Khan (Assistant Professor)	Dr. Usman Hanif (Assistant Professor)	Dr. Hammad Anis (Assistant Professor)

Dr. Rao Arsalan Khushnood
(Assistant Professor)

ACKNOWLEDGEMENTS

Since I got admission as a graduate student in the NUST Institute of Civil Engineering, National University of Science and Technology, H-12 Islamabad, this period was one of the wealthiest and most exciting years of my life. In this journey, I met many people with whom I learned a lot and whom I will never forget. The following lines are dedicated to thanking the ones that contributed to my studies and my project in one way or another.

First, I would like to thank my supervisor, Dr. Azam Khan, Assistant Professor, NUST Institute of Civil Engineering, for his generosity, kindness, flexibility, cooperation, and guidance. Despite a hectic schedule, he went above and beyond the call of duty to provide excellent and prompt guidance for unconditional support and encouragement throughout my project work. I must also acknowledge his availability, dedication, guidance, and reviewing the drafted report.

I also owe a debt of gratitude to my project evaluation committee members/examiner Engr. Dr. Rao Arsalan Khushnood, Engr. Dr. Hamad Anis and Engr. Dr. Usman Hanif. Their constant support, intellectual, logical, and rational, thoughtful comments and suggestions for improving my thesis, and assistance during the execution of the computational work improved the quality of work.

I am grateful to my friends and colleagues who provided continual moral encouragement and never gave up on me when it seemed like this project would never be completed. At this stage, I would also like to thank my friends and colleagues, Engr. Moiz Tariq, Engr. Hassan Sardar, Engr. Hassan Irfan, Engr. Sultani Mulk Khan, Engr. Junaid Shah Khan for their constant support and help during the coursework and research work.

Most importantly, I am greatly indebted to my parents for the endless encouragement, patience, and support they have given me over the past year and my entire life. Thanks for reminding me that knowledge is power; experiences are priceless.

Wednesday, August 25, 2021. ***Asad Ullah***

TABLE OF CONTENTS

TITLE PAGE i

DECLARATION PAGE iv

PLAGIARISM CERTIFICATE v

SIGNATURE PAGE vi

ACKNOWLEDGEMENTS vii

TABLE OF CONTENTS viii

LIST OF FIGURES xi

LIST OF TABLES xiv

ABSTRACT xv

1 INTRODUCTION 1

1.1 Background 1

1.2 Types of RC beam failure under impact loading 4

1.3 Problem Statement 6

1.4 Research Significance 6

1.5 Research Objectives 7

2 REVIEW OF LITERATURE 8

2.1 Overview 8

2.2 Effect of strain-rating on the properties of materials 9

2.2.1 Plain concrete 9

2.2.2 Steel reinforcement 14

2.3 Effect of strain rate on RC beam 14

2.3.1 Analytical and numerical studies 14

2.4 Study of RC beams under Impact Loading 15

2.4.1 Experimental testing 15

2.4.2 Mathematical and analytical based studies 23

2.5 Summary 24

3 Methodology 28

3.1 Proposed Dynamic Rigid-Plastic Model Incorporating Strain-rate Effet 28

3.1.1 Representation of kinetics and kinematics as the nodal description 29
3.1.2 Material Model 31
3.1.3 The Mathematical Formulation 35
3.1.4 Solution steps of formulation 37
3.2 LCP Formulation Incorporating M-V Interaction 38
3.2.1 Representation of kinetics and kinematics as the nodal description 38
3.2.2 Material Model 41
3.2.3 The Mathematical Formulation 43
3.2.4 Initiation of LCP formulation 45
3.2.5 Plastic Unstressing 47
3.3 Existence and uniqueness of optimal solutions 48
3.4 Peak Impact Force Model 50
3.4.1 Parameters affecting the impacted force on RC beam from a drop-weight 50
3.4.2 Experimental database 51
3.4.3 Fundamentals of gene programming 52
3.4.4 Proposed GEP model for estimating peak impact force 54
3.5 Statistical Parameters for Validation 57
3.5.1 Predicted to experimental ratio (PER) 57
3.5.2 Coefficient of Variation (CoV) 57
3.5.3 Coefficient of Determination 58

4 RESULTS & DISCUSSION 60
4.1 Organization 60
4.2 Model Validation 60
4.3 Viscoplastic LCP Validation 60
4.3.1 Experimental Database 60
4.3.2 Validation of midspan deflection 63
4.4 Bending shear LCP 70

4.4.1 Experimental Database 70
4.4.2 Validation of midspan deflection 72
4.5 Peak Impact Force 76
4.5.1 Experimental Database 76
4.5.2 Validation with experimental tested data 77
4.5.3 Sensitivity of the proposed model 79
4.5.4 Comparison with numerical model 82
4.5.5 Comparison with the available model 84
4.5.6 Remarks about shear force, and bending moment plots 86

5 CONCLUSION AND RECOMMENDATION 88
5.1 Recommendations 91

References 92

LIST OF FIGURES

Figure 1. 1: Strain rates corresponding to different loading conditions 3

Figure 1. 2: Different tendencies for different types of loading 4

Figure 1. 3: Response of RC beams under impact loading: (a) Loading procedure and local response. (b) Global bending failure. (c) Local failure in shear. (d) Global failure in shear. (e) Global shear-flexure failure. 5

Figure 2. 1: RC beams failure (Mylrea [60]) 16

Figure 2. 2: Parallelogram of hysteretic loop (Kishi et al. [61]). 17

Figure 2. 3: Hysteratic loop of force vs displacement (Kishi et al. [14]) 18

Figure 2. 4: Instrumental setup of impacted RC beam (Fujikake et al. [59]) 19

Figure 2. 5: Cracking profiles of type-a and -b series beams (Saatci and Vecchio [13]) 21

Figure 3. 1: Discritized simply-supported beam under impact loading 28

Figure 3. 2: Stress-resultants, strain-resultant rates, chord deformation rates, and independent chord forces. 29

Figure 3. 3: Centroidal-velocities in a system of lumped mass 30

Figure 3. 4: Material model 31

Figure 3. 5: Flow path for the proposed viscoplastic LCP model 37

Figure 3. 6: Discritized simply-supported beam under dropweight impact 38

Figure 3. 7: Independent nodal velocities and member deformation rates 39

Figure 3. 8: Stress-resultants, strain-resultant rates, chord deformation rates, and independent chord forces: (a) Planar element allowing plastic-interaction of the bending moment and the shear force. (b) Planar element allowing plastic bending moment. (c) centroidal-velocities in a system of lumped mass 40

Figure 3. 9: Bending-shear interaction 43

Figure 3. 10: Flow path of bending-shear LCP model 48

Figure 3. 11: Flow chart for the GEP 54

Figure 3. 12: Gene expression tree for peak impact force 56

Figure 3. 13: Graphical Representation of Coefficient of Determination 58

Figure 4. 1: Frequencies of different experimental parameters. (a) Impact Mass. (b) Beam net length. (c) Drop mass velocity. (d) Compressive strength. (e) Beam depth. (f) Beam-width. (g) Shear reinforcement ratio. (h) Tensile reinforcement ratio. 63

Figure 4. 2: Comparison of predicted and experimental results of midspan maximum deflection 63

Figure 4. 3: : Influence of parameters on the estimative performance of the developed formulation. (a) Projectile velocity. (b) Impacted mass. (c) Mass ratios. (d) Beam depth 64

Figure 4. 4: Zhao et al. vs Visoplastic LCP 65

Figure 4. 5: Comparison of viscoplastic LCP and Adhikary et al. 66

Figure 4. 6: Khan et al. vs viscoplastic LCP model prediction 67

Figure 4. 7: Comparison of viscoplastic vs Kishi and Mikami model 68

Figure 4. 8: Tachibana et al. vs viscoplastic LCP 69

Figure 4. 9: Frequencies of different experimental tested beams parameters. (a) Drop mass velocity. (b) Impacted Mass. (c) Beam net length. (d) Compressive strength. (e) Beam depth. (f) Beam-width. (g) Shear reinforcement ratio. (h) Tensile reinforcement ratio. 72

Figure 4. 10: Comparison of predicted and experimental results of midspan maximum deflection 73

Figure 4. 11: Influence of parameters on the estimative performance of the developed formulation. (a) Projectile velocity. (b) Impacted mass. (c) Mass ratios (d) Beam depth 74

Figure 4. 12: Khan et al. vs bending-shear LCP 75

Figure 4. 13: Comparison of bending shear LCP with Adhikary et al. model 76

Figure 4. 14: Comparison of predicted and experimental results of peak impacted force (a) Training data (b) Validation data (c) All data 79

Figure 4. 15: Parametric study 80

Figure 4. 16: The effect of main parameters on the precision of developed GEP 81

Figure 4. 17: Response of RC beam model in ABAQUS (a) Maximum midspan deflection (b) Peak impact force 83

Figure 4. 18: Comparison of GEP with Pham and Hao model 85

Figure 4. 19: GEP model vs Zhao et al. model 86

Figure 4. 20: Calculation of the shear force, and bending moment diagram 87

LIST OF TABLES

Table 1. 1: Responses of RC beam under different impact loading condition 5

Table 3. 1: Distribution of key influence parameters 51

Table 3. 2: Model Construction Parameter 56

Table 4. 1: Statistical analysis of maximum mid-span deflection prediction models of RC beams under Impact loading 69

Table 4. 2: Statistical analysis of maximum midspan deflection prediction models of RC beams under Impact loading 76

Table 4. 3: Distribution of key influence parameters 77

Table 4. 4: Comparison of GEP result with Experimental result and ABAQUS solution 84

Table 4. 5: Comparison with available models 86

ABSTRACT

A numerical model is produced herein for predicting the dynamic plastic structural responses of RC skeletal structures under drop-weight impact loading. The numerical formulation has the mathematical form of a linear complementarity problem (LCP) that incorporates the strain-rate sensitivity. This formulation offers a systematic numerical process that is automatic from the commencement until the dynamic response termination. The maximum deflection obtained from the viscoplastic LCP of midspan impacted simply supported beam is statistically compared to the experimental dataset of RC beams. So, an extensive experimental database of 118 simply supported RC beams under midspan impact is selected. All cases within the database experiencing either flexure or flexure-shear failure, whereas only shear failure cases are excluded.

Similarly, another numerical model is developed here having the same mathematical form of a linear complementarity problem (LCP) but the only difference from the previous one is that it incorporates bending shear interaction obeying the square yield criterion. The maximum deflection as a result output obtained from this interaction-based LCP of midspan impacted simply supported reinforced concrete beam is statistically compared to the experimental dataset of tested RC beams carried out by different researchers available in the Literature. For this purpose, an extensive experimental database of 46 simply supported reinforced concrete (RC) beams under midspan impact has been constructed. All cases within the database experienced either flexure-shear or shear failures, whereas those specimen which failed in pure bending are excluded.

For structures and load-bearing members under extreme impact loading, the prediction of peak impact force is the most challenging task. Owing to the non-uniqueness in the acceleration field of the rigid-plastic model, the peak impact force is also non-unique, therefore, an efficient and accurate empirical model is produced to estimate this force for the particular case of a simply supported (RC) beam under drop-weight impact. A gene expression programming (GEP) approach is employed to formulate this empirical model

reflecting the contribution of various material and geometric factors like compressive strength of concrete, shear span to depth ratio, and strength and area of tensile reinforcement. The effect of other factors including the impact velocity and impactor weight is also investigated. A database containing 126 impact force experiments of the simply supported RC beams is analyzed statistically on the basis of variation of these factors and is used to develop the proposed models. This model is also compared statistically and analyzed with the available proposed models. Numerical confirmation of the empirical model of peak impact force is obtained by reference to finite element (FE) code ABAQUS with plane stress elements. Overall, the proposed model offers highly promising results, which can be applied to predict the shear force and bending moment diagrams, thus rendering it ideal for practical application.

1 INTRODUCTION

1.1 Background

Different components of reinforced concrete (RC) structure may subject to various kinds of extreme dynamic loading throughout its service life ranging from low to high rates of loading i.e. from earthquake to impact and then to blast loading. Due to development of infrastructures throughout the world, there are chances that the components of these structures can be subjected to impact loading from several events or accidents. Typical examples include the impact loading on different highway structural elements (i.e. bridge piers, side guard rails, traffic signal poles, electric distribution poles, girder of overhead passing or bridges) from vehicle striking impacts, falling rocks in mountainous regions on different structures, industrial plants may suffer potential damage of critical components caused by heavy falling objects happened from pipe and the turbine breaks, offshore and marine structures may be on threat from collision of ships or ice with them, different types of building may be expected to tornado or debris impact from tsunami, columns in multistory buildings or bridges pier may be impacted by moving vehicles, structures for protection subjected to projectiles or aircraft impact. During these collisions, the impact causes huge amount of abnormal forces on these structures. Therefore, it is very important to predict the response of these structures under these extreme loading for better and safe design [1,2].

Due to complex nature of loading and inelastic structural response, the analysis of structure under time-dependent short-term loading is not straightforward. In a perfectly elastic viscous damping system with small displacement, the system can be easily solved by solving linear second order differential equation of motion. But in cases like elasto-plastic system under these dynamic loading, the mathematics becomes more complex and non-linear. Because when these engineering structures such as beam, frame, plate, or shell are subjected to impact loading, the first portion of structural response is the elastic one. But when yield limit is reached at any point, a more complicated response of both elastic and plastic deformation is distributed along the structure. We can't separate the plastic deformations as they are scattered with the elastic. Therefore, the closed-form analytical solution of elasto-plastic structures is immensely difficult or

sometimes not even possible. Therefore, powerful numerical solutions such as finite element analysis (FEA) are adopted to obtain an approximate solution [3].

In order to solve the complexity, different researchers have used different techniques. Among those, the most simple and powerful approach of rigid-plastic analysis has been widely accepted and extensively used. This method is bearing outstanding results in the limiting analysis of steel and concrete under static loading but has also shown promising results in analyzing the structures under extreme dynamic loading. The reason behind its simplicity is that this method neglects the elastic strain of materials. The dynamic response of different types of structure such as beam, plates, and shells, etc. [2] are expressed in the form of differential equations which can be solved analytically, or numerically, for given initial end boundary conditions. At each instant of time, the plasticity occurred only at a fixed point or zone in a structure, while everywhere else will only rigid-body motion occurs. This rigid-plastic theory is formulated on an assumption that the amount of the energy transferred to structure is quite huge than the amount of strain energy, it can store. That's why this technique is very efficient for better understanding of the mechanism by which plastic deformation contributes to residual damage and energy absorption in ductile structure [4].

Quadratic programming has shown promising results when incorporated to rigid planar frame (assumed that all the connecting elements are rigid) subjected to impulsive or short-term pulse loading [5]The kinematic and kinetic laws are represented in nodal or mesh descriptions along with the plasticity relation are converted into linear complementarity problem (LCP) with the help of Newmark's integration scheme [6,7]. Later [8] change the incremental form of LCP into rate form, for the accurate representation of non-holonomic of the plasticity relation. Secondly, he replaced Wolfe's type solver with Lemke's Algorithm for its robustness in addressing the solution of semi-definite LCP.

Along with all the above discussion, it is also very important to acknowledge the effect of loading rate on different structures. The strain rates incorporated by different loading encounter in practice has been shown by [9] as given in Fig. 1.1. As been clear from the wide spectrum, that very low strain rate ($\sim 10^{-8} - 10^{-7}$ /s) normally occurs during creeping. For static conditions, the strain rate normally lies in range of 10^{-6} to 10^{-4}

/s. Moreover, during earthquake it could be in the domain of 10^{-3} – 1 /s, and for impact loading, it can be increased up to 50 /s. The strain rate greater than impact scenario will fall in blast loading regime. In earthquake regimes, the inertial effect on structure is insignificant, but for high strain loading, the inertial effect is dominant than structural response [10].

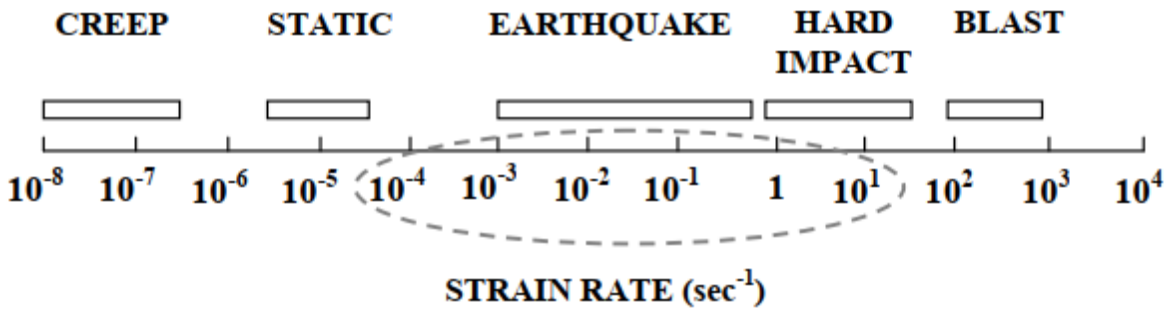

Figure 1. 1: Strain rates corresponding to different loading conditions

The phenomenon of impact loading is very complex not only due to the reason that it's an extreme high dynamic loading but also due to involvement of inertial effect, energy transferring mechanics, and distribution of stress-waves along the structure. Due to this, different influencing factors such as compressive strength f_c', mass and initial velocity of drop hammer, and contact region's stiffness affect the behavior of structure. Additionally, the structural response under drop-weight impact loading is divided into two stages: the primary response stage (local failure) and the secondary response stage (overall failure), and these behaviors are dependent on high rates of loading and stress-waves propagation. The different proportional increase of stress-waves and high rates effect occurred in different structural members for different types of loading is shown in Fig. 1.2 [11].

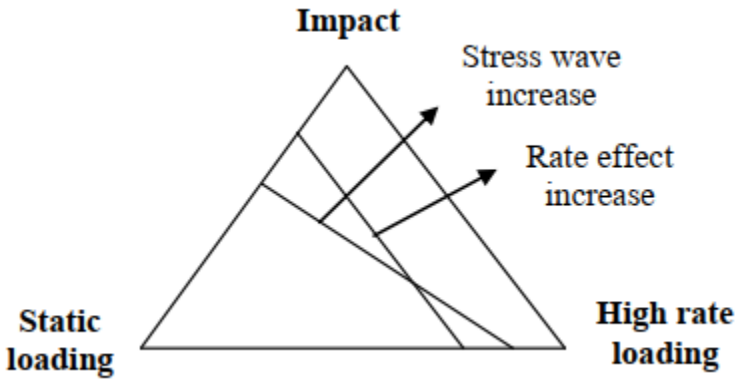

Figure 1. 2: Different tendencies for different types of loading

1.2 Types of RC beam failure under impact loading

Like all other engineering structural members, RC beams under impact loading also show different failure responses. The study of published articles on the dynamic plastic behavior of RC beams under these loads reveals that the magnitude of impact loading, beam-flexural capacities, and beam-shear capacities result in different failure responses [12–14]. Consider the dynamic behavior of a simply supported RC beam shown in Fig. 1.3. The first diagram shows that sudden impact on the midspan of the RC beam generates wave packets with the higher frequency component moving out ahead of the main disturbance. These waves reflect off the support and generate an irregular wave distribution in the domain between the support and the impacted point. It transpires that different failure modes result depending upon the impact loading rate, Fig. 1.3(b)-(e) and Table 1.1. Under low rate-long duration impact, the beam exhibits a ductile response with vertical flexural cracks forming at the tension zone, Fig. 1.3(b). On the other hand, high rate-short duration impact may be governed by transverse shear effects at the impacted point, as shown in Fig. 1.3(c). Furthermore, in the case of low-shear strength under the same loading may have significant shear effects at the support, Fig. 1.3(d). Finally, a global flexure-shear failure may be initiated if the beam has moderate shear and bending strength, Fig. 1.3(e). In this failure shape, the damages start with the surfacing of vertical flexural cracks at the tension zone and similar flexural cracks at the top surface of beam due to the hogging moments.

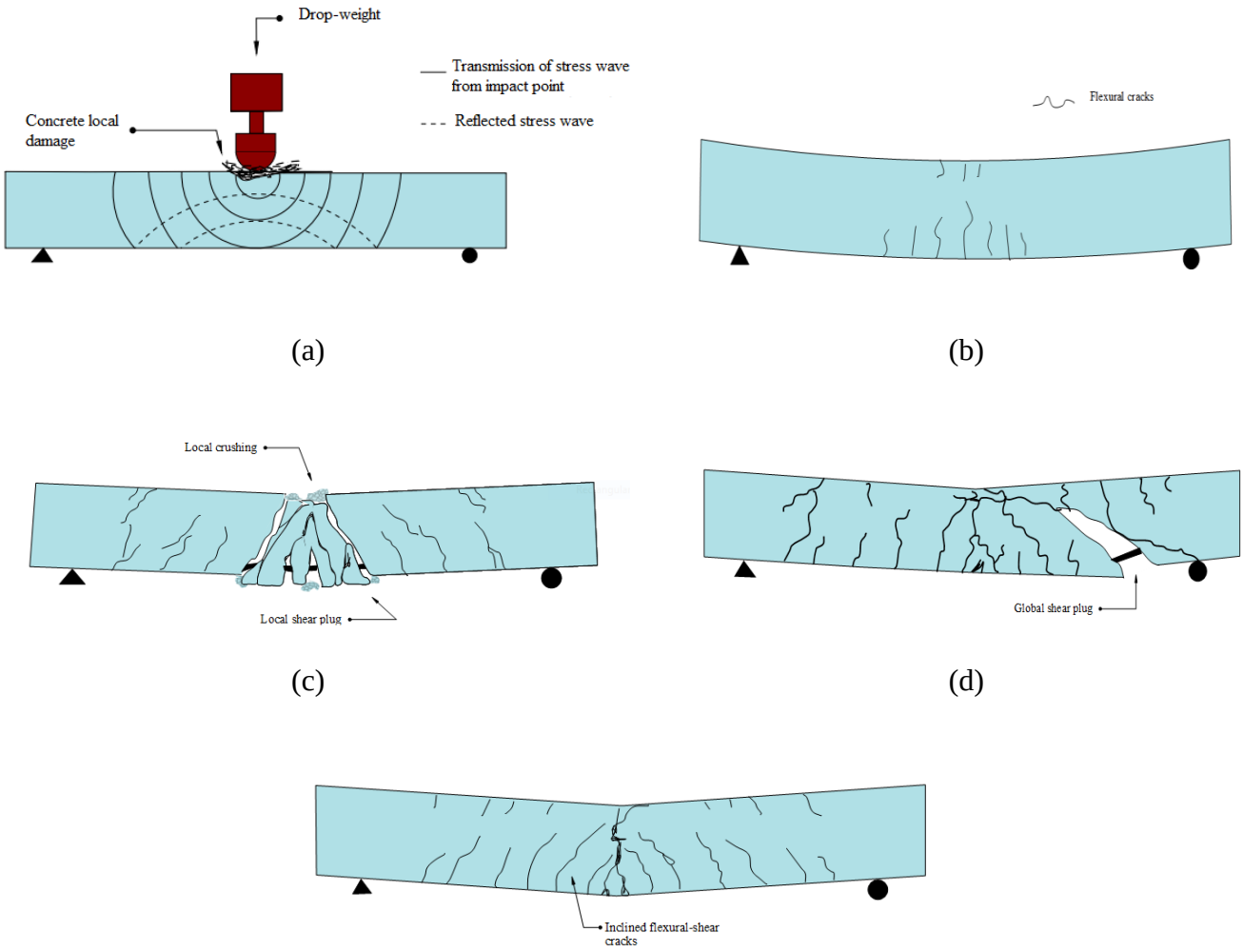

Figure 1. 3: Response of RC beams under impact loading: (a) Loading procedure and local response. (b) Global bending failure. (c) Local failure in shear. (d) Global failure in shear. (e) Global shear-flexure failure.

Table 1. 1: Responses of RC beam under different impact loading conditions

Specimen	*Flexural and shear resistance*	*Impact loading condition*	*Failure type*
Fig1.b	Middle range resistance	Low rate and extended duration	Vertical flexural cracks from tension zone
Fig1.c	Middle range resistance	High rate and short duration	Local shear plugs at the impact point

Fig1.d	Low shear strength	Medium rate impact loading	Global brittle shear plugs near the support
Fig1.e	Middle range resistance	Medium rate impact loading	Global bending-shear failure

1.3 Problem Statement

A simplified method, such as rigid plastic theory which has shown promising performance in analyzing structures under extreme dynamic loading doesn't incorporate the effect of strain-rate. Along with it, to better capture the shear behavior, it is necessary to incorporate the bending moment and shear force interaction in rigid plastic bending response. Moreover, to simplify the design approach, the peak impact force can then be employed to derive bending moment and shear force diagrams. It is therefore essential to propose simplified models that incorporate strain-rate effect, bending-shear interaction, and predict the peak impact load with reasonable accuracy.

1.4 Research Significance

Predicating the response of an RC beam under drop-weight impact loading is a complex phenomenon. The following three approaches are generally used for this purpose;

- Spring Mass System.
- Analytical approach on the basis of conservation of energy.
- Analytical approach on the basis of various contact laws.

The application of these procedures is not straightforward and sometimes not even possible. On other hand, a simplified method, such as rigid plastic theory, can prove very useful in capturing this complex response of RC structures. The dynamic behavior of RC structures is highly sensitive to strain rate, resulting in a considerable increase in the yield stress with an increased rate of straining. This property of viscoplasticity should be incorporated in any simplified model for accurately predicting the peak response of these structures under drop-weight impact loading. Along with it, RC beams that fail in bending in static loading often fail in shear behavior during high impact loading. Therefore, it is necessary that the rigid-plastic

bending response may be extended to incorporate bending moment and shear force interactions. Moreover, proper design procedure, protection, and strengthening of all these structures against drop-weight impact loads are necessary. To achieve these goals, being able to accurately predict the impact loads is essential.

1.5 Research Objectives

A systematic study on RC beam has been carried out in this research, which will address the research gaps and also improve the understanding of RC beam under drop-weight impact loading. The main objectives of this study are as given below:

1. To propose a simplified mathematical model based on rigid-plasticity incorporating the effect of strain rate for predicting the midspan displacement of RC beam under drop-weight impact loading.
2. To propose a simple mathematical and computational method, founded upon the rigid-plastic theory incorporating the bending-shear interaction for calculating the dynamic responses of RC skeletal structures under drop-weight loading.
3. To develop an efficient model to produce the peak impact load on RC beam from a drop-weight.
4. Validation of the developed models with the available experimental data.
5. Validating the proposed models with the existing models available in the Literature.

2 REVIEW OF LITERATURE

2.1 Overview

Impact loading response is an ever-growing field of studies that encompasses various engineering problems, as exemplified by vehicle collisions, the impact of rockfalls, and terrorist activities. Although RC structures are very pronounced universally, the understanding of the impact response of these structures is still limited. A considerable variation exists in response parameters prediction as per various codes of practice [15,16], mostly not asking for the dynamic analysis of the impacted RC components. However, the dynamic response of RC structures, such as beams, indicates that there can be instances when the dynamic behavior is significantly different from the static loading [13,14,17–23]. Indeed, the ability to predict the response of these structures under impact loadings is essential for appraising the safety of these structures to the potential damage of structural components [24]. Most of the techniques exploring the nonlinear dynamic plastic response under impact loading require expertise and are computationally expensive [25]. However, rigid-plastic approximations offer a simplified and computationally efficient procedure for dynamic analysis, owing to the exclusion of the elastic response [26].

The role of elasticity in structural response due to the extreme dynamic loads can be neglected if the plastic deformation is substantially large. In such cases, it is suitable to consider that the stress resultants on a section are coupled to deformation by a rigid-perfectly plastic constitutive law [2]. This simple theory in impact dynamics has well played an essential role in producing computationally efficient approaches that allow considerable physical insight into the underlying mechanics of motion [27]. Although the application of the rigid-plastic theory to dynamic problems was suggested by Taylor [28], the first systematic study in this context appears to have been made by Lee and Symonds [29]. This study yielded vast literature on the investigations of structures submitted to extreme dynamic loading [30–38]. Yet, it is noteworthy that each closed-form theoretical solution requires to postulate a kinematically admissible velocity profile for the evolution of displaced configuration.

Like most structural materials, reinforced concrete exhibits different dynamic responses and failure modes from the quasistatic loads [13,14,17–23]. This behavioral change is due to the involvement of high rate of loading due to which it changes the material responses. This variation is explained in detail in following sections.

2.2 Effect of strain-rating on the properties of materials

Since the key mechanical properties of the materials i.e., plain concrete and reinforcement are strongly dependent on the strain rate effect. So, in order to accurately predict the responses of these structures, the effect of strain rate on these basic materials over a wider range should be considered.

2.2.1 Plain concrete

There are three different factors that influenced the behavior of structure under impact load. They are (a) Growth of cracks with time; (b) Viscous properties of material between cracks; (c) Inertial effect on structures that change the stresses and strains [O3]. We can incorporate the strain rate effect by various methods. According to the theory of Mihashi and Wittmann [39], cracks occur on atomic scale when material is under loading and the growth of these cracks increases with the time of application of load. Long duration of loading causes more cracks than the short term high loading because the quantitative numbers of these cracks are supposed to be fixed over time. Due to this reason, long term loading reduces the strength of materials by increasing the number of cracks while short term high loading increases the strength on other hand. This increase in the strength can be given by the following equations;

$$\frac{f_d}{f_s} = \left(\frac{\dot{\sigma}}{\dot{\sigma}^o}\right)^{\alpha} \tag{2.1}$$

where f_d is dynamic strength, f_s is the static strength under the monotonic loading, $\dot{\sigma}$ is the stress rate due to dynamic load, $\dot{\sigma}^o$ is the stress rate under static loading, and α is the parameter that depends on loading, material types, and way of loading. The effect of inertia on materials has been studied by Reinhardt and Weerheijm [40]. They studied a cluster of cracks that are perpendicular to the direction of tension loading. They observed that crack faces move with certain velocity under the application of loading and they

computed the energy balanced for this movement. They found out that the amount of energy applied is too much large to be absorbed in fractural process and as a result, most of energy is stored at crack tips. They concluded that stress distribution changes at tips and as a result stress intensity factor reduces with increasing load rate. Therefore, increase in the strength of materials occur under high loading rate. Bazant et al. [41,42] consider the effect of loading rate in two stages i.e. for viscosity he used visco-elastic model and the increasing growth of the cracks with time is due to the theory of activation energy. He didn't consider the inertial effect and the expression is given below;

$$\sigma(\epsilon) = \sigma^{o}(\epsilon)\left[1 + C_1 LN\left(\frac{2\dot{\epsilon}}{C_2}\right)\right] \tag{2.2}$$

where σ is the stress due to dynamic loading, σ^{o} the stress at static loading, $\dot{\epsilon}$ is the strain rate, C_1 and C_2 are the constants found from experiments. Ozbolt et al. [43] performed experiments and compare their results with the available theoretical models and find out the Reinhardt and Weerheijm [40] model has better accuracy than other models. This has been lately demonstrated that for low to medium range strain rate upto 10 s^{-1}, total resistance offered is due to materials viscosity and growth rate of microcracks, but for strain rate higher than 10 s^{-1}, the inertial effect is dominant and is responsible for structural resistance.

Several numerical studies have been done on the compression properties of concrete under high loading rate for over several decades. Some of the key findings are as given; both the compressive capacity and stiffness have direct relation with strain-rate, the effect of high strain rate is more on normal strength concrete than the higher strength concrete, similarly concrete in dry state is less sensitive to strain rate than concrete in wet state, and the slope of descendent portion of stress-strain plot increases with the increasing strain-rate.

In comparison to concrete compressive strength, limited test data is available for the tensile strength of concrete. Several techniques like cylinder split test, uniaxial direct tension test, Split Hopkinson Pressure Bar (SHPB), etc are adopted to check the strain rate effect on concrete in tension. According to the tests performed by Sauris and Shah [44], they concluded that concrete is more sensitive to strain rating in tension

than compression. Split-Hopkinson-Bar procedure was adopted by Zielinski and Reinhardt [45], to study the properties of concrete and mortar paste at high strain rating. They concluded that there was excessive cracks formation over the whole specimen, as a result, increase in strength occur. They also find out that increase of strength in concrete is more than mortar because of the reason that crack propagation was arrested by tougher aggregates and as result increased the amount of store energy. Furthermore, Malvar and Ross [46] have done a detailed study on the behavior of concrete under high loading rate.

The most comprehensive model to incorporate the strain rate effect on the compressive and tensile strength of concrete is that of the CEB code [47]. Dynamic increase factor (DIF) is used to represent the effect of strain rate i.e. the ratio of the dynamic strength to the static strength. Increase in the compressive strength is evaluated by the following equation;

$$DIF_c = \begin{cases} \left(\frac{\dot{\epsilon}}{\dot{\epsilon_s}}\right)^{1.026\alpha_s} & \dot{\epsilon} \leq 30\ s^{-1} \\ \gamma_s \left(\frac{\dot{\epsilon}}{\dot{\epsilon_s}}\right)^{1/3} & \dot{\epsilon_s} > 30\ s^{-1} \end{cases} \tag{2.3}$$

where $\dot{\epsilon}$ is the strain rate ranges from $30 \times 10^{-6} - 300\ s^{-1}$, $\dot{\epsilon_s} = 30 \times 10^{-6}\ s^{-1}$ (the static strain-rate), $\log \gamma_s = 6.156\alpha_s - 2$, $\alpha_s = 1/(5 + 9f_{cs}/f_{co})$, $f_{co} = 10$ MPa, f_{cs} is the static concrete compressive strength.

The equation for dynamic increase factor for the concrete compressive strength given by Soroushian et al. [48] is as follows;

$$DIF_c = 1.48 + 0.160 \log_{10} \dot{\epsilon} + 0.0127(\log_{10} \dot{\epsilon})^2 \tag{2.4}$$

where $\dot{\epsilon}$ is the strain-rate (s^{-1}) larger than 10^{-5}. Although, they tried to find out the reason for the scatteredness of data over wide range spectrum. They concluded that moisture content is the reason for this variation. So, from this, they concluded that strength increase is directly related to moisture content. The tested result didn't show any effect of moisture content on the static strength in compression. In addition, the strength increase was same for two samples that have same moisture content but different ages. The suggested equations for dry and wet state concrete are as given below;

For dry concrete,

$$DIF_c = 1.48 + 0.206 \log_{10} \dot{\epsilon} + 0.0221 (\log_{10} \dot{\epsilon})^2 \quad (2.5)$$

For wet concrete,

$$DIF_c = 2.54 + 0.580 \log_{10} \dot{\epsilon} + 0.0543 (\log_{10} \dot{\epsilon})^2 \quad (2.6)$$

Series of SHPB tests were carried out by Ross et al. [49,50] and Tedesco and Ross [51] in order to check the strain-rate effect and moisture content on improved strength of concrete. The equations suggested by them are given below;

$$DIF_c = 0.00965 \log_{10} \dot{\epsilon} + 1.058 \geq 1.0 \quad for\ \dot{\epsilon} \leq 63.1\ s^{-1} \quad (2.7)$$

and

$$DIF_c = 0.758 \log_{10} \dot{\epsilon} - 0.289 \leq 2.5 \quad for\ \dot{\epsilon} > 63.1\ s^{-1} \quad (2.8)$$

Grote et al. [G2] did experimental investigation to find out the strength increase in concrete and mortar at high strain rates ranging from 10^{-3} - 10^{4} and under high confining pressure from 0 – 1.5 GPa. The formula is as given;

$$DIF_c = 0.0235 \log_{10} \dot{\epsilon} + 1.07 \quad for\ \dot{\epsilon} \leq 266\ s^{-1} \quad (2.9)$$

and

$$DIF_c = 0.882\ (\log_{10} \dot{\epsilon})^3 - 4.4(\log_{10} \dot{\epsilon})^2 + 7.22\ (\log_{10} \dot{\epsilon}) - 2.64 \quad for\ \dot{\epsilon} > 266\ s^{-1} \quad (2.10)$$

The application of SHPB was carried out by Li and Meng [52] and found that hydrostatic effect is more with the increasing dynamic effect having the strain rate greater than 10^2 s^{-1} because of the inertial effect on the structure. The following DIF equations for compression is given by them;

$$DIF_c = 1 + (\log_{10} \dot{\epsilon} + 3) \times 0.03438 \quad for\ \dot{\epsilon} \leq 100\ s^{-1} \quad (2.11)$$

and

$$DIF_c = 8.5303 - 7.1372\log_{10}\dot{\epsilon} + 1.729(\log_{10}\dot{\epsilon})^2 \quad for\ \dot{\epsilon} > 100\ s^{-1} \tag{2.12}$$

The incorporation of strain rate effect in the compressive strength equation given by Drucker-Prager is carried out by using the equation of Yamaguchi et al. [53] which is given below;

$$DIF_c = 1.021 - 0.05076\log_{10}\dot{\epsilon} + 0.2583(\log_{10}\dot{\epsilon})^2 \tag{2.13}$$

The dynamic increase in the compressive strength of concrete find out by Fujikake et al. [54] by performing compressive tri-axial loading on concrete is as follows;

$$DIF_c = \left(\frac{\dot{\epsilon}}{\dot{\epsilon}_{sc}}\right)^{0.006\left[\log\left(\frac{\dot{\epsilon}}{\dot{\epsilon}_{sc}}\right)\right]^{1.05}} \tag{2.14}$$

where $\dot{\epsilon}_{sc} = 12 \times 10^{-5}\ s^{-1}$ and $\dot{\epsilon} < 10\ s^{-1}$.

However, the DIF for tension as per CEB [47] is noted down;

$$DIF_t = \begin{cases} \left(\frac{\dot{\epsilon}}{\dot{\epsilon}_s}\right)^{1.016\delta_s} & \dot{\epsilon} \le 30\ s^{-1} \\ \beta_s \left(\frac{\dot{\epsilon}}{\dot{\epsilon}_s}\right)^{1/3} & \dot{\epsilon} > 30\ s^{-1} \end{cases} \tag{2.15}$$

where $\dot{\epsilon}$ is the strain rate ranges from $3 \times 10^{-6} s^{-1} - 300\ s^{-1}$, $\dot{\epsilon}_s = 3 \times 10^{-6}\ s^{-1}$ (the static strain rate), $log\beta_s = 7.11\delta - 2.33$, $\delta_s = 1/(10 + 6f_{sc}/f_{co})$, $f_{co} = 10$ MPa, f_{cs} is the static concrete compressive strength.

Although, Malvar and Ross [46] find out that there is some difference between the available data and new data and hence modified the equation of CEB. The modified equation is as follow;

$$DIF_t = \begin{cases} \left(\frac{\dot{\epsilon}}{\dot{\epsilon}_s}\right)^{\delta} & \dot{\epsilon} \le 1\ s^{-1} \\ \beta \left(\frac{\dot{\epsilon}}{\dot{\epsilon}_s}\right)^{1/3} & \dot{\epsilon} > 1\ s^{-1} \end{cases} \tag{2.16}$$

where $\dot{\epsilon}$ is the strain rate from $10^{-6} s^{-1} - 160\ s^{-1}$ range, $\dot{\epsilon}_s = 10^{-6}\ s^{-1}$ (the static strain rate), $log\beta = 6\delta - 2$, $\delta = 1/(1 + 8f_{sc}/f_{co})$, $f_{co} = 10$ MPa, f_{cs} is the static concrete compressive strength.

It is clear from the above that there are plenty of equations for both the dynamic increase of concrete compressive and tensile strength. These $DIF_{c/t}$ are influenced by different factors such as aggregate size, water to cement ratio, cement content, aggregate shape, age and curing of concrete, etc. There is a lot of experimental data required to check the validity of equations over a wide spectrum.

2.2.2 Steel reinforcement

The strain-rate effect on steel reinforcements has been studied by various researchers. Fu et al. [55] and Malvar [46] have conducted a detailed study on the strain-rate effect on the reinforcing bars. Wakabayashi et al. [56] concluded that yielding stress of bar is affected by strain rate but strain hardening is not quite affected. According to the finding of Soroushian and Choi [57], the yielding stress is very sensitive to strain rating than ultimate strength and has no effect on elastic modulus. Therefore, they concluded that only static yield stress is changed by the strain rating. They also find out that steels having lower yielding stress is more sensitive than higher yielding stress bars. Malvar [58] also find out that the dynamic increase factor has inverse relation with the yielding stress of bar. An equation is formulated for DIF_s on the basis of available experimental data. The following formulation is valid for yield stresses in the regime of 290-710 MPa and strain rates from 10^{-4} s^{-1} to 10 s^{-1};

$$DIF_s = \left(\frac{\dot{\epsilon}}{10^{-4}}\right)^{\alpha} \tag{2.17}$$

where for yield stress, $\alpha = \alpha_{fy}$; $\alpha_{fy} = 0.074 - 0.04 f_y/414$; while for the ultimate stress, $\alpha = \alpha_{fu}$; $\alpha_{fu} = 0.019 - 0.009 f_y/414$; $\dot{\epsilon}$ is the strain rate in the form of s^{-1} and f_y is the static yield strength in MPa.

2.3 Effect of strain rate on RC beam

2.3.1 Analytical and numerical studies

Kulkarni and Shah [10] used simple sectional analysis to incorporate rate effect on the response of an RC beam. However, this approach of sectional response including the rate-dependent materials property doesn't capture the shape of curves adequately. This variation is due to the enhanced bond properties under high

rate loading which causes the extreme localized bars yielding. Thus to avoid this problem, they then used the shape of average stress-strain curve along with the characterization of localized yielding.

Non-linear analytical model was proposed by Fujikake et al. [59] to capture the load-midspan deflection relation of an RC beam under drop-weight impact. He produces the load-deflection relation from the moment-curvature sectional relation of RC beam by incorporating both the influence of strain rate on concrete and steel reinforcement.

Adhikary et al. [19] carried out numerical simulation on RC beam and check out the influence of different factors on DIF and then provide two empirical equations for dynamic increase factors: one having the shear reinforcement and the other without shear reinforcement which is given below;

$$DIF = \left[1.89 - 0.067\rho_g - 0.42\rho_v - 0.14\left(\frac{a}{d}\right)\right] e^{\left[-0.35-0.052\rho_g+0.179\rho_v+0.18\left(\frac{a}{d}\right)\right]\delta} \tag{2.18}$$

$$DIF = \left[0.004\rho_g + 0.136\left(\frac{a}{d}\right) - 0.34\right] log_e\,\delta + \left[0.009\rho_g + 0.41\left(\frac{a}{d}\right) + 0.157\right] \tag{2.19}$$

where ρ_g is the longitudinal bars reinforcement ratio, ρ_v is the transverse bars reinforcement ratio, $\frac{a}{d}$ is the shear span to the effective depth ratio, and δ is the loading rate.

2.4 Study of RC beams under Impact Loading

2.4.1 Experimental testing

Mylrea [60] is one of the pioneers to perform the impact test on RC beams, the characteristic of beam is 254 x 406.4 mm, of 2.44 m length with varying amount of longitudinal and no shear reinforcement of different grades subjected to impact mass of 254 kg and 925 kg. The beams were severely damaged with diagonal shear cracks. The failure mode is shown in Fig. 2.1.

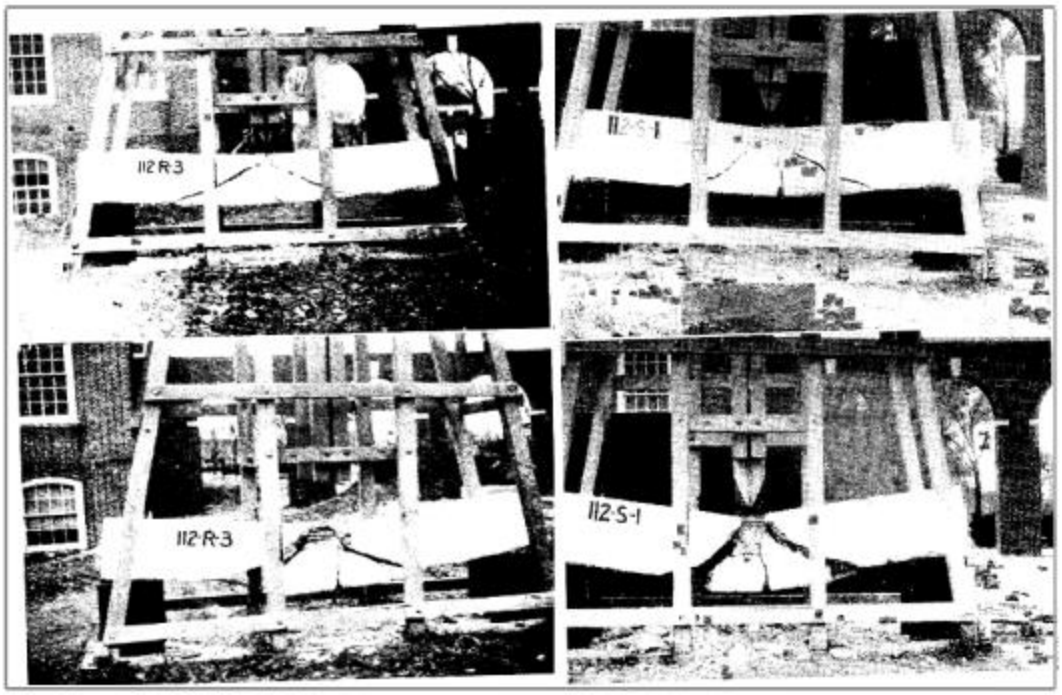

Figure 2. 1: RC beams failure (Mylrea [60])

There was still enough potential strength for collapse when the bars yield. Just like the steel reinforcing bar, the structural performance against impact loading of beams having rail-steel and other hard steel was quite impressive.

Kishi et al. [61] tested eight RC beams having length of 2m under midspan drop-weight of 200 kg steel impactor. In these tests, the variables are cross-section dimensions, impact velocity, and reinforcement ratios. Parallelogram is adopted to approximate the hysteretic loop between the reaction force and mid-span deflection, as shown in Fig. 2.2.

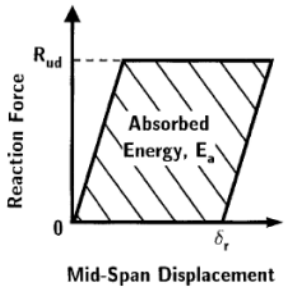

Figure 2. 2: Parallelogram of hysteretic loop (Kishi et al. [61]).

To design flexure failure RC beam under dop-weight impact, the author assumed the dynamic increasing factor of 2 and the ratio of the stored energy to the input energy equal to 0.7. A simple empirical equation was developed for static bending resistance of an RC beam under impact load. The equation is as follows;

$$P_{usd} = 0.35\frac{E_{kd}}{\delta_{rd}} \tag{2.20}$$

where P_{usd} is the static bending strength, E_{kd} is the imparted kinetic energy and δ_{rd} is the mid-span residual displacement.

Twenty seven simply supported rectangular shear-failure type RC beams (150 x 250 mm) without shear reinforcement under midspan impact of 300 kg weight were tested by Kishi et al. [14]. The contact surface of the dropping steel weight is spherical having curvature of 1407 mm radius. The test variables include longitudinal reinforcement, shear span to effective depth ratio, static shear strength to bending strength ratio, and span. It was concluded that for lower static condition of shear to bending ratio (i.e. < 1), shear failure occurs under impact loading. While beams having this ratio just greater than or near to 1, mostly fail in flexure under low impact but fail in shear mode under high impact loading. The hysteretic loop was assumed to be triangular between the force and displacement as shown in Fig. 2.3. The author assumed the dynamic increase ratio of 1.5 and energy ratio of 0.7 for the designing of shear type failure beam under impact loading. The static shear resistance of beams can be calculated as;

$$V_{usd} = 0.8\frac{E_{kd}}{\delta_{rd}} \tag{2.21}$$

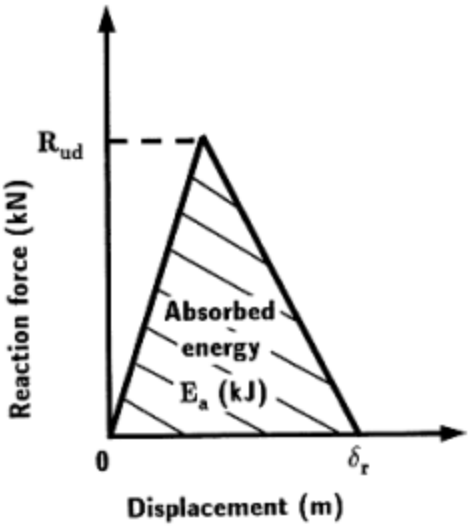

Figure 2. 3: Hysteretic loop of force vs displacement (Kishi et al. [14])

Bhatti et al. [62] also conducted testing on shear failure RC beam to compare it with the simple elasto-plastic FE modeling. The beams were rectangular having dimension of 200 x 400 mm and length equal to 2400 mm. The support condition was simply supported and was impacted at mid-span by dropping 400 kg mass from a defined height. The following experimental results were then compared with FE model: a) Impacting force, reaction forces, and displacement time histories. b) Hysteretic loop of impact loading against mid-span deflection and reaction forces versus mid-span deflection. c) crack propagation on beam's sides.

Impact test on twelve RC simply supported rectangular shape beams having cross-sectional dimensions of 150 x 250 mm and length of 1700 mm was carried out by Fujikake et al. [59]. All the beams are under reinforced and static shear to bending resistance ranges from 1.5-2.6, so that they fail flexurally. All the beams were impacted by dropping a steel mass of 400 kg having hemispherical contact tip having radius of 90 mm. The variables were drop-height and longitudinal reinforcement. The experimental instrumentations setup is shown in the following figure.

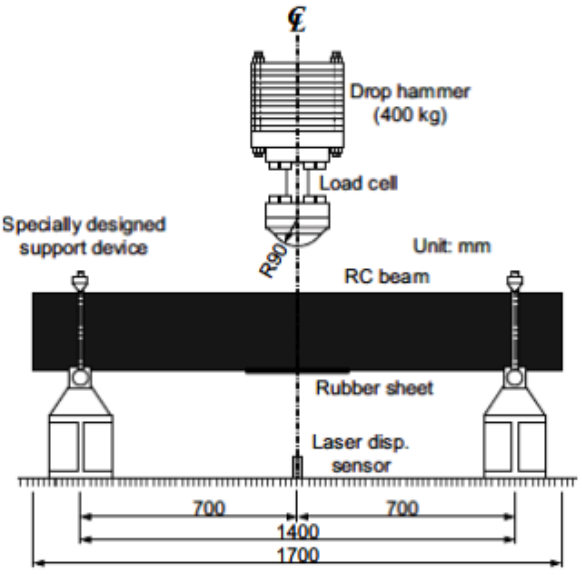

Figure 2. 4: Instrumental setup of impacted RC beam (Fujikake et al. [59])

It was found out that magnitude of longitudinal bars reinforcement affects the failure behavior. For beams having lower amount of longitudinal bars reinforcement only fails in flexure mode, while beams having greater reinforcement not only in flexure but also fail locally near the impact point. This local failure is considerably reduced by increasing the compressive reinforcement. It was also found out that maximum impacted force, maximum mid-span deflection, impulse, duration of the impacted load, and time taken to reach maximum mid-span deflection is considerably increased with the corresponding increase in the drop-height. Although, the impacted load duration, maximum deflection, and the time required for this maximum deflection are affected by the flexural rigidity.

Chen and May [63] also contributed to check the performance of RC beams under drop-weight impact loading. In order to do so, he tested eighteen RC beams in which fourteen have 2.7 m spans while the remaining four are 1.5 m in length. All the beams were tested by dropping a mass of 98.7 kg having striking velocity of 7.3 m/s. Support conditions (i.e. simply supported and pin ended), contact surface of striker (i.e. hemispherical and flat) and the interface surface between the striker and beam (e.g. plywood) were the variables. The time histories of the impact force, acceleration, and strain in longitudinal reinforcements were measured during testing, and crack profiles were produced from the video capture during testing.

There were three types of failure occur: a) the flexure failure with some cracks in the impacted region, b) the local crushing of concrete at impact point and yielding of reinforcement, c) flexure cracks like case (a) but some scabbing of concrete at bottom surface also occur. It was concluded from the testing that support conditions have less effect on impact forces as compared to the length of beams and the behavior of interface and flat head are same.

To understand the effect of shear behavior on RC beams under impact loading, Saatci and Vecchio [13] tested eight specimens by drop-weight with a velocity of 8 m/s. Two masses were used for dropping i.e a lighter weight equal to 211 kg and heavier weight equal to 600 kg. The contact surfaces of both masses are flat and a square steel plate of 305 x 305 mm cross-section and 50 mm thick was used as an interface. A-series beams were tested by dropping a lighter weight first and then followed by heavier weight two times, while for b-series beams, they were tested two times with heavier and third time with lighter weight. All the beams have varying shear reinforcement spacing in order to understand the effect of shear.

Crack propagation of both a and type-b series beams are given in Fig. 2.5. According to the static test, SS3 and SS2 fail in flexure modes, whereas, SS1 and SS0 fail in shear behavior. But under impact loading, all the beams have severe cracking under impact point forming shear plug along with some other inclined cracks adjacent to shear plug and some vertical flexure types cracks at mid-span and around supports. In flexure-critical beams, the formation of shear plug is earlier than all other cracks. While for shear-critical beams along with shear plug, severe inclined cracks starting from impact point to the supports formed which is the indication of lower shear resistance of these beams compared to flexure ones. Several impacts cause the shear plug to move further down in flexure-critical beams while it increases the severity of inclined cracks in shear-critical beams and thus fails the beams at that point.

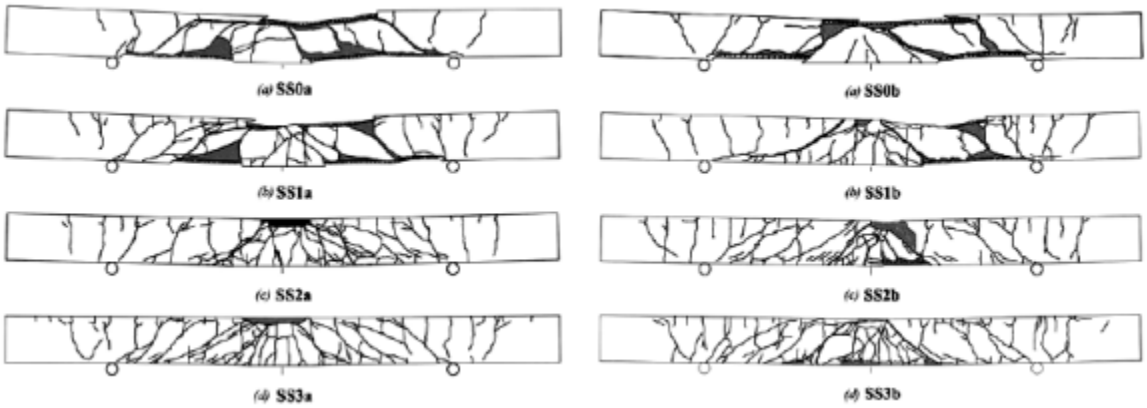

Figure 2. 5: Cracking profiles of type-a and -b series beams (Saatci and Vecchio [13])

Regardless of the static behavior of beams, all the beams were severely damaged under the impact loading. Those beams having greater shear capacity absorb greater impact energy than those which have less capacity as there was excessive damage in those beams under same or even smaller impact force. This means that shear mechanism should need to be used for predicting the impact behavior. As the structure response under impact loading is mainly initially controlled by the inertial force, therefore the mass and geometries of RC beams such as length of beam greatly affect the behavior of beams. It was found out that different parameters that can influence the impact behavior need to be investigated by testing increasing number of specimens.

A series of low impact speed testing was performed by Tachibana et al. [64] having span, cross-section, and longitudinal reinforcement as variables. The contact surface of the striker is curved having radius equal to 75 mm. Steel weight of masses 150, 300, and 450 kg was used as drop-weight from a specific height at the mid-span of beam. All the beams were expected to fail in flexure mode under static loading because the ratio of shear resistance to bending resistance was more than one. Moreover, an equation is developed by the author to produce the maximum midspan deflection of the beam based on the imparted energy, and ultimate static flexural strength. The equation is as follows;

$$\delta_{max} = 0.522 \frac{E_{col}}{P_u} \tag{2.22}$$

where δ_{max} is the maximum midspan deflection (mm), E_{col} is the imparted kinetic energy (J), P_u is the static ultimate flexural resistance (kN). This equation is valid in the range of 16.7 – 66.7 kN and 150 – 5400 J.

Thirty six simply supported RC beams having rectangular cross-section of 150 – 250 mm in width, 200 – 400 mm in depth, and 2 – 3 m in length have been tested under drop-weight impact loading. Longitudinal reinforcement ratio varies from 0.8 – 3.17%, and the shear reinforcement was placed with changing spacing of 100, 125, and 150 mm. All the beams were statically flexure-critical, as having ratio of shear to flexure resistance greater than 1. Three different masses of 300, 400, and 500 kg were used as drop-weight with the dropping velocity in the range of 3.1 – 7.7 m/s. The striking face of all the masses was spherical having 1407 mm radius. Flexural cracks in lower as well as in upper fibers were occur along with diagonal shear cracks formed from the impacted point toward the end support and the severity of these shear cracks increased with the increasing impact velocity. The maximum and residual mid-span deflections are related to the imparted input energy and on the basis of these following empirical equations were proposed;

$$\alpha_{def} = \frac{0.63}{P_{usc}} \tag{2.23}$$

$$\alpha_{rs} = \frac{0.42}{P_{usc}} \tag{2.24}$$

By rearranging the above equations, the followings relation can be as follows;

$$P_{usc} = 0.63\ E/D_{max} \tag{2.25}$$

$$P_{usc} = 0.42\ E/\delta_{rs} \tag{2.26}$$

where P_{usc} is the static flexural strength (kN), E is the imparted kinetic energy (J), D_{max} is the maximum mid-span displacement and δ_{rs} is the residual mid-span displacement (mm). These equations predict well for $E < 15$ kJ, $P_{usc} < 240$ kN, and the static shear to flexure resistance ratio $\alpha > 1.5$.

2.4.2 Mathematical and analytical based studies

Bhatti et al. [62] used a simple FE elasto-plastic model to compare the results with the experimental findings. He used a bilinear curve for concrete compression and cutoff model for tension in concrete. He modeled steel bars as an elasto-plastic material with strain-hardening. The effect of strain rate on concrete and bars were neglected. The output results such as impacted force, reaction force, and midspan deflection time histories were compared with the experimental results. Moreover, hysteretic loops of impacted force with corresponding mid-span displacement and reaction versus displacement, crack patterns and energy absorption were predicted with reasonable accuracy.

Non-linear finite element analysis (NLFEA) procedure was adopted by Saatci and Vecchio [65] for modeling RC beams under drop-weight impact loading. The efficiency of the modeling can be confirmed from the comparison of time histories data of midspan deflection and strain in longitudinal reinforcement along with the cracking profiles obtained from NLFEA and experimental testing. Distributed stress field model (DSFM) was very effective in producing the response of shear critical RC beams under impact loading including the strain rate dependents material properties.

Two degrees of freedom mass-spring damping system was adopted by Fujikake et al. [59] to model RC beam under dropweight impact loading. The global stiffness of the spring was obtained from the load versus midspan deflection relation having rate effect whereas the stiffness of the contact spring was calculated through the contact theory of Hertz. The global value of damping was assumed as zero while the contact spring damping value was considered half of the critical damping coefficient. In case of global flexure failure, the output of model in terms of impacted force, reaction force, and midspan deflection time histories were predicted well but in case of both local and global flexure failure large variation was observed.

Alternatively, Zhao et al. [66] evaluated the mid-span deflection on the basis of the conservation of energy procedure as given below;

$$E_{kstab} + (M + m)gs_{max} = \int_0^{s_{max}} F(s)ds \tag{2.27}$$

where E_{kstab} is the imparted kinetic energy, M is the impact mass, m is the effective calculated mass of beam, g is the gravity of acceleration, s_{max} is the maximum mid-span deflection, and F is the strength of the beam under drop-weight loading at mid-span.

Khan et al. [8] used mathematical computation to address the response of beam under impact loading. The kinetic, kinematic and material plasticity relations were used to produce a numerical model in the form of Linear Complementarity Problem (LCP) capable of examining the rigid plastic behavior of simply supported beams under impact loading. This procedure doesn't employ the strain rate effects as well as not incorporating the shear bending interaction for shear critical beams.

2.5 Summary

Based on the above literature review, following conclusion points can be summarized:

(a) The dynamic-behavior of RC structures is highly sensitive to strain-rate, resulting in a considerable increase in the yield stress with an increased rate of straining [9,19,46,55,58,67]. This property of viscoplasticity should be incorporated in any simplified model for accurately predicting the peak response values of these structures under dropweight impact loading. Therefore, the study of the dynamic properties of RC structures has received considerable attention, and many forms of the rate-dependent constitutive laws have been proposed [19,68,69]. The most commonly used form is that due to Cowper and Symonds [70]. They have proposed an exponential strain rate law, whose constants can be determined for many common materials [2]. Adopting the usual assumptions of beam theory, Aspden and Campbell [71] integrated this exponential law through the thickness of a rectangular beam, thereby establishing an expression relating bending moment to the associated curvature rate. This moment expression is widely accepted due to its very good agreement with the experimental data. A vast experimental literature is available which shows that the strain rate effects can significantly change the dynamic response of RC structures under high impact loading.

(b) Many experimental, analytical, and numerical studies by authors have been conducted toward understanding flexure failure modes of RC beams under dropweight impact loading. On the other

hand, the effect of transverse shear forces on the response of these beams has not been adequately understood [72]. Although several experimental investigations have signified the importance of shear in the impact response of RC structures. [14,62,72]. Similarly, Saatci et. al [13] have identified shear-plug under the impact point. Truly, it has been tested numerically and shown theoretically by Saatci et. al [65] that failure due to shear can be developed in impacted beams. It transpires that the rigid-plastic bending response may be extended to incorporate bending moment and shear force interactions, where the significance of interaction depends on the magnitude of shear force relative to the bending moments [73].

(c) A rigid-plastic beam subjected to extreme dynamic load develops bending and shear deformations which contribute to the resulting motion. The shear deformation leads to a decrease in the bending deformation since part of the imparted kinetic energy is used in shearing. The significance of bending-shear interaction in the plastic deformation of the structures depends on the bending strength relative to shear strength as well as the magnitude of the applied load. The shear effects get larger as the ratio of shear strength to the bending gets smaller and as the ratio of the magnitude of the applied load to the bending strength gets larger [74]. In rigid-plastic structures, these shear effects are localized at a discontinuity interface which consumes plastic-deformation in the dynamic-plastic response. This interface can be termed as a shear hinge which is assumed to have an infinitesimal length for a rigid-perfectly plastic idealization because the characteristic length of the shear interface is very small in comparison with the length of the beam. Also, the shear interface is always stationary; that is, the size of the shear hinge deformation does not increase during the following beam response [75,76].

(d) Many commercial software packages, such as ABAQUS and LS-DYNA, are founded upon the finite element methods, which can be employed to determine the dynamic response of impacted RC structures [12,77–81]. However, even for application to simple problems, their use is likely to be both computationally expensive and time-consuming [17]. Mathematical programming, on the contrary, has proven to be an effective and efficient computational tool for solving this class of

dynamic problems [27]. Moreover, it has the potential to proffer a systematic numerical formulation for the analysis of problems based on the method of finite element (FE). More specifically, a mathematical formulation in the state of Linear Complementarity Problem (LCP) can capture the rigid-plastic behavior of structures under high intensity dynamic loading based on the fundamental principles of mechanics and got the potential to incorporate strain-rate effects and shear bending interaction straightforwardly. Although full of potential, this mathematical programming tool has not been exploited to any great extent to encode and solve problems in dynamic plasticity.

(e) It can be inferred from the above discussion that the simple rigid-plastic theory in the impact dynamics of RC structure has a vast potential for offering computationally efficient procedures that allows considerable physical insight into the underlying mechanics of motion [27]. Therefore, in this work, firstly a simple mathematical and computational method is developed, which is founded upon the rigid-plastic theory incorporating the strain-rate sensitivity for calculating the dynamic behavior of RC skeletal structures under dropweight impact loading. The formulation is represented as a viscoplastic linear complementarity problem (LCP). Then the same approach was used for the formulation of the LCP model but this time it uses a rectangular yield curve for the relation between transverse shear force, and the bending moment. The solution strategy is based upon the Lemke's Algorithm [6,82–86], which can deal in best way with the sign-unrestricted variables, and structural semidefinite matrices. An essential feature of this current work is incorporating strain-rate sensitivity that is accounted for in the LCP using the bending equation of Aspden and Campbell [71]. The material constants of this equation have been determined from the experimental data of RC beams collected from the literature. The bending-shear interaction curve was incorporated in the LCP again to capture the response of shear critical RC beam. It is known that the maximum deflection is considered an important parameter for determining the damage degree [59,64,87].

(f) Due to the limitation of the LCP model for producing the peak impact force of RC beams uniquely under impacted loading, a regression-based model of peak impact force using the Gene Expression

programming algorithm is proposed. The peak dropweight impact force can be employed to derive the shear force and bending moment diagrams, thus providing a capability to examine the dynamic response characteristics of impacted RC beams, and simplifying the design approach.

3 Methodology

In this chapter, the mathematical formulation is carried out for beams under dropweight impact loading. The mathematical work is formulated in the form of Linear Complementarity Problem (LCP). There are two LCP formulations one is incorporating strain rate effect while the other one includes the bending-shear interaction. Due to the limitation of these LCPs, we are unable to get peak impact force directly, therefore, an empirical model was proposed through gene expression programming to predict the peak impact force by incorporating the midspan deflection obtained from the above LCPs.

3.1 Proposed Dynamic Rigid-Plastic Model Incorporating Strain-rate Effet

This section presents a simple rigid-plastic lumped mass model to analyze reinforced concrete beams and frames under impact loads shown in Fig. 3.1. Thus, the fundamental conditions of the kinetics, the kinematics, and the material constitution are combined in a consistent way to develop a multi-degrees of freedom model [8].

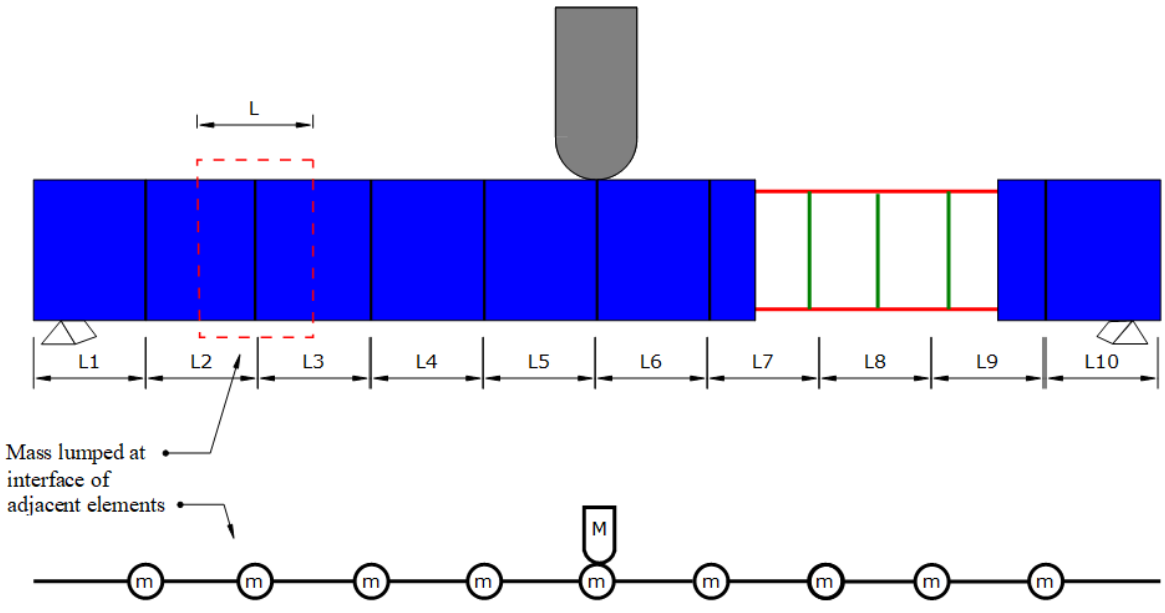

Figure 3. 1: Discritized simply-supported beam under impact loading

3.1.1 Representation of kinetics and kinematics as the nodal description

The RC structure in Fig. 3.1 is explored in the nodal description of kinetics and kinematics. Let this structure be subdivided into N finite elements, in which the independent movements of the interconnecting nodes are governed by β degrees of freedom. Any kinematically consistent velocity distribution or profile may be specified entirely in terms of β independent nodal velocities $\dot{q}_j \ \ (j = 1,2, \ldots \ldots, \beta)$. For an assembly of the inextensible planar elements, with α static indeterminacy and S plastic rotational deformations occurring at the element extremities, the kinematic indeterminacy number can be established as $\beta = S - \alpha$.

When each of the β independent nodal velocities $\dot{\mathbf{q}}$ is released, a velocity profile is generated, for which the independent member deformation rates $\dot{x}_h \ (h = 1, 2, \ldots \ldots, 2N)$; indicated in Fig. 3.2, the velocities related to center of gravity of mass $\dot{u}_k (k = 1, 2, \ldots \ldots, \gamma)$; indicated in Fig. 3.3, and the load point velocities $\dot{\delta}_\ell \ (\ell = 1, 2, \ldots \ldots, n)$ can be easily obtained through geometric considerations. Hence, the nodal representation of the kinematic equations has the form:

$$\begin{bmatrix} \dot{\mathbf{x}} \\ \dot{\mathbf{u}} \\ \dot{\boldsymbol{\delta}} \end{bmatrix} = \begin{bmatrix} \mathbf{A} \\ \mathbf{A}_d \\ \mathbf{A}_0 \end{bmatrix} \dot{\mathbf{q}} \tag{3.1}$$

where the coefficient matrix is constant, provided that the motion falls within small displacements.

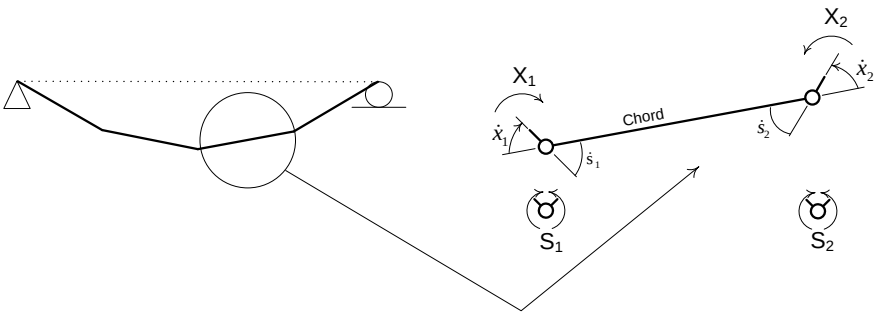

Figure 3. 2: Stress-resultants, strain-resultant rates, chord deformation rates, and independent chord forces.

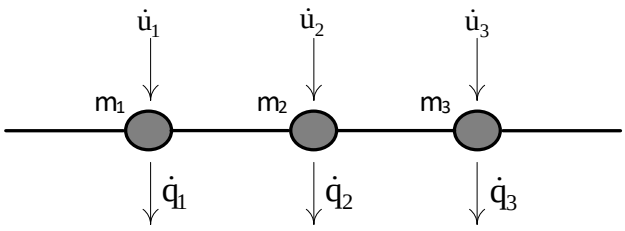

Figure 3. 3: Centroidal-velocities in a system of lumped mass

Let the structure be subjected to n discrete time-dependent loads λ_ℓ $(\ell = 1, 2, \ldots\ldots, n)$ applied at nodes. By employing the principle of D' Alembert, during every instant of the accelerated motion of a structure, the loads applied, and the inertial forces $\mu_k (k = 1, 2, \ldots\ldots, \gamma)$ are in state of equilibrium with the independent member forces X_h $(h = 1, 2, \ldots\ldots, 2N)$. Corresponding to the independent nodal displacements, the nodal forces of constraint $Q_j (j = 1, 2, \ldots\ldots, \beta)$ are applied. For satisfaction of the dynamic equilibrium, it is necessary that the constraints Q_j must vanish, giving the nodal kinetics description for the assembly of all elements:

$$\mathbf{Q} = \mathbf{0} = [\mathbf{A}^T \quad \mathbf{A}_d^T \quad \mathbf{A}_0^T] \begin{bmatrix} \mathbf{X} \\ -\boldsymbol{\mu} \\ -\boldsymbol{\lambda} \end{bmatrix} \tag{3.2}$$

where the transposed (T) coefficient matrix remains constant by virtue of small displacements. It may be observed that (3.1) and (3.2) satisfy the adjoint relationship of kinetic-kinematic duality.

The independent relations (3.1) and (3.2) have no cause-effect relationship between the kinetic and kinematic variables. Nevertheless, the relation

$$\boldsymbol{\mu} = -\boldsymbol{m}\, \ddot{\boldsymbol{u}} \tag{3.3}$$

implicitly links the inertia forces $\mu_k (k = 1, 2, \ldots\ldots, \gamma)$, located at the mass centroid, with the corresponding centroidal accelerations $\ddot{u}_k (k = 1, 2, \ldots\ldots, \gamma)$ of the actual motion of the system. In this inertial law, the diagonal mass matrix $m_k (k = 1, 2, \ldots\ldots, \gamma)$ constitutes the mass or moment of inertia related to the corresponding centroidal accelerations.

3.1.2 Material Model

To analyze the nonlinear flexural response of RC beams, the cause-effect relation between the stress-resultant S_1^i (bending moment M_i) and its dual rate of strain-resultant $\dot{s}_1^i$ (the rotation rate $\dot{\theta}_i$) at different critical section $i, (i = 1,2, \dots, \chi)$, is illustrated in Fig. 3.4. These quantities are also depicted in the discrete structural model of Fig. 3.1. It is noted that the plastic moment $X_*^{+i} \geq 0$ when the stress-resultant S_1^i is positive. In Fig. 3.4, it is evident that the critical section yielding i is defined by two variables, i.e., the plastic potential $y_*^{+i} \geq 0$, and other is the plastic multiplier rate $\dot{x}_*^{+i} \geq 0$. A similar argument applies to $X_*^{-i} \geq 0$, $y_*^{-i} \geq 0$, $\dot{x}_*^{-i} \geq 0$ when S_1^i has got negative value.

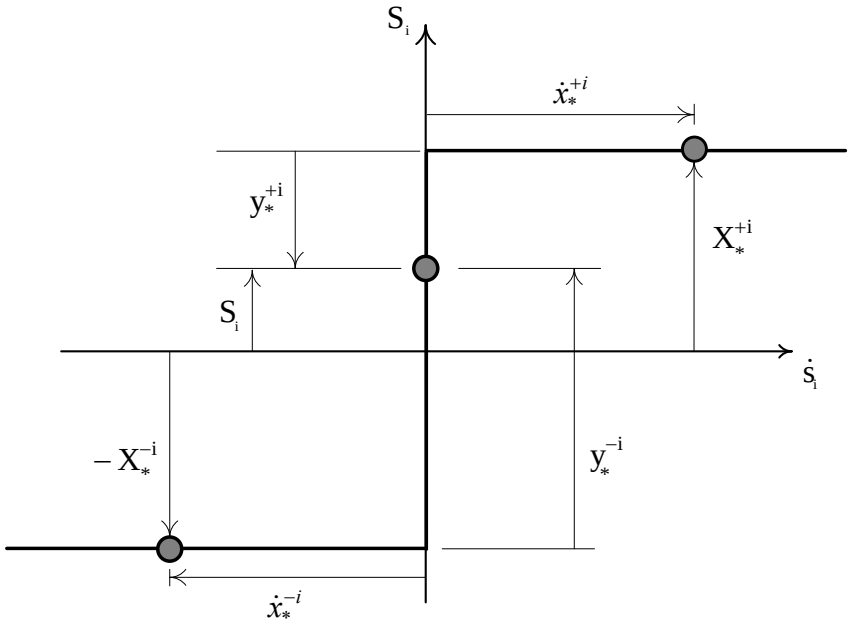

Figure 3. 4: Material model

Now, let the current plastic deformation at the critical section i be $s_1^i = x_*^{+i}$ as in Fig. 3.4. Ensuring the irreversible nature of plasticity, the plastic deformation rate at the i[th] section is $(\dot{x}_*^{+i} > 0)$, and accordingly, the yield mode at this section is $(y_*^{+i} = 0)$ only if the yield limit is attained, whereas, if the yield limit is not attained $(y_*^{+i} > 0)$, then the plastic deformation cannot be active $(\dot{x}_*^{+i} = 0)$. The mutual exclusivity

each pair of corresponding variables have, ($\dot{x}_*^{+i} > 0$, $y_*^{+i} = 0$), and ($y_*^{+i} > 0$, $\dot{x}_*^{+i} = 0$), is assured by the provision of complementarity condition: $y_*^{+i}\, \dot{x}_*^{+i} = 0$. Now, the rigid perfectly plastic constitutive relation for each critical section i is written in matrix notation:

$$\begin{bmatrix} \mathbf{0} & \mathbf{N}^T \\ \mathbf{N} & \mathbf{0} \end{bmatrix} \begin{bmatrix} \dot{\mathbf{x}}_* \\ \mathbf{S} \end{bmatrix} + \begin{bmatrix} \mathbf{y}_* \\ \mathbf{0} \end{bmatrix} = \begin{bmatrix} \mathbf{X}_* \\ \dot{\mathbf{s}} \end{bmatrix} \tag{3.4}$$

$$\mathbf{y}_* \geq \mathbf{0} \tag{3.5}$$

$$\mathbf{y}_*^T \dot{\mathbf{x}}_* = 0 \tag{3.6}$$

$$\dot{\mathbf{x}}_* \geq \mathbf{0} \tag{3.7}$$

where **N** is the matrix defining the exterior unit normal to the yield function; $N = [\mathbf{I} \quad -\mathbf{I}]$, and **I** is the matrix of identity.

Relations (3.4) to (3.7), is the representation of the nonholonomic constitutive law of one-dimensional (1D) perfect plasticity, that can be adopted for the RC structural elements system. These relations can be also used for the situation where yielding is controlled by several stress resultants. In such situations, the yielding surface can be piecewise linearized into a polytope which represents the hyperplanes of the polyhedral yield surface [88].

It is of interest to develop a governing mathematical system that couples the constitutive relations, (3.4) to (3.7), with the kinetic and the kinematic relations, (3.1) to (3.3). Fig. 3.2 clearly illustrates that the independent member forces **X,** and the independent deformation rates of member $\dot{\mathbf{x}}$ can be defined by the respective resultant of stresses **S,** and the resultant of all strain rates $\dot{\mathbf{s}}$. These can be collected for all the constituent finite elements:

$$\dot{\mathbf{x}} = \mathbf{T}\dot{\mathbf{s}} \tag{3.8}$$

$$\mathbf{S} = \mathbf{T}^T\mathbf{X} \tag{3.9}$$

3.1.2.1 Strain Rate Effect

Like many structural materials, RC structures are also significantly stronger when loaded at a very high rate than when subjected to normal rate service loads. For such cases, the yield stress increases considerably with an increased rate of straining to render the participation of strain rate effects in the dynamic plastic response [9,19,46,55,58,67]. Therefore, it is intended herein to include the rate-dependent plastic moment into the preceding formulation. Notably, a vast amount of literature is available on the strain rate-sensitive behavior at the material constitutive level. However, a limited attempt is made to investigate the structural behavior under varying loading rates. For this reason, the contemporary literature has advocated the use of dynamic increase factor, that is, the ratio of the dynamic strength to corresponding static strength, in the numerical formulations, which encompasses not only the material strain-rate effect but also various structural influencing parameters.

Under the impact loads, reinforced concrete structures show much greater capacities to absorb energy. The strain-rate effect in these structures is influenced by various material and geometric factors, as pointed out by the parametric study [68] on the dynamic increase factor (DIF). Based on this study, two empirical equations are proposed for the DIF of the RC beams: one having the shear bar reinforcement, and the other without shear bar reinforcement. Thus

$$DIF = \left[1.89 - 0.067\rho_g - 0.42\rho_v - 0.14\left(\frac{a}{d}\right)\right] e^{\left[-0.35-0.052\rho_g+0.179\rho_v+0.18\left(\frac{a}{d}\right)\right]\delta} \tag{3.10}$$

$$DIF = \left[0.004\rho_g + 0.136\left(\frac{a}{d}\right) - 0.34\right] log_e\,\delta + \left[0.009\rho_g + 0.41\left(\frac{a}{d}\right) + 0.157\right] \tag{3.11}$$

where ρ_g is the longitudinal bar reinforcement ratio, ρ_v is the transverse bar ratio, $\frac{a}{d}$ is the ratio of shear span to effective depth, and δ is the loading rate.

To incorporate the aforementioned DIF equations in the plastic moment capacities, choosing a constitutive equation keyed to the experimental test programs is essential. In the body of researches into the strain-rate effects, the simple equation suggested by Cowper and Symonds [70] has been extensively used for various

metal alloys, such as steel and aluminum. From this precedent, it has been decided in the present investigation to use this equation to reinforce concrete structures. The constitutive equation suggested by Cowper and Symonds [70] is

$$\dot{\epsilon} = D\left(\frac{\sigma_o'}{\sigma_o} - 1\right)^p , \quad \sigma_o' \geq \sigma_o \tag{3.12}$$

where σ_o' is the dynamic stresses at yielding, $\dot{\epsilon}$ is the corresponding strain rate, σ_o is the static state yield stress, and both D and p are material constants. It is of interest to note that the ratio $\frac{\sigma_o'}{\sigma_o}$ can be considered as DIF straightforwardly. Now, equation (3.12) may be written as

$$log_e \dot{\epsilon} = p\, log_e(DIF - 1) + log_e D \tag{3.13}$$

which has the same form as a line with the parameter p as the slope, while the $log_e D$ as the intercept. Hence, these coefficients can be determined from the experimental data of RC structures.

The constitutive equation derived in (3.13) has been recast by Aspden and Campbell [71], integrating (3.12) through the depth H of a rectangular cross-section. So, the resulting equation is

$$\frac{M_o'}{M_o} = \left\{1 + \left[\frac{H}{2z\left(1+\frac{1}{2p}\right)^p}\frac{\dot{x}}{D}\right]^{\frac{1}{P}}\right\} \tag{3.14}$$

where M_o' is dynamic bending moment, $\dot{x}$ is the generalized strain rate and z is the plastic hinge length. Due to the inherent difficulty of defining the actual variation of the curvature along the plastic zone, an estimation of the plastic hinge length may be had by the following proposed empirical formula [89]

$$z = d + 0.05 \times l \tag{3.15}$$

where d is the effective depth of beam cross-section and l is the net span length of RC beam.

In order to incorporate strain rate sensitivity in the proposed mathematical formulation for rigid-plastic dynamics, equation (3.14) can be expressed as;

$$\mathbf{X}_{*n+1} = \mathbf{V}_n \mathbf{X}_*^{\boldsymbol{o}} \tag{3.16}$$

where $\mathbf{X}_{*n+1}$ is the plastic capacity at the corresponding active node in the structural system at time $t = t_{n+1}$, $\mathbf{X}_*^{\boldsymbol{o}}$ is the corresponding plastic capacity for the original state of the structural material and $\mathbf{V}_n$ is the viscoplastic function, evaluated at time $t = t_n$.

3.1.3 The Mathematical Formulation

The vectorial relations (3.1) to (3.3), together with the triad of complementarity conditions (3.5) to (3.7), can be combined into a set of differential equations having second-order derivatives with respect to time. Nevertheless, this set is made more complex by the complementarity conditions. As no mathematical system is known to this kind of mathematical problem, adopting a numerical solution appears reasonable. Therefore, a time depending scheme is incorporated in order to allow the solution procedure to be advanced from a time station t_n to $t_{n+1} = t_n + \Delta t$, where subscript n is an integer defining consecutive discrete time stations and Δt is the intervening increments of time. Then, the centroidal velocities and corresponding accelerations can be expressed in the time-integration scheme of Newmark:

$$\ddot{\mathbf{u}}_{n+1} = b_0(\dot{\mathbf{u}}_{n+1} - \dot{\mathbf{u}}_n) - b_1 \ddot{\mathbf{u}}_n \tag{3.17}$$

and

$$\dot{\mathbf{u}}_{n+1} = \mathbf{u}_n + b_2 \dot{\mathbf{u}}_n + b_3 \ddot{\mathbf{u}}_n + b_4 \ddot{\mathbf{u}}_{n+1} \tag{3.18}$$

in which integration constants are

$$b_0 = \frac{1}{\bar{\gamma} \Delta t}, \tag{3.19}$$

$$b_1 = \frac{1-\bar{\gamma}}{\bar{\gamma}}, \tag{3.20}$$

$$b_2 = \Delta t, \tag{3.21}$$

$$b_3 = (0.5 - \bar{\alpha}) \Delta t, \tag{3.22}$$

$$b_4 = \bar{\alpha} \Delta t^2 \tag{3.23}$$

It is found after thorough investigations that suitable results are obtained for rigid-plastic dynamics if $\bar{\alpha} = 0.25$ and $\bar{\gamma} = 0.5$.

Collecting together (3.1), (3.2), (3.3), and (3.4) to (3.7), (3.8), (3.9), and (3.16), at time $t = t_{n+1}$, and coupling with the Newmark's scheme (3.17) to (3.23) the governing system becomes:

$$\begin{bmatrix} -b_0\mathbf{M}_q & \mathbf{0} & -\mathbf{A}^{\mathrm{T}} \\ \mathbf{0} & \mathbf{0} & \mathbf{N}^T\mathbf{T}^T \\ -\mathbf{A} & \mathbf{TN} & \underline{\mathbf{0}} \end{bmatrix} \begin{bmatrix} \dot{\mathbf{q}}_{\mathrm{n+1}} \\ \dot{\mathbf{x}}_{*n+1} \\ \mathbf{X}_{n+1} \end{bmatrix} + \begin{bmatrix} \mathbf{0} \\ \mathbf{y}_{*n+1} \\ \mathbf{0} \end{bmatrix} = \begin{bmatrix} -\mathbf{Y}_{n+1} \\ \mathbf{X}_{*\mathrm{n+1}} \\ \mathbf{0} \end{bmatrix} \tag{3.24}$$

$$\mathbf{y}_{*n+1} \geq \mathbf{0} \tag{3.25}$$

$$\mathbf{y}_{*n+1}^T \dot{\mathbf{x}}_{*n+1} = 0 \tag{3.26}$$

$$\dot{\mathbf{x}}_{*n+1} \geq \mathbf{0} \tag{3.27}$$

with variables $\dot{\mathbf{q}}_{\mathrm{n+1}}, \mathbf{X}_{n+1}$ unrestricted

The right-hand side sub-vector $\mathbf{Y}_{n+1}$ of (24) is given by:

$$\mathbf{Y}_{n+1} = \mathbf{A}_0^T\boldsymbol{\lambda}_n + \mathbf{M}_q(b_0\dot{\mathbf{q}}_n + b_1\ddot{\mathbf{q}}_n) \tag{3.28}$$

and the mass matrix $\mathbf{M}_{\mathbf{q}}$ is given by the relation:

$$\mathbf{M}_q = \mathbf{A}_d^T\mathbf{m}\mathbf{A}_d \tag{3.29}$$

The approximating governing system (3.24) to (3.27) has a computational structure of a linear complementarity problem (LCP). It may be noticed that the variables i.e. $[\dot{\mathbf{x}}_*, \mathbf{y}_*]$, are restrained into the complementary pairs, whereas the leading sub-matrix related to variables[$\dot{\mathbf{q}}$, $\mathbf{X}$] is negative semi-definite. In this work, the governing system is solved efficiently by Lemke algorithm due to its simplicity and robustness.

3.1.4 Solution steps of formulation

Having the response parameters $\mathbf{q}_n, \dot{\mathbf{q}}_n, \ddot{\mathbf{q}}_n, \mathbf{X}_n, \mathbf{x}_{*n}, \dot{\mathbf{x}}_{*n}, \mathbf{x}_n$ of the structural system at time $t = t_n$ be known, the right hand side of (3.24) can be calculated with the plastic capacities $\mathbf{X}_{*n+1}$ determined using (3.16). Similarly, the right-hand side sub-vector $\mathbf{Y}_{n+1}$ in (3.28) requires generalized accelerations in the master directions that can be found by imposing the kinetic equation (3.2)

$$(\ddot{\mathbf{q}}_m)_{n+1} = (\mathbf{A}_{dm}^T \, \boldsymbol{m} \, \mathbf{A}_{dm})^{-1}(\mathbf{A}_{0m}^T \, \boldsymbol{\lambda}_{n+1} - \mathbf{A}_m^T \, \mathbf{X}_{n+1}) \tag{3.30}$$

To initiate the solution sequence at time $\mathrm{t} = \mathrm{t}_0$, the generalized velocities $\dot{\mathbf{q}}_0$, the generalized acceleration $\ddot{\mathbf{q}}_0$ and the initial plastic capacities $\mathbf{X}_*^{\boldsymbol{o}}$ must be established. When the motion is excited by impact, $\dot{\mathbf{q}}_0$ is known, $\ddot{\mathbf{q}}_0 = \mathbf{0}$ since $\boldsymbol{\lambda} = \mathbf{0}$ and $\mathbf{X}_0 = \mathbf{0}$ in (3.30), and $\mathbf{X}_*^{\boldsymbol{o}}$ is the vector of plastic capacities with viscoplastic matrix $\mathbf{V}_0 = \mathbf{1}$ in (3.16). The iterative strategy is shown in Fig. 3.5.

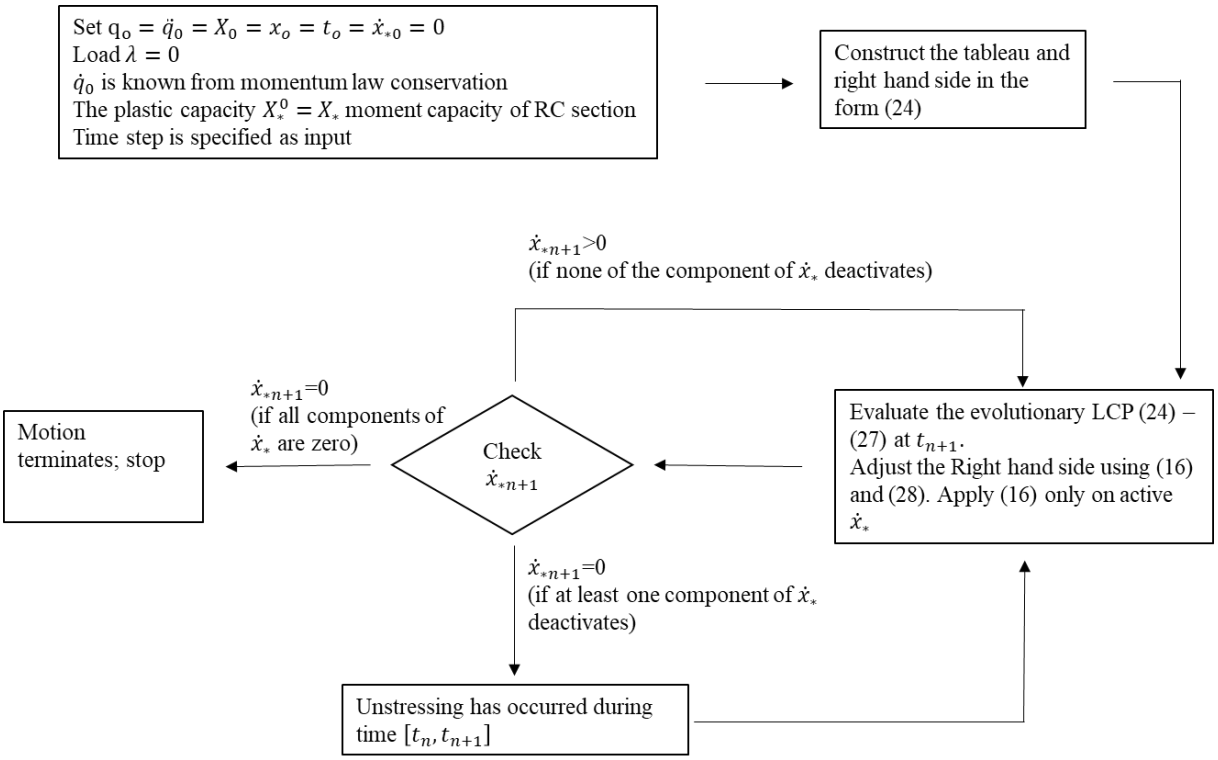

Figure 3. 5: Flow path for the proposed viscoplastic LCP model

3.2 LCP Formulation Incorporating M-V Interaction

This section presents a simple rigid-plastic lumped mass model to analyze reinforced concrete beams and frames under impact loads shown in Fig. 3.6. Thus, the fundamental conditions of the kinetics, the kinematics, and the material constitution are combined in a consistent way to develop a multi-degrees of freedom model [8].

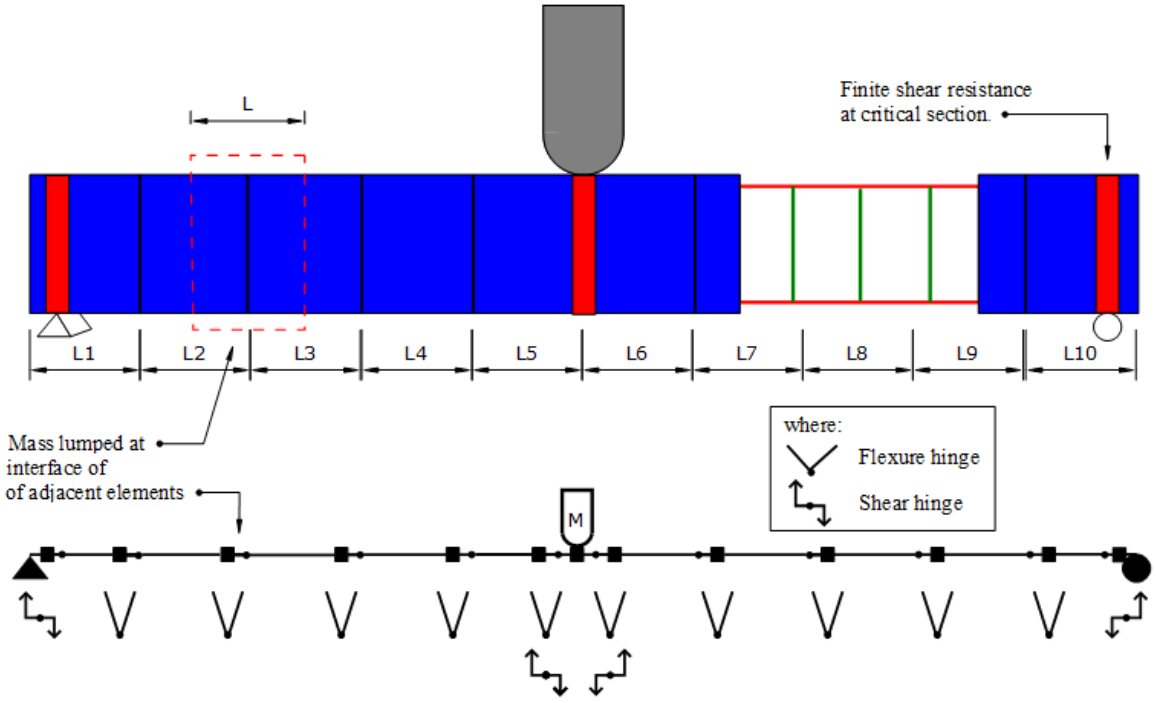

Figure 3. 6: Discretized simply-supported beam under dropweight impact

3.2.1 Representation of kinetics and kinematics as the nodal description

The RC structure in Fig. 3.6 is explored in the nodal description of kinetics and kinematics. Let this structure be subdivided into N finite elements, in which the independent movements of the interconnecting nodes are governed by β degrees of freedom. Any kinematically consistent velocity distribution or profile may be specified entirely in terms of β independent nodal velocities $\dot{q}_j \ \ (j = 1,2, \dots \dots, \beta)$. For an assembly of the inextensible planar elements, with α static indeterminacy and S plastic rotational deformations occurring at the element extremities, the kinematic indeterminacy number can be established as $\beta = S - \alpha$.

Fig. 3.7 exemplifies the type of discrete structural model that is referred to herein for the sake of simplicity. The flexural deformability is assumed at all the critical sections marked by dots except the support region. In comparison, the shear deformability is assumed only at the support points and the point of impact at the midspan. If attention is confined to the impact point of Fig. 3.7, it is clear that both the bending and shear deformation can occur simultaneously. This impacted member is dissected from the beam and subjected to independent member force in Fig. 3.8(a). This figure clearly shows that the onset of plasticity is governed by bending moments and shear forces at each of the critical sections. With regard to the remaining elements of Fig. 3.7 that are governed by bending moments only, the independent member forces and the deformation rates are shown in Fig. 3.8(b).

When each of the β independent nodal velocities $\dot{\mathbf{q}}$ is released, a velocity profile is generated, for which the independent member deformation rates $\dot{x}_h\ (h = 1, 2, \ldots\ldots, 2N)$; indicated in Fig. 3.7, the velocities related to center of gravity of mass $\dot{u}_k (k = 1, 2, \ldots\ldots, \gamma)$; as shown in Fig. 3.8(c), and the load point velocities $\dot{\delta}_\ell\ (\ell = 1, 2, \ldots\ldots, n)$ can be easily obtained through geometric considerations. Hence, the nodal representation of the kinematic equations has the form:

$$\begin{bmatrix} \dot{\mathbf{x}} \\ \dot{\mathbf{u}} \\ \dot{\boldsymbol{\delta}} \end{bmatrix} = \begin{bmatrix} \mathbf{A} \\ \mathbf{A}_d \\ \mathbf{A}_0 \end{bmatrix} \dot{\mathbf{q}} \tag{3.31}$$

where the coefficient matrix is constant, provided that the motion falls within small displacements.

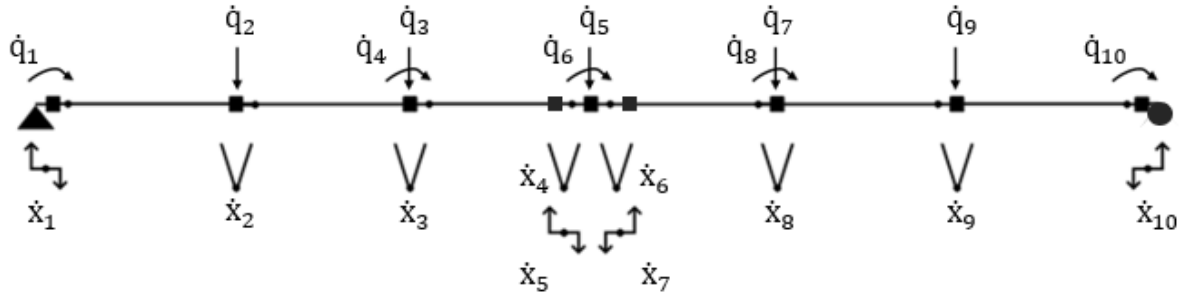

Figure 3. 7: Independent nodal velocities and member deformation rates

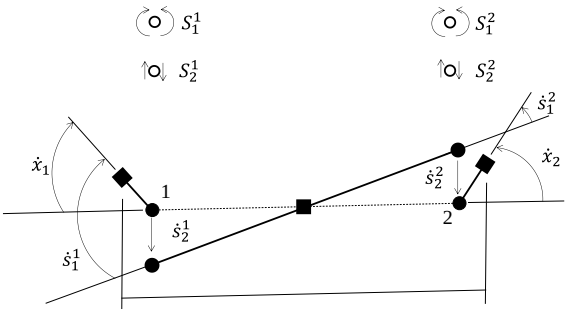

(a)

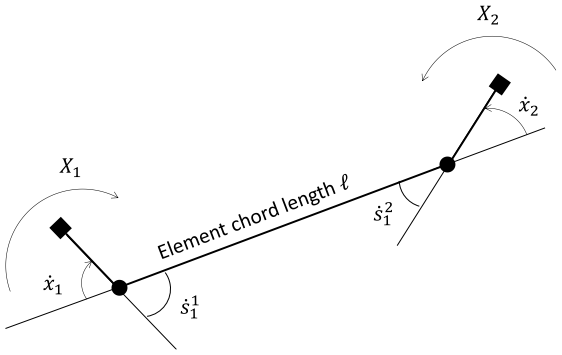

(b)

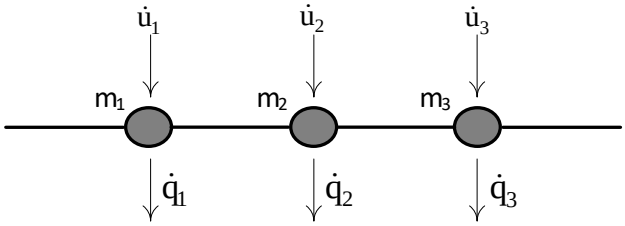

(c)

Figure 3. 8: Stress-resultants, strain-resultant rates, chord deformation rates, and independent chord forces: (a) Planar element allowing plastic-interaction of the bending moment and the shear force. (b) Planar element allowing plastic bending moment. (c) centroidal-velocities in a system of lumped mass

Let the structure be subjected to n discrete time-dependent loads λ_ℓ $(\ell = 1, 2, \ldots\ldots, n)$, applied at nodes. By employing the principle of D' Alembert, during every instant of the accelerated motion of a structure, the loads applied and the corresponding inertial forces $\mu_k (k = 1, 2, \ldots\ldots, \gamma)$, are in the state of equilibrium with the independent member forces X_h $(h = 1, 2, \ldots\ldots, 2N)$. Corresponding to the independent nodal

displacements, the nodal forces of constraint $Q_j(j = 1, 2, \ldots\ldots, \beta)$ are applied. For satisfaction of the dynamic equilibrium, it is necessary that the constraints Q_j must vanish, giving the nodal kinetics description for the assembly of all elements:

$$\mathbf{Q} = \mathbf{0} = [\mathbf{A}^T \quad \mathbf{A}_d^T \quad \mathbf{A}_0^T] \begin{bmatrix} \mathbf{X} \\ -\boldsymbol{\mu} \\ -\boldsymbol{\lambda} \end{bmatrix} \tag{3.32}$$

where the transposed (T) coefficient matrix remains constant by virtue of small displacements. It may be observed that (3.31) and (3.32) satisfy the adjoint relationship of kinetic-kinematic duality.

The independent relations (3.31) and (3.32) have no cause-effect relationship between the kinetic and kinematic variables. Nevertheless, the relation

$$\boldsymbol{\mu} = -\boldsymbol{m}\,\ddot{\boldsymbol{u}} \tag{3.33}$$

implicitly links the inertia forces $\mu_k(k = 1, 2, \ldots\ldots, \gamma)$, located at the mass centroid, with the corresponding centroidal accelerations $\ddot{u}_k(k = 1, 2, \ldots\ldots, \gamma)$ of the actual motion of the system. In this inertial law, the diagonal mass matrix $m_k(k = 1, 2, \ldots\ldots, \gamma)$ constitutes the mass or moment of inertia related to the corresponding centroidal accelerations.

3.2.2 Material Model

The current investigation employs a rectangular yield criteria representing the relation of the bending moment, and the transverse shear force. An insight into this simple yield criterion [75] can be gained by separating the plasticity relation at any critical section i into the three constituent relation rules:

The yield criteria rule:

$$\begin{bmatrix} \boldsymbol{y}_*^{+1} \\ \boldsymbol{y}_*^{-1} \\ \boldsymbol{y}_*^{+2} \\ \boldsymbol{y}_*^{-2} \end{bmatrix} = \begin{bmatrix} \boldsymbol{X}_*^{+1} \\ \boldsymbol{X}_*^{-1} \\ \boldsymbol{X}_*^{+2} \\ \boldsymbol{X}_*^{-2} \end{bmatrix} - \begin{bmatrix} +\mathbf{1} & \mathbf{0} \\ -\mathbf{1} & \mathbf{0} \\ \mathbf{0} & +\mathbf{1} \\ \mathbf{0} & -\mathbf{1} \end{bmatrix} \begin{bmatrix} \boldsymbol{M} = \boldsymbol{S}_1 \\ \boldsymbol{V} = \boldsymbol{S}_2 \end{bmatrix}; \qquad \begin{bmatrix} \boldsymbol{y}_*^{+1} \\ \boldsymbol{y}_*^{-1} \\ \boldsymbol{y}_*^{+2} \\ \boldsymbol{y}_*^{-2} \end{bmatrix} \geq \mathbf{0} \tag{3.34}$$

$$\boldsymbol{y}_* = \boldsymbol{X}_* - \boldsymbol{N}^{\boldsymbol{T}}\boldsymbol{S} \qquad\qquad \boldsymbol{y}_* \geq \mathbf{0}$$

The Normal Flow Rule:

$$\begin{bmatrix}\dot{s}_1=\dot{\theta}\\ \dot{s}_2=\dot{\gamma}\end{bmatrix} = \begin{bmatrix}+1 & -1 & 0 & 0\\ 0 & 0 & +1 & -1\end{bmatrix}\begin{bmatrix}\dot{x}_*^{+1}\\ \dot{x}_*^{-1}\\ \dot{x}_*^{+2}\\ \dot{x}_*^{-2}\end{bmatrix};\qquad \begin{bmatrix}\dot{x}_*^{+1}\\ \dot{x}_*^{-1}\\ \dot{x}_*^{+2}\\ \dot{x}_*^{-2}\end{bmatrix}\geq 0 \tag{3.35}$$

$$\dot{s}=N\dot{x}_* \qquad\qquad \dot{x}_*\geq 0$$

The Association Rule:

$$\begin{bmatrix}y_*^{+1}\\ y_*^{-1}\\ y_*^{+2}\\ y_*^{-2}\end{bmatrix}\begin{bmatrix}\dot{x}_*^{+1}\\ \dot{x}_*^{-1}\\ \dot{x}_*^{+2}\\ \dot{x}_*^{-2}\end{bmatrix}=0 \tag{3.36}$$

$$y_*^T\dot{x}_*=0$$

Interaction between the bending moment S_1, and shear force S_2 at any critical section is characterized by the yield criterion shown in Fig. 3.9. Evidently, the rectangular shape surface is bounded by X_*^{+1}, X_*^{+2}, being the plastic-moment capacity M_p, and plastic-shear force capacity V_p, for the positive bending, and the shear, and by X_*^{-1}, X_*^{-2}, the capacities corresponding for the negative bending, and shear. Also illustrated in figure below are four plastic-potential elements; y_*^{+1}, y_*^{+2}, y_*^{-1}, y_*^{-2}, vanishing any one of these potential indicate commencement of plastic deformation. The deformation rate of the plastic rotation $\dot{s}_1$, and the shear deformation rate $\dot{s}_2$ can be superimposed on the S_1 and S_2 axes. For example: if the potential $y_*^{-2}=0$, then the normal flow criteria rule (3.35), and association criteria rule (3.36), suggest $\dot{s}_2=(-1)\dot{x}_*^{-2}, \dot{x}_*^{-2}\geq 0$, as the upcoming increment of plastic-deformation, that have the direction along the outward-pointing normal to the corresponding yield surface at the point of intiation. At the vertex of the rectang yield locus, where the potentials $y_*^{+1}=0$, $y_*^{-2}=0$, the next increment of the deformation could lie in the cone defined by the normal to the locus on either side $\dot{s}_1=(+1)\dot{x}_*^{+1}$, $\dot{x}_*^{+1}\geq 0$, and $\dot{s}_2=(-1)\dot{x}_*^{-2}$, $\dot{x}_*^{-2}\geq 0$.

Eventually, it is very important to mention that the total transverse shear slide is bounded to some portion

of the beam depth [25].

It is of interest to develop a governing mathematical system that couples the constitutive relations, (3.34) to (3.36), with the kinetic and the kinematic relations, (3.31) to (3.33). Fig. 3.8(b) clearly illustrates that the independent member forces **X** and the independent member deformation rates $\dot{\mathbf{x}}$ can be defined by the respective stress-resultants **S** and the strain resultant rates $\dot{\mathbf{s}}$. These can be collected for all the constituent finite elements:

$$\dot{\mathbf{x}} = \mathbf{T}\dot{\mathbf{s}} \tag{3.37}$$

$$\mathbf{S} = \mathbf{T}^T\mathbf{X} \tag{3.38}$$

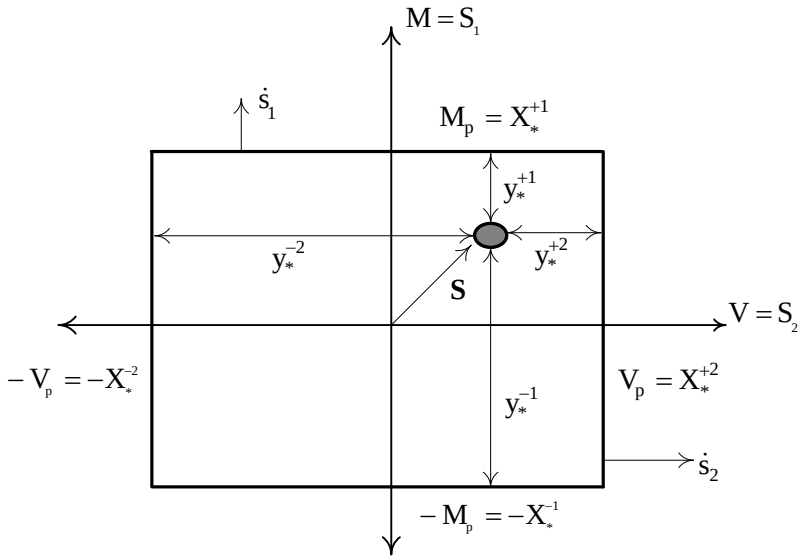

Figure 3. 9: Bending-shear interaction

3.2.3 The Mathematical Formulation

The vectorial relations (3.31) to (3.33), together with the triad of complementarity conditions (3.34) to (3.36), can be combined into a set of differential equations having second-order derivaties with respect to time. Nevertheless, this set is made more complex by the complementarity conditions. As no mathematical system is known to this kind of mathematical problem, adopting a numerical solution appears reasonable.

Therefore, a time depending scheme is incorporated in order to allow the solution procedure to be advanced from a time station t_n to $t_{n+1} = t_n + \Delta t$, where subscript n is an integer defining consective discrete time stations and Δt is the intervening increments of time. Then, the centroidal velocities and corresponding accelerations can be expressed in the time-integration scheme of Newmark:

$$\ddot{\mathbf{u}}_{n+1} = b_0(\dot{\mathbf{u}}_{n+1} - \dot{\mathbf{u}}_n) - b_1\ddot{\mathbf{u}}_n \tag{3.39}$$

and

$$\dot{\mathbf{u}}_{n+1} = \mathbf{u}_n + b_2\dot{\mathbf{u}}_n + b_3\ddot{\mathbf{u}}_n + b_4\ddot{\mathbf{u}}_{n+1} \tag{3.40}$$

in which integration constants are

$$b_0 = \frac{1}{\bar{\gamma}\Delta t}, \tag{3.41}$$

$$b_1 = \frac{1-\bar{\gamma}}{\bar{\gamma}}, \tag{3.42}$$

$$b_2 = \Delta t, \tag{3.43}$$

$$b_3 = (0.5 - \bar{\alpha})\Delta t, \tag{3.44}$$

$$b_4 = \bar{\alpha}\Delta t^2 \tag{3.45}$$

It is found after thorough investigations that suitable results are obtained for rigid-plastic dynamics if $\bar{\alpha} = 0.25$ and $\bar{\gamma} = 0.5$.

Collecting together (3.31), (3.32), (3.33), and (3.34) to (3.36), (3.37), and (3.38), at time $t = t_{n+1}$, and coupling with the Newmark's scheme (3.39) to (3.45) the governing system becomes:

$$\begin{bmatrix} -b_0\mathbf{M}_q & \mathbf{0} & -\mathbf{A}^{\mathrm{T}} \\ \mathbf{0} & \mathbf{0} & \mathbf{N}^T\mathbf{T}^T \\ -\mathbf{A} & \mathbf{TN} & \underline{\mathbf{0}} \end{bmatrix} \begin{bmatrix} \dot{\mathbf{q}}_{\mathrm{n+1}} \\ \dot{\mathbf{x}}_{*n+1} \\ \mathbf{X}_{n+1} \end{bmatrix} + \begin{bmatrix} \mathbf{0} \\ \mathbf{y}_{*n+1} \\ \mathbf{0} \end{bmatrix} = \begin{bmatrix} -\mathbf{Y}_{n+1} \\ \mathbf{X}_{*\mathrm{n+1}} \\ \mathbf{0} \end{bmatrix} \tag{3.46}$$

$$\mathbf{y}_{*n+1} \geq \mathbf{0} \tag{3.47}$$

$$\mathbf{y}_{*n+1}^{T}\dot{\mathbf{x}}_{*n+1} = 0 \tag{3.48}$$

$$\dot{\mathbf{x}}_{*n+1} \geq \mathbf{0} \tag{3.49}$$

with variables $\dot{\mathbf{q}}_{n+1}, \mathbf{X}_{n+1}$ unrestricted

The right-hand side sub-vector $\mathbf{Y}_{n+1}$ of (3.46) is given by:

$$\mathbf{Y}_{n+1} = \mathbf{A}_0^T\boldsymbol{\lambda}_n + \mathbf{M}_q(b_0\dot{\mathbf{q}}_n + b_1\ddot{\mathbf{q}}_n) \tag{3.50}$$

and the mass matrix $\mathbf{M_q}$ is given by the relation:

$$\mathbf{M}_q = \mathbf{A}_d^T\mathbf{m}\mathbf{A}_d \tag{3.51}$$

The approximating governing system (3.46) to (3.49) has a computational structure of a linear complementarity problem (LCP). It may be noticed that the variables i.e. $[\dot{\mathbf{x}}_*, \mathbf{y}_*]$, are restrained into the complementary pairs, whereas the leading sub-matrix related to variables[$\dot{\mathbf{q}}$, $\mathbf{X}$] is negative semi-definite. In this work, the governing system is solved efficiently by Lemke algorithm due to its simplicity and robustness.

3.2.4 Initiation of LCP formulation

The incremental numerical process shown in (3.46) to (3.49), representing the evolutive sequence of the dynamic response, is not self-starting. Therefore, it is necessary to establish a subroutine for calculating the relevant accelerations at a certain instant of time. These accelerations are of particular relevance at the commencement of the motion and at the deactivation of previously active section. At similar instant, the vector of plastic-multiplier rates $\dot{\mathbf{x}}$, can be separated into Y yielded plastic hinges and R rigid plastic hinges. So, these subsets of the multiplier rates $\dot{\mathbf{x}}$ can be expressed as:

$$Y = \{(\dot{\mathbf{x}}_{*y}, \mathbf{y}_{*y})|\dot{\mathbf{x}}_{*y} > \mathbf{0}, \mathbf{y}_{*y} = \mathbf{0}\} \tag{3.52}$$

$$R = \{(\dot{\mathbf{x}}_{*r}, \mathbf{y}_{*r})|\dot{\mathbf{x}}_{*r} = \mathbf{0}, \mathbf{y}_{*r} \geq \mathbf{0}\} \tag{3.53}$$

The time-derivative of the discrete law (3.34) to (3.36) is formulated as:

$$\begin{bmatrix} \mathbf{0} & \mathbf{0} & \boldsymbol{N}_{\boldsymbol{y}}^{\boldsymbol{T}} \\ \mathbf{0} & \mathbf{0} & \boldsymbol{N}_{\boldsymbol{r}}^{\boldsymbol{T}} \\ \boldsymbol{N}_{\boldsymbol{y}} & \boldsymbol{N}_{\boldsymbol{r}} & \mathbf{0} \end{bmatrix} \begin{bmatrix} \ddot{\boldsymbol{x}}_{*\boldsymbol{y}} \\ \ddot{\boldsymbol{x}}_{*\boldsymbol{r}} \\ \boldsymbol{S} \end{bmatrix} + \begin{bmatrix} \mathbf{0} \\ \boldsymbol{y}_{*\boldsymbol{r}} \\ \mathbf{0} \end{bmatrix} = \begin{bmatrix} \boldsymbol{X}_{*\boldsymbol{y}} \\ \boldsymbol{X}_{*\boldsymbol{r}} \\ \ddot{\boldsymbol{s}} \end{bmatrix} \tag{3.54}$$

$$\mathbf{y}_{*r} \geq \mathbf{0} \tag{3.55}$$

$$\mathbf{y}_{*r}^{T} \ddot{\mathbf{x}}_{*r} = 0 \tag{3.56}$$

$$\ddot{\mathbf{x}}_{*r} \geq \mathbf{0} \tag{3.57}$$

$\ddot{\mathbf{x}}_{*y}$ *unrestricted.* (3.58)

It is to Tamuzh [90] that the relation (3.54) to (3.58) is due. The comparison of these relations with the equations of nonholonomic laws (3.34) to (3.36), it is clear that the former fails completely in representing the latter in two important situations. Firstly, (3.58) has no restriction on $\dot{\mathbf{x}}_{*y}$ to become non-positive, which is certainly opposing (3.35). Secondly, the above relations has no restriction on $\dot{\mathbf{x}}_{*r}$**,** related with the yield conditions, which have activated during the finite time interval, to decrease.

The following three criteria can be employed to identify the interval end:

a) The time at which the relevant functions are not differentiable any more, or

b) Upon the unstressing of any yielded nodes in set y, or

c) Upon the activation of any yielded node in set of r.

At that determined instant, the sets *Y* and *R* must be separated, and then the modified plasticity-relations can be used accurately for a contiguous finite time interval.

It has already been said that the LCP system (3.46) to (3.49) is not self-starting. To initiate this system, regardless of the prescribed displacements $\mathbf{q}_0$ and velocities $\dot{\mathbf{q}}_0$, it is not easy to infer the initial accelerations $\ddot{\mathbf{q}}_0$, and the independent member forces $\mathbf{X}_0$. Differentiating with respect to time the kinematic relation

(3.31), and together with (3.54) to (3.58), Sahlit [7] re-established the governing system in terms of accelerations:

$$\begin{bmatrix} -\mathbf{M}_q & \mathbf{0} & \mathbf{0} & -\mathbf{A}^{\mathrm{T}} \\ \mathbf{0} & \mathbf{0} & \mathbf{0} & \mathbf{N}_{\mathrm{y}}^{\mathrm{T}}\mathbf{T}^{\mathrm{T}} \\ \mathbf{0} & \mathbf{0} & \mathbf{0} & \mathbf{N}_{\mathrm{r}}^{\mathrm{T}}\mathbf{T}^{\mathrm{T}} \\ -\mathbf{A} & \mathbf{T}\mathbf{N}_y & \mathbf{T}\mathbf{N}_r & \underline{\mathbf{0}} \end{bmatrix} \begin{bmatrix} \ddot{\mathbf{q}} \\ \ddot{\mathbf{x}}_{*\mathrm{y}} \\ \ddot{\mathbf{x}}_{*r} \\ \mathbf{X} \end{bmatrix} + \begin{bmatrix} \mathbf{0} \\ \mathbf{0} \\ \mathbf{y}_* \\ \mathbf{0} \end{bmatrix} = \begin{bmatrix} -\mathbf{A}_0^T\lambda_0 \\ \mathbf{X}_{*\mathrm{y}} \\ \mathbf{X}_{*r} \\ \mathbf{0} \end{bmatrix}$$

(3.59)

$$\mathbf{y}_{*r} \geq \mathbf{0} \tag{3.60}$$

$$\mathbf{y}_{*r}^T\ddot{\mathbf{x}}_{*r} = 0 \tag{3.61}$$

$$\ddot{\mathbf{x}}_{*r} \geq \mathbf{0} \tag{3.62}$$

with variables $\ddot{\mathbf{q}}, \ddot{\mathbf{x}}_{*\mathrm{y}}, \mathbf{X}$ unrestricted

If the structure is coerced into motion by an initial impulse or by an initial velocity field, the vector of initial loading is null $\boldsymbol{\lambda}_0 = \mathbf{0}$ at the start of motion. Accordingly, the set of *Y* active plastic hinges $\left(\dot{\mathbf{x}}_{*\boldsymbol{y}} > \mathbf{0}\right)$ are easily deductible.

3.2.5 Plastic Unstressing

The LCP formulation (3.46) to (3.49) only allows the plastic unstressing at the commencement of each time interval but not within the increment Δt. This loss of accuracy over a time step leads to spurious oscillations in the stress resultants. Therefore, it is imperative to include a subroutine that calculates the unstressing time instant $t_{n+\varepsilon}$ within the interval Δt [7]. Thus, the evolutive sequence of dynamic response is terminated temporarily at the instant when unstressing is detected. Subsequently, the velocity profile and the partition active *Y* and in-active *R* critical sections are adjusted. Once the relevant structural variables at $t_{n+\varepsilon}$ are determined, then, the evolutive process of the LCP system (3.46) to (3.49) is re-initiated with $t_{n+\varepsilon}$ as the starting-time. The iterative procedure for the whole dynamic response is shown in Fig. 3.10.

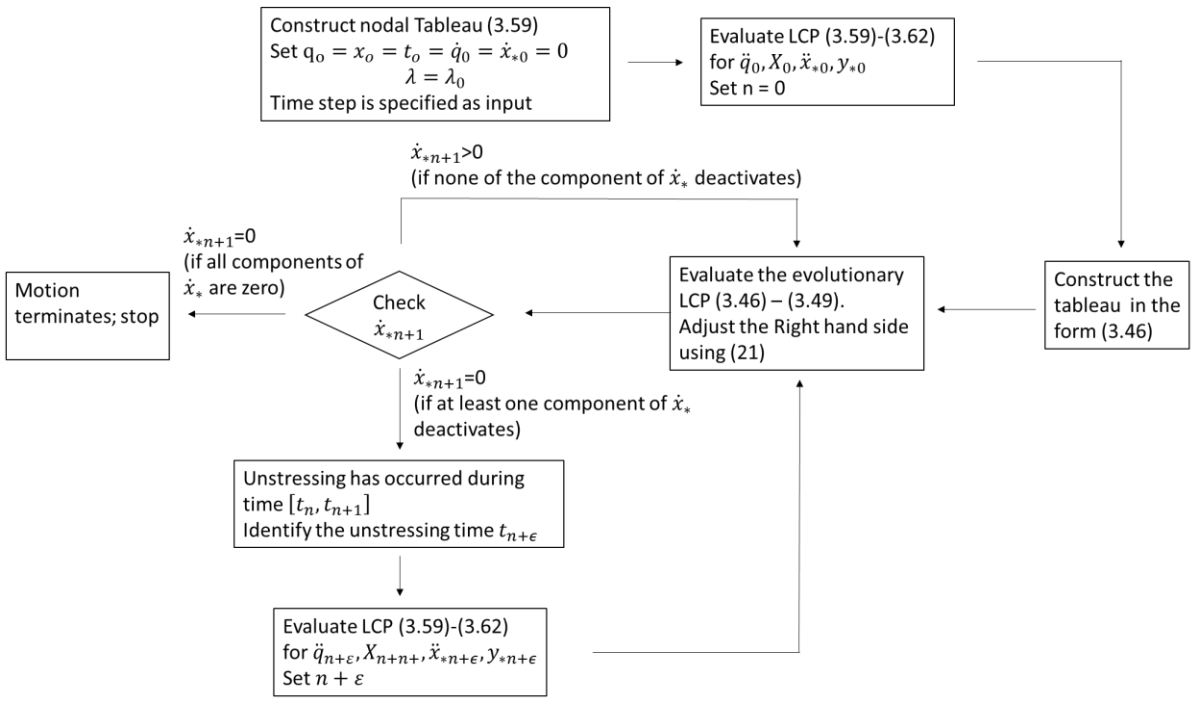

Figure 3. 10: Flow path of bending-shear LCP model

3.3 Existence and uniqueness of optimal solutions

A fundamental problem in the dynamic analysis of structural systems is determining the acceleration field at some instant of time when the velocity field and the applied loads are known at that instant. The governing system (3.59)-(3.62) in terms of accelerations, separated into Y yielded plastic hinges and r rigid plastic hinges, is examined here to address the uniqueness of acceleration.

In both (3.46) and (3.49), the independent member forces X are not guaranteed to be uniquely defined due to the null matrice shown with the underbar. Also, a more detailed discussion is necessary in order to establish the uniqueness in the acceleration field since the mass or inertia matrix $\mathbf{M}_{\mathrm{q}}\left(\mathbf{A}_d^T\mathbf{m}\mathbf{A}_d\right)$ is positive semidefinite. It has been defined in Subsection 3.2.1 that **m** is the mass matrix that alludes to the accelerations of the inertia coordinates or the dynamic degrees of freedom **u**, whereas $\mathbf{M}_{\mathrm{q}}$ is the mass matrix that refers to the accelerations of the generalized or Lagrange coordinates **q**. With each nodal mass, the γ accelerations $\ddot{\mathbf{u}}$ of the masses may form a subset of the β independent nodal acceleration $\ddot{\mathbf{q}}$, and $\gamma \leq \beta$ correspondingly. The vector of β generalized accelerations $\ddot{\mathbf{q}}$ can then be partitioned into a master set

γ −vector $\ddot{\mathbf{q}}_m = \ddot{\mathbf{u}}$ and a slave set $(\beta - \gamma)$ −vector $\ddot{\mathbf{q}}_s$. The accelerations $\ddot{\mathbf{u}}$ need not form a strict subset of the accelerations $\ddot{\mathbf{q}}$ being merely linearly dependent on some of them. By partitioning vector $\ddot{\mathbf{q}}$ into a master set $\ddot{\mathbf{q}}_m$ and a slave set $\ddot{\mathbf{q}}_s$, the accelerations $\ddot{\mathbf{u}}$ becomes:

$$\ddot{\mathbf{u}} = [\mathbf{A}_{\mathrm{dm}} \quad \mathbf{0}] \begin{bmatrix} \ddot{\mathbf{q}}_m \\ \ddot{\mathbf{q}}_s \end{bmatrix} \tag{3.63}$$

where $\mathbf{A}_{\mathrm{dm}}$is the positive definite square matrix of order $(\gamma \times \gamma)$ which need not be equal to the identity matrix $\mathbf{I}_{\gamma}$. Because of the partition (33) attained in the matrix $\mathbf{A}_{\mathrm{d}}$, the inertia matrix $\mathbf{M}_{\mathrm{q}}$ maybe recast as:

$$\mathbf{M}_{\mathrm{q}} = \begin{bmatrix} \mathbf{A}_{\mathrm{dm}}^{\mathrm{T}} \\ \mathbf{0}^{\mathrm{T}} \end{bmatrix} \mathbf{m} [\mathbf{A}_{\mathrm{dm}} \quad \mathbf{0}] = \begin{bmatrix} \mathbf{A}_{\mathrm{dm}}^{\mathrm{T}} \mathbf{m} \mathbf{A}_{\mathrm{dm}} & \mathbf{0} \\ \mathbf{0} & \mathbf{0} \end{bmatrix} \tag{3.64}$$

Clearly, the mass submatrix $\mathbf{A}_{\mathrm{dm}}^{\mathrm{T}} \mathbf{m} \mathbf{A}_{\mathrm{dm}}$,corresponding to the master acceleration $\ddot{\mathbf{q}}_m$, is positive definite because $\mathbf{m}$ and $\mathbf{A}_{\mathrm{dm}}$ are each square matrices of full rank γ. So, it can be deduced that the acceleration components $\ddot{\mathbf{q}}_m$ are uniquely defined. In contrast, the uniqueness of the slave acceleration components $\ddot{\mathbf{q}}_s$, cannot be guaranteed since all the mass influence coefficients associated with these components are zero.

If $\gamma = \beta$, the slave set is null, and the entire acceleration field must be uniquely defined. The implication of a unique acceleration field is that a unique dynamic response occurs in terms of the velocities for the discrete model of structure. The uniqueness of the acceleration and velocity fields agrees with Tamuzh's principle [90] and Martin's theorem[91], respectively.

Non-uniqueness in the spread of the independent member forces $\mathbf{X}$ is only possible in hyperstatic structural systems. It may occur in parts of the structure that are not moving and at critical sections in which plastic flow occurs when the dimension of the corresponding generalized stress vector exceeds the number of activated yield planes. For isostatic structural systems, matrix $\mathbf{A}$ in (3.32) is the square matrix of full rank β. Because the inertia forces $\boldsymbol{\mu}$ are uniquely defined in terms of (3.33) and (3.63), and for a given loading $\boldsymbol{\lambda}$, the equation (3.32) may be solved uniquely for the independent member forces $\mathbf{X}$.

3.4 Peak Impact Force Model

Due to the limitation of the LCP model for producing the peak impact force of RC beams uniquely under dropweight impact loading, a regression-based model of peak impact force adopting the Gene Expression Programming (GEP) programming is proposed. The maximum impacted force can be employed to derive the shear force and the bending moment diagrams, thus providing a capability to examine the dynamic behavior of impacted RC beams, and simplifying the design approach.

3.4.1 Parameters affecting the impacted force on RC beam from a drop-weight

To establish an empirical model describing the impacted force on RC beam from a dropweight over it, it is necessary to set out the affecting parameters. It may be inferred from the literature [19,62,92–94] that the impacted force on the RC beam greatly depended on various parameters, such as concrete strength in compression, longitudinal reinforcement, yield strength of longitudinal reinforcement, vertical shear reinforcement, mass, and velocity of the drop-weight, and different geometrical properties of RC beam. The influence of these parameters has been shown by extensive experimental studies of Hughes & Mahmoud [95], Louw et al. [96], May et al. [97], Zhan et al. [98], Goldston et al. [22]. From this precedent, Zhan et al. [98], May et al. [97], and Louw et al. [96] identify that the concrete strength in compression shows an increasing positive relation with the impact force from a drop-weight. A similar increasing trend has been observed by Adhikary et al. [92] through numerical simulation. This trend follows intuition since as the compressive strength is increased, the beam capacity and the stiffness are increased, thereby resulting in an increased peak impact force because stiffer elements attract more force. In the same context, increasing the width or depth of the beam will attract more impact force than increasing the length of the beam.

Longitudinal tensile reinforcement is another important parameter affecting the peak impact force on the RC beam. In this instance, Goldston et al. [22], Hughes & Mahmoud [95], Adhikary et al [19], and Zhan et al. [98] have observed the influence of longitudinal tensile reinforcement on the impact force because as the area of tensile reinforcement increases, both the peak ultimate bending moment strength as well as there is corresponding increase in the ultimate load-carrying resistance. Zhan et al. [98], and Fujikake et al. [59]

also observed that the stiffness of the RC beam increases with the increase in the longitudinal tensile reinforcement which tends to rise the peak impact force. The yield strength of the longitudinal reinforcement also contributes to the impact force as it increases the brittleness of the RC beam. Similar behavior has been produced by Adhikary et al. [92] with the help of numerical study. Adhikary et al. [19], and Bhatti et al. [62] have shown the increasing trend of peak impact force with the increasing vertical shear reinforcement. This trend is due to the reason that transverse reinforcement provides extra confinement to the concrete in core, thereby increasing lateral restraint strength against buckling of the longitudinal bars. Input kinetic energy ($K.E = 1/2*M*V^2$) has a vital role in the impact analysis of RC beam under dropweight. With increasing input kinetic energy, the increase in the peak impact load has been reported by various researchers [62,93,94].

3.4.2 Experimental database

In a way to accurately predict the peak impact force on RC beam from a dropweight, a collection of 126 experimental tests from previous studies is compiled into a database [18,59,62,64,72,98–102]. Within the database, all beams are of rectangular cross-sections subjected to impact load at the midspan having either flat or spherical contact surface. For GEP analysis, only a randomly selected portion of 84 experiments is used to develop the model. The remaining 42 samples are employed for the model validation.

3.4.2.1 Distribution of key influence parameters

The important influence parameters of RC simply supported beam is examined herein. The influence parameters, such as the impact velocity, impact mass, geometrical size of the beam, concrete strength in compression, longitudinal reinforcement, and shear reinforcements, are given in Table 3.1. It is clear from the table that the velocity of the projectile ranges from 1-16 m/sec, and the impact mass M is in the range of 33-1700 kg. Further, the net span of simply supported RC beams ranges from 1000 to 5000 mm, the width and height of RC beams lie within the range limit 100-300 mm and 120-500 mm, respectively, and the longitudinal tensile and shear reinforcement ratio falls in the range 0.29-3.1% and 0-1.4%, respectively.

Table 3. 1: Distribution of key influence parameters

Parameters	Ranges
Velocity	1-16 (m/s)
Mass	33-1700 (kg)
Compressive strength	20-42 (MPa)
Net span length	1000-5000 (mm)
Beam width	100-300 (mm)
Beam height	120-500 (mm)
Tensile reinforcement ratio	0.29-3.1 (%)
Shear reinforcement ratio	0-1.4 (%)

3.4.3 Fundamentals of gene programming

Gene expression programming (GEP) is a progressive genetic algorithm (GA), that outputs mathematical models from the supplied data and processes the data in domain-independent mode [103–105]. GEP is different from the genetic algorithm Gas, and the genetic programming GP in terms of the representation of chromosomes. The chromosomes are strings of constant length in GAs, but these entities in GPs, have different shapes and sizes and also they are non-linear. GEP, on the other hand, encapsulates both the linear entity of constant length, as well as ramified structure of different sizes and shapes.

As with other evolutionary algorithms, for executing the evolutionary process, several trials are conducted by iteratively altering the chromosomes number, the amount of genes, head size, and linking functions. Thus, GEP optimizes solutions by selecting the best candidates among the supplied initial population based on their fitness. Notably, a complicated function can stem from increasing the quantity of genes and chromosomes number, but the function can precisely fit the results. Hence, there exists a tradeoff between the attainment of a simplified mathematical model, by controlling the number of genes and chromosomes, and the achievement of the desired level of accuracy.

A basic step in the GEP algorithm is the convergence to the global optimal solution. It can sometimes happen that the algorithm is not able to select an optimal solution among several competing candidate solutions. In this state, the algorithm can lead to an indefinite sequence of steps resulting in either a non-

terminating program or yielding an illogical expression. This predicament can be resolved by either varying the number of genes and chromosomes or adjusting the linking function. In this context, the contribution of an analyst decides if and what solution proposed by GEP should be extended for statistical analysis [106]. The benefits of GEP have attracted extensive applications in the field of structural engineering over the last decade. Several authors have elegantly employed GEP to develop models for estimating the capacity of various structural components. Recently, GEP has been successfully used for predicting the behavior of RC beam from a drop-weight, especially where the code formulations are not available.

The different steps of GEP optimization are illustrated in Fig. 3.11. The optimization process starts with the selection of control parameters, such as the function set, the ending set, the fitness function, the controlling parameters, and the stopping condition. Before the execution of the evolutionary algorithm, the fitness function is identified, and then the problem is coded to produce a random string of the initial population, or in Genetic Programming parlance 'Chromosomes'. These strings translate into an expression tree corresponding to a mathematical formulation. The outcomes from the mathematical formulation are checked with the actual values of the fitness scores of each chromosome. In appreciating results scenarios, the algorithms are put to stop. In case, if the error level is not according to desire, some of the chromosomes are again selected using the roulette-wheel sampling and then proceed to obtain new generations. When we get the error level of our choice, decoding of chromosomes is done for the best solutions to the problem [107,108].

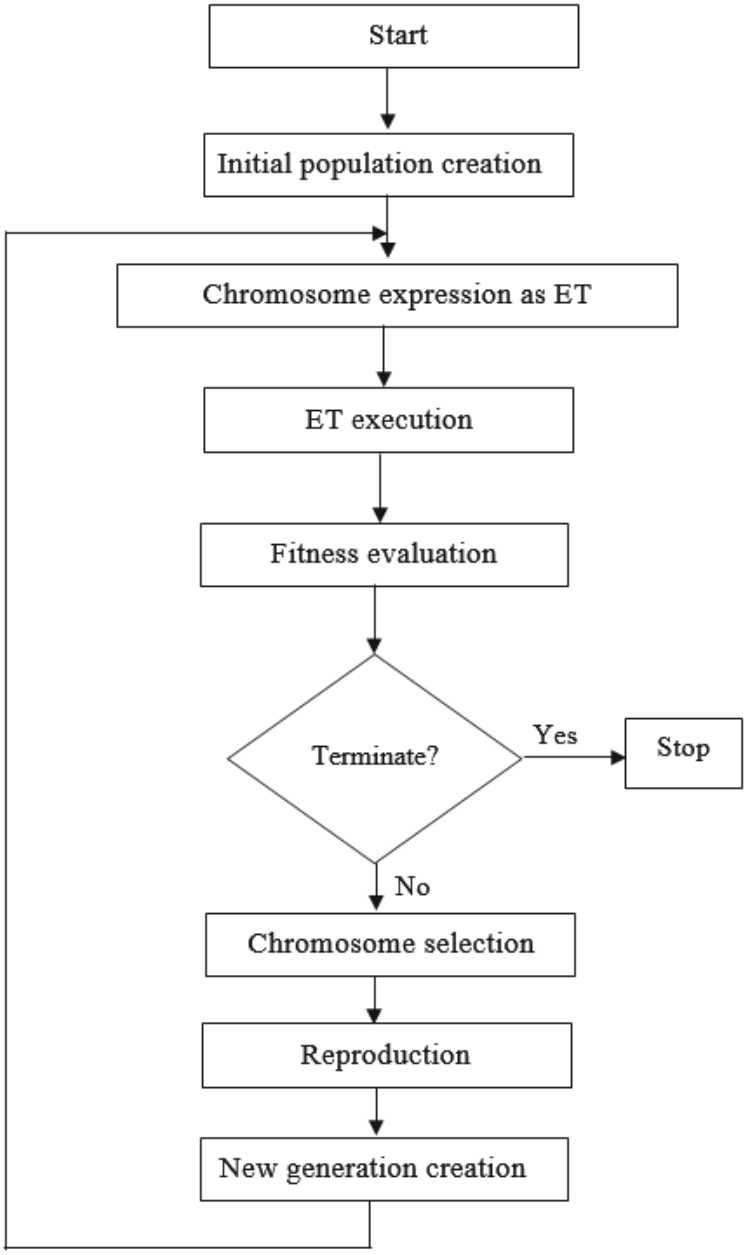

Figure 3. 11: Flow chart for the GEP

3.4.4 Proposed GEP model for estimating peak impact force

This work aims to develop a precise model that is capable of predicting the peak impact force on RC beam. This model has been constructed by incorporating mechanical and geometrical properties, reinforcement ratio, and detailing of steel reinforcement in the RC beam were included into the model preparation. More

specifically, beam width, beam depth, concrete compressive capacity, yielding stress capacity of steel reinforcing bars, longitudinal reinforcement area, and transverse reinforcement ratio are identified as important influencing factors on the suggested model. Out of 126 experimental datasets, a randomly selected portion of 84 data beams is for training purposes, and the remaining 42 data beams as a validation set.

An empirical model is produced through GEP evolutionary algorithm for estimating the peak impacted force on the RC beam, given in Eq. (3.65). The expression tree of the proposed model is also given in Fig. 3.12. In addition, the operational and functional details in the developed model are listed in Table 3.2. It is remark that the selection of the parameters influences the model capability of the GEP.

$$F_p = a + b + c\ (kN) \tag{3.65}$$

$$a = \left[\left(\frac{1}{3.07+2V}\right)^{\frac{5}{2}} + \left(\frac{V}{l_n+\frac{A_s f_y}{f_c'}+s-2390.26}\right)\right]^{-1} \tag{3.66}$$

$$b = \left[\left\{\frac{f_c'}{\frac{a}{d}-2.93} + \left(LN(V) \times \left(b - \rho_v f_y + 40.27\right)\right)\right\} - \left(f_c' \times \sqrt{V}\right)\right] \tag{3.67}$$

$$c = \left\{\left((6.83 + f_c') \times V\right) + b + 3h - \frac{a}{d} - \frac{M}{V} - 2s - d - 404.96\right\} \tag{3.68}$$

where b, h, and d are the respective breadth, height, and effective depth of the beam, V, and M are the initial velocity and mass of dropweight respectively, l_n and $\frac{a}{d}$ represents the respective net span and the ratio of shear span to depth of the beam, $A_s f_y$ is the product of area and yield strength of longitudinal reinforcement, LN is the natural log, f_c' is the concrete compressive stresses, $\rho_v f_y$ is the product of shear bars ratio and yield strength of transverse reinforcement, and s is the mid-span deflection.

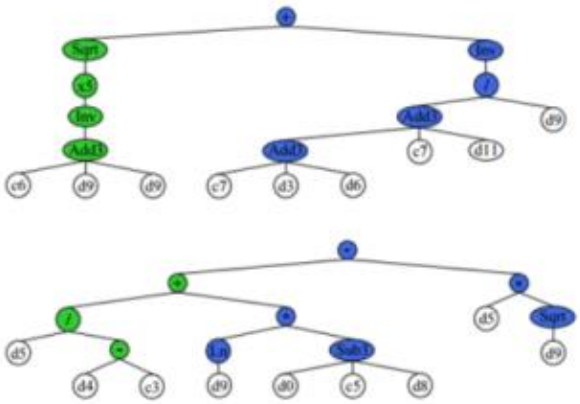

G1C7	-1195.14
G1C6	3.08
G2C3	2.94
G2C5	-40.27
G3C6	-404.96
G3C0	6.84

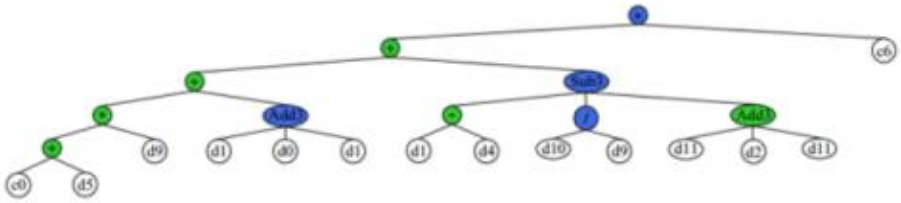

d0 b ***d1*** h ***d2*** d ***d3*** l_n ***d4*** $\frac{a}{d}$ ***d5*** f_c' ***d6*** $\frac{A_s f_y}{f_c'}$ ***d8*** $\rho_v f_{vy}$ ***d9*** V

d10 M ***d11*** s

Figure 3. 12: Gene expression tree for peak impact force

Table 3. 2: Model Construction Parameter

Function set	Ln, +, -, /, *, sqrt, x2,3,4,5
Chromosomes	110
Size of head	11
Link function	Addition
Quantity of genes	3
Rate of Mutation	0.0014
Rate of inversion	0.1
One-point recombination rate	0.0027
Two-point recombination rate	0.0027
Rate of Gene recombination	0.0027
Rate of Gene transposition	0.0027
Constants / gene	10

Lower/Upper bound of constants	-20/20

3.5 Statistical Parameters for Validation

In this section, few statistical parameters are picked to find the accuracy of the proposed models. Predicted to experimental ratio (PER), coefficient of Variation (CoV), coefficient of determination (R^2), and the average absolute error (AAE) to compare the response of RC beam under impact loading by proposed models with the previously proposed in the literature. Based on these statistical parameters, the accuracy and efficiency of the proposed models will be accessed.

3.5.1 Predicted to experimental ratio (PER)

The predicted to experimental ratio is generally used to check, how much accurate and efficient the models are to predict accurately the response of RC beams subjected to dropweight loading. For a model to estimate a good prediction, the net value of the performance factor should be closer to 1. The value of the predicted to experimental ratio will be equal to 1, Mathematically the predicted to experimental ratio is shown in Eq. (3.69)

$$(PER) = \frac{v_{Est}}{v_{Exp}} \tag{3.69}$$

3.5.2 Coefficient of Variation (CoV)

The dispersion of the statistical points in the data sets around the mean is calculated by the coefficient of variation (CoV). It is the ratio between the standard deviation and the mean of the total data set. This factor is usually helpful in calculating the extent of variation between the data series, even if the mean of the data set is different from each other. The range of the variability of data sample in relation to the mean of the population is shown by the coefficient of variation (CoV). Mathematically the coefficient of variation is defined as

$$Coefficient\ of\ Variation\ (CoV) = \frac{Standard\ Deviation}{Mean} \tag{3.70}$$

3.5.3 Coefficient of Determination

Total variation is defined as, the variability among the values of the variable that is dependent i.e. Y and is given by: $= \sum(y - \bar{y})^2$ (3.71)

The expression shown in Eq (3.71) is composed of two parts:

- The one expressed by regression line i.e. $\sum(\hat{y} - \bar{y})^2$
- The one is not to be defined by regression line, i.e. $\sum(y - \hat{y})^2$

$$Total\ Variation = Unexplained\ Variation + Explained\ Variation$$

$$\sum(y - \bar{y})^2 = \sum(y - \hat{y})^2 + \sum(\hat{y} - \bar{y})^2 \quad (3.72)$$

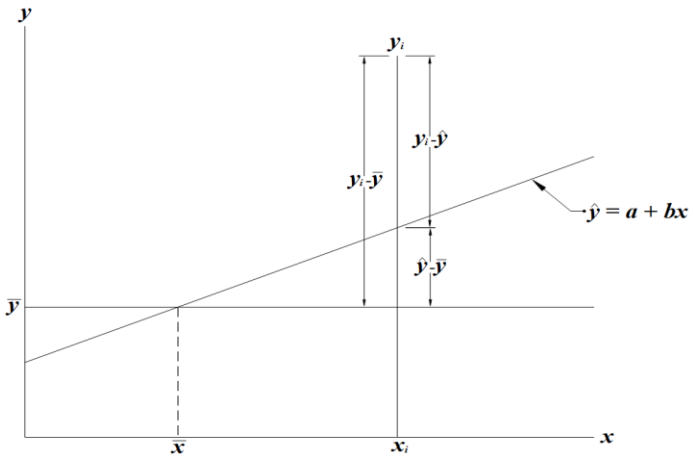

Figure 3. 13: Graphical Representation of Coefficient of Determination

The ratio of the explained variation to the total variation is termed as coefficient of determination and is represented as R^2. Mathematically, the coefficient of determination (R^2) is given by:

$$Coefficient\ of\ Determination = \frac{Explained\ Variation}{Total\ Variation}$$

$$R^2 = \frac{\sum(\hat{y}-\bar{y})^2}{\sum(y-\bar{y})^2} \quad (3.73)$$

$$R^2 = 1 - \frac{\sum(y-\bar{y})^2}{\sum(y-\bar{y})^2} \quad (3.74)$$

Average absolute error (AAE) is also used for validation purposes, which represents the total error between the predicted and experimental results. The AAE is therefore

$$AAE\ (\%) = \frac{1}{n} \times \Sigma \left[\frac{|Experimental\ value - predicted\ value|}{Experimental\ value} \right] \tag{3.75}$$

Yet another statistical evaluation parameter effective in evaluating the accuracy and consistency of the proposed numerical model is the slope of the best fit line (m). For the dataset having the least average absolute error, the slope of the trendline is close to the benchmark value of 1, that is the trendline is on a 45-degree angle. Thus,

$$m = \tan^{-1}\left(\frac{y_2 - y_1}{x_2 - x_1}\right) \tag{3.76}$$

where, x and y represent the abscissa and ordinate values, respective wise.

4 RESULTS & DISCUSSION

4.1 Organization

In this chapter the proposed models i.e. LCP having strain-rate effect, LCP incorporating M-V interaction, and peak impact force model are validated using different statistical tools. The statistical analysis is not only applied to the current model but is also applied to the previously proposed models to estimate the robustness and efficiency of the current models over the previously proposed models. The variation of results is also represented graphically for better understanding.

4.2 Model Validation

Model Validation is an important step after the selection of the model. This step actually confirms the application of the proposed model on the given set of experimental data. In this research study, the model is not only validated with experimental data set but also validate with the previous literature and code provisions.

In most of studies it has been observed that only R^2 is used as statistical tool for the validation of the model. Statistical literature reveals that higher R^2 does not always guarantee that the model will fit the data. It is also observed that a prediction model that does not fit the data points well, cannot give a good estimated result to the underlying engineering questions. Apart from using only one statistical tool for the validation purpose, it is necessary to apply different statistical tools available in the literature, to validate your proposed model. In this research study, the statistical tool selected is discussed in detail in section 3.5. Using those statistical tools, a detailed statistical analysis is performed. The results obtained from the statistical analysis will be discussed in detail for all the cases.

4.3 Viscoplastic LCP Validation

4.3.1 Experimental Database

An extensive experimental database of 143 simply supported RC beams has been constructed from the literature [18,59,109,62,64,72,78,99–102] by employing a consistent set of inclusion criteria. Within the database, all beams are of rectangular cross-sections subjected to impact load at the midspan having either

flat or spherical contact surface. Out of this dataset of 143 RC beams, the specimens failing in bending and bending-shear are included. Therefore, 25 specimens are removed from the data due to shear failure, and the validation of the proposed viscoplastic LCP is carried out with the remaining 118 beams.

4.3.1.1 Distribution of key influence parameters

The important influence parameters of RC simply supported beam is examined herein. The influence parameters, such as the impacted dropweight velocity, and mass, geometric size of beam, concrete compressive capacity, longitudinal reinforcement, and shear reinforcement, are given in Fig. 4.1. It is visible from the figure that the velocity of the projectile ranges from 1-16 m/sec, whereas most of the data lie in 3-8 m/sec regime. Similarly, the impact mass M is in the range of 100-1800 kg, having a large number of tested beams within 300-600 kg. Further, the net span of simply supported RC beams ranges from 1000 to 5000 mm, the width and height of RC beams lie within the range limit 100-300 mm and 150-500 mm, respectively, and the longitudinal tensile and shear reinforcement ratio falls in the range 0.25-3.25% and 0-1.4%, respectively.

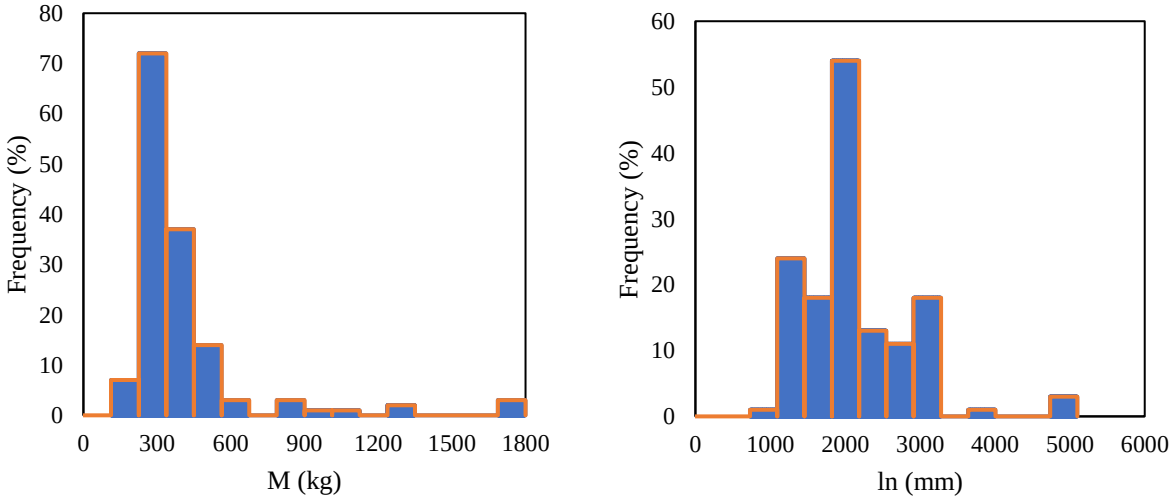

(a) (b)

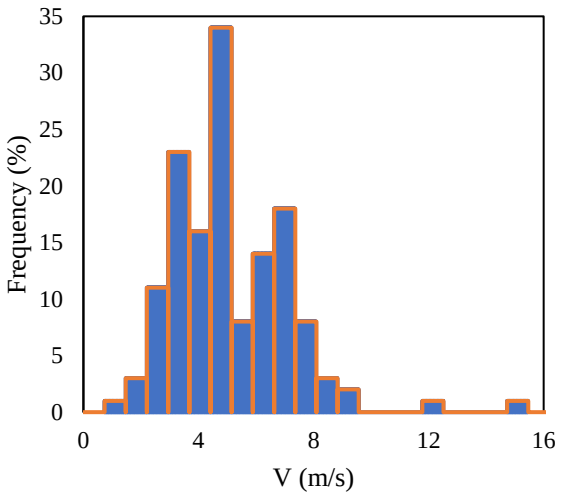
Frequency (%)
0
5
10
15
20
25
30
35
0
4
8
12
16
V (m/s)

(c)

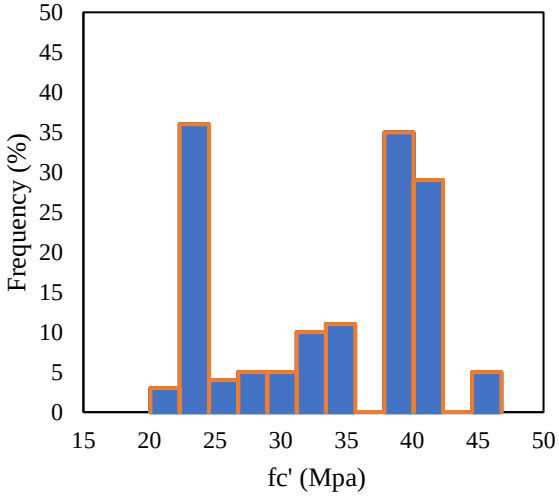
Frequency (%)
0
5
10
15
20
25
30
35
40
45
50
15
20
25
30
35
40
45
50
fc' (Mpa)

(d)

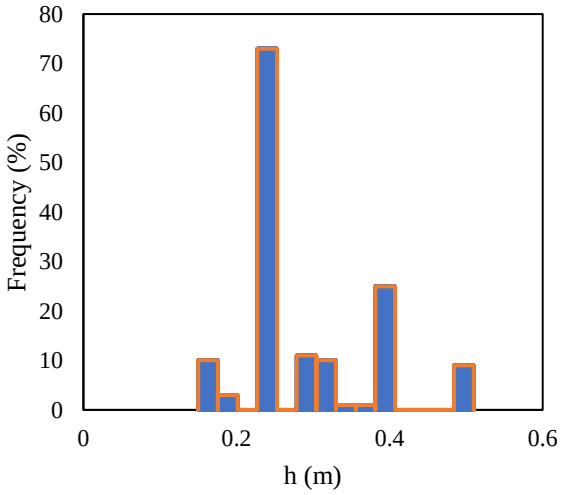
Frequency (%)
0
10
20
30
40
50
60
70
80
0
0.2
0.4
0.6
h (m)

(e)

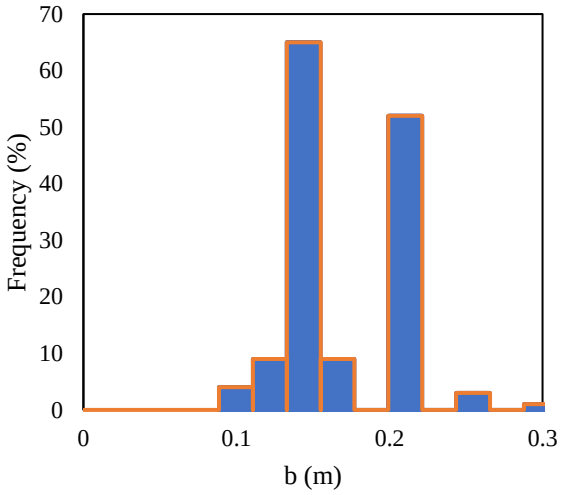
Frequency (%)
0
10
20
30
40
50
60
70
0
0.1
0.2
0.3
b (m)

(f)

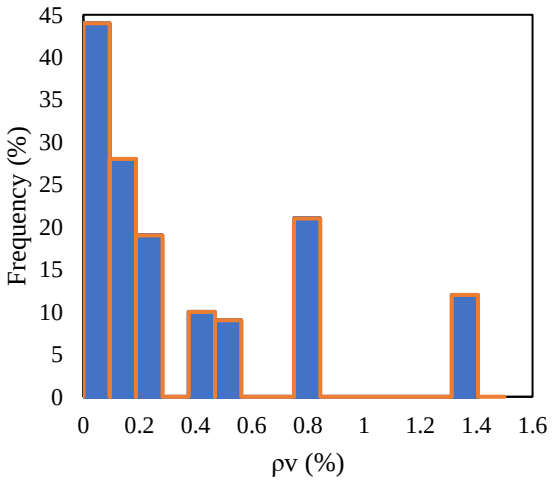
Frequency (%)
0
5
10
15
20
25
30
35
40
45
0
0.2
0.4
0.6
0.8
1
1.2
1.4
1.6
ρv (%)

(g)

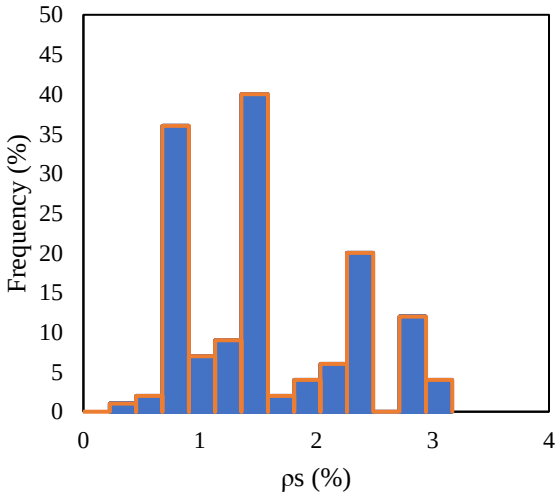
Frequency (%)
0
5
10
15
20
25
30
35
40
45
50
0
1
2
3
4
ρs (%)

(h)

Figure 4. 1: Frequencies of different experimental parameters. (a) Impact Mass. (b) Beam net length. (c) Drop mass velocity. (d) Compressive strength. (e) Beam depth. (f) Beam-width. (g) Shear reinforcement ratio. (h) Tensile reinforcement ratio.

4.3.2 Validation of midspan deflection

4.3.2.1 Validation with experimental tested data

A statistical comparison is undertaken between the developed viscoplastic LCP model, and the experimental results, as shown in Fig. 4.2. To validate this LCP model with the collected dataset, the statistical presentation of midspan deflection is evaluated using the coefficient of determination (R^2). This is the variance-dependent coefficient whose value near 1 indicates best prediction. In this context, the correlation factor of the experimental and predicted results is R^2 = 0.98, indicating better prediction. Furthermore, the best-fit line for the predicted peak midspan deflection is y =0.97x, which is closely aligned with the 45^o benchmark, suggesting a solid relation between the experimental and the predicted results.

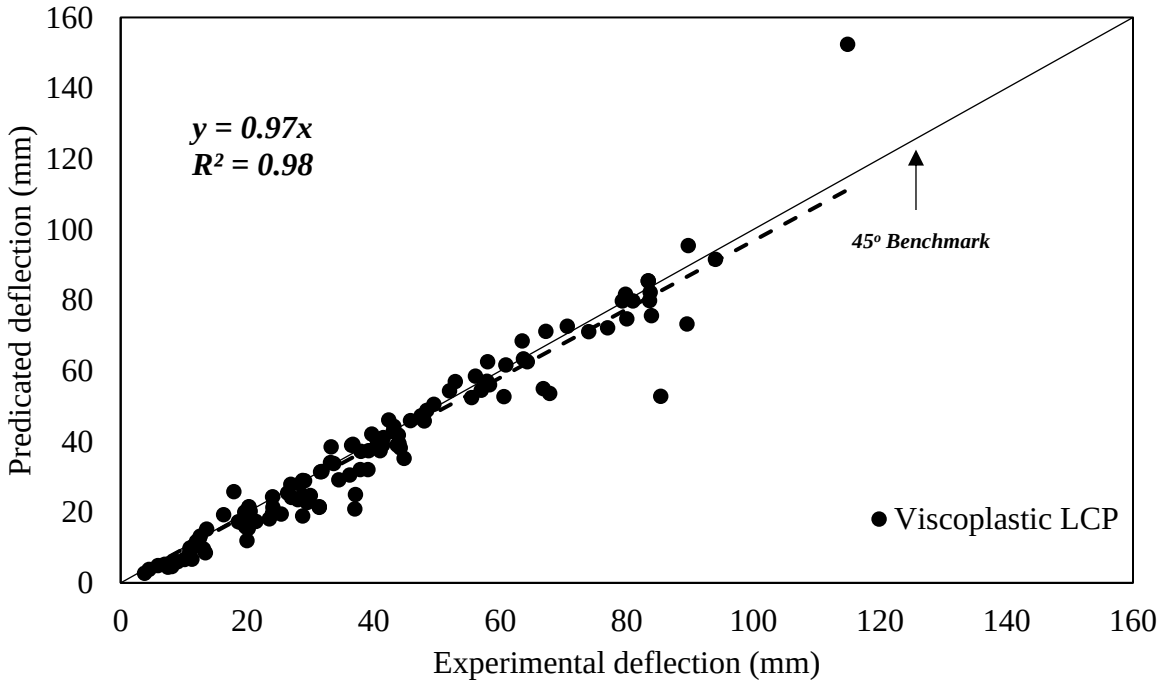

Figure 4. 2: Comparison of predicted and experimental results of midspan maximum deflection

Another statistical indicator is the predicted to the experimental deflection ratio (PER), whose value close to 1 specify better prediction. The average PER is 0.92, close to a benchmark value of 1, with a coefficient of variation (CoV) of 16.5%. Fig. 4.3 presents the sensitivity analysis of different parameters in the

proposed viscoplastic LCP formulation for predicting the maximum mid-span deflection. It is clear from Fig. 4.3(a) that the influence of the velocity on the model accuracy has a virtual average of 0.92 for maximum mid-span deflection within the interval (0.6-1.5). This clearly demonstrates that the proposed model has adequate performance for various ranges of velocity. The mid-span deflection predicted by the viscoplastic LCP model is compared with the experimental impact mass, as shown in Fig. 4.3(b). The accuracy and better reliability of the proposed model are still in the range of (0.6-1.5). Fig. 4.3(c) and (d) also confirm the satisfactory performance of the LCP model with experimental mass ratio and depth of the beam, respectively. Evidently, the proposed LCP method is predicting deflection with reasonable accuracy as PER ranges between 0.6-1.5. It can also be found that the overall deflection of PER is insignificantly affected by changing the impact parameters, which means that this formulation can be well used for a wide spectrum of these impacted parameters.

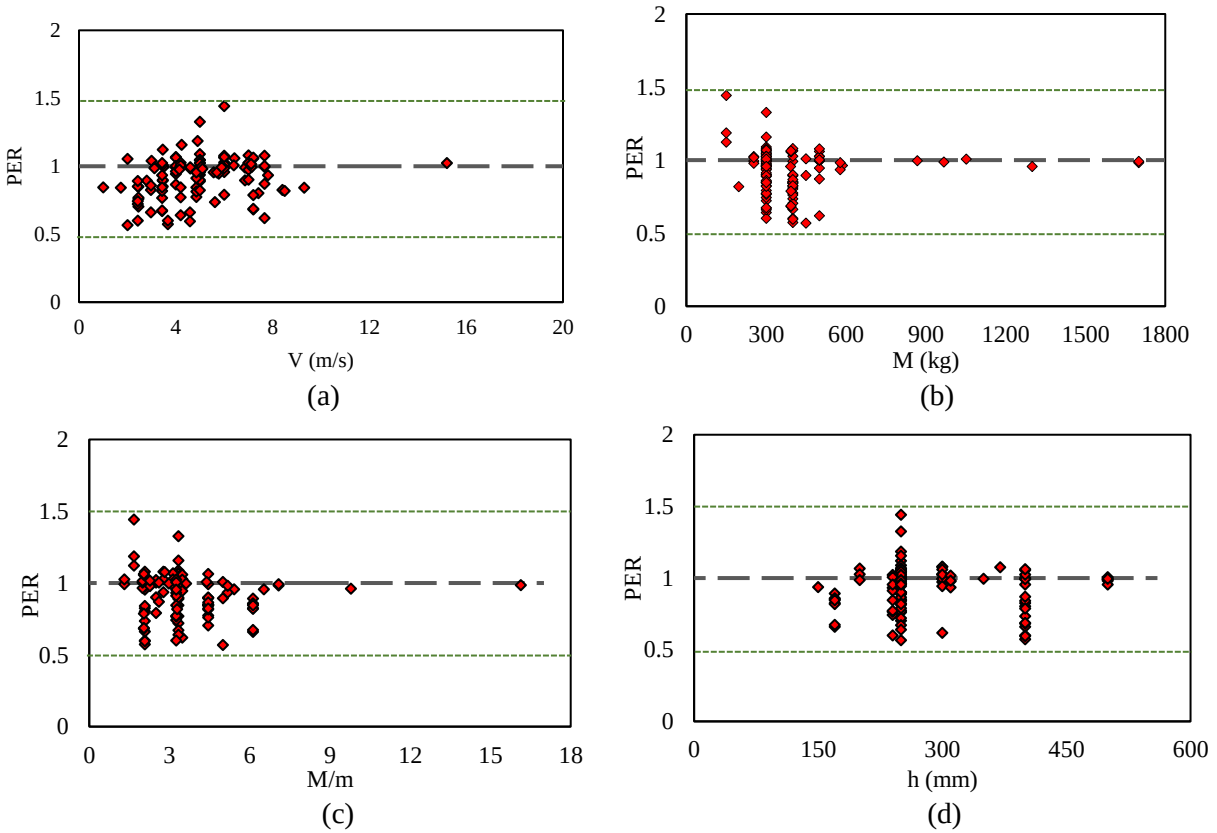

Figure 4. 3: : Influence of parameters on the estimative performance of the developed formulation. (a) Projectile velocity. (b) Impacted mass. (c) Mass ratios. (d) Beam depth

4.3.2.2 Validation with the available models

A comparison of various available models through statistical parameters is shown in Table 4.1. It is really important to note down the reliability of developed formulation is best than all other models because of higher value of R^2, and the resulting slope of the best-fit line (m) is closest to the slope of the benchmark line.

4.3.2.2.1 Zhao et al. Model

The comparison of viscoplastic LCP with the Zhao et al. model is shown in Fig. 4.4. This model is valid to 118 tested beams data. The R^2 of the Zhao et al. model is 0.96 with AAE of 26.9%. The mean PER value is 1.07 with coefficient of variation of 30.2%.

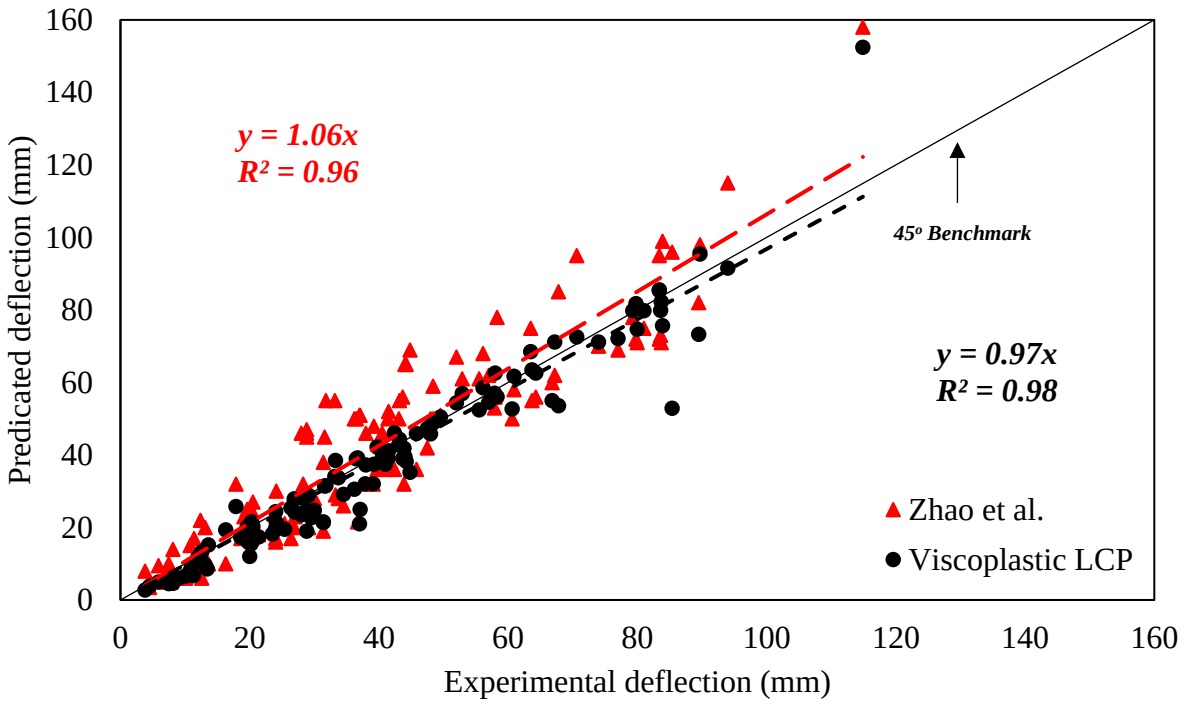

Figure 4. 4: Zhao et al. vs Visoplastic LCP

4.3.2.2.2 Adhikary et al. Model

The comparison of viscoplastic LCP with the Adhikary et al. model is shown in Fig. 4.5. This model is valid to 114 tested beams data. Therefore, only that 114 data were used for LCP model as well. The R^2 of the LCP model becomes 0.99 with AAE equal to 12.5%. The average PER value becomes 0.91 with CoV

equal to 16.3%. Similarly, the R^2 of the Adhikary et al. model is 0.95 with AAE of 25.5%. The mean PER value is 0.85 with coefficient of variation of 34.1%.

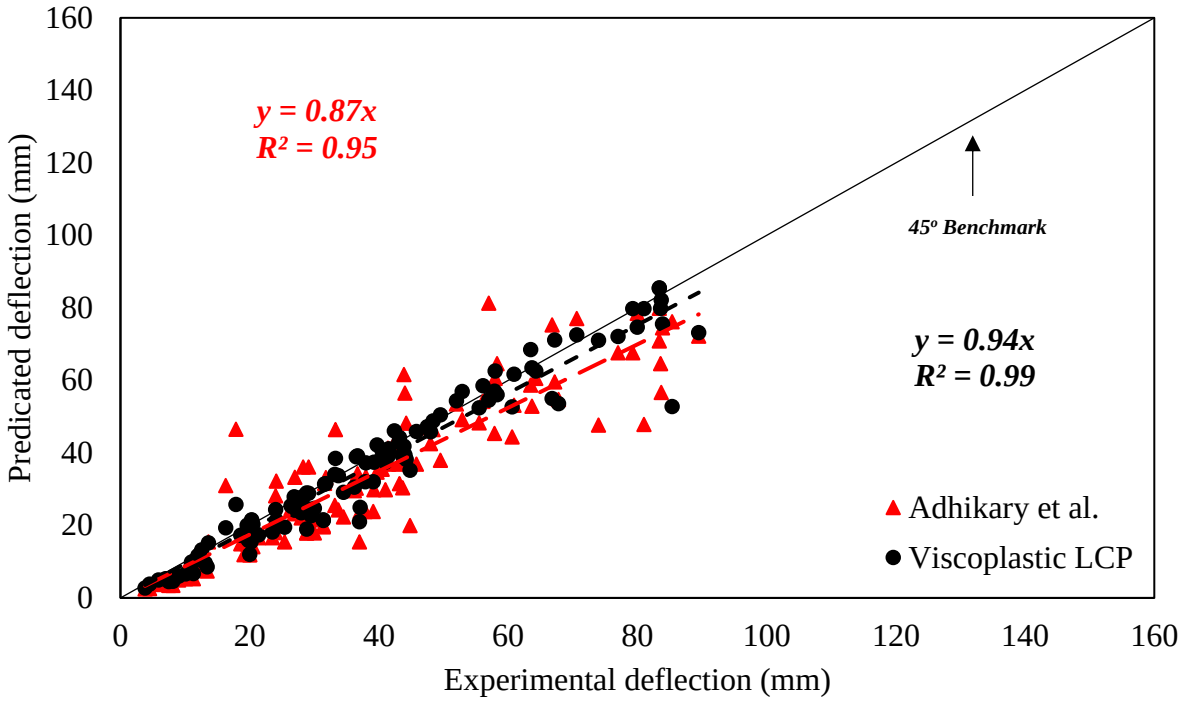

Figure 4. 5: Comparison of viscoplastic LCP and Adhikary et al.

4.3.2.2.3 Khan et al. Model

The comparison of viscoplastic LCP with the Khan et al. model is shown in Fig. 4.6. This model is valid to 118 tested beams data. The R^2 of the Khan et al. model is 0.94 with AAE of 30.8%. The mean PER value is 1.26 with coefficient of variation of 30.5%.

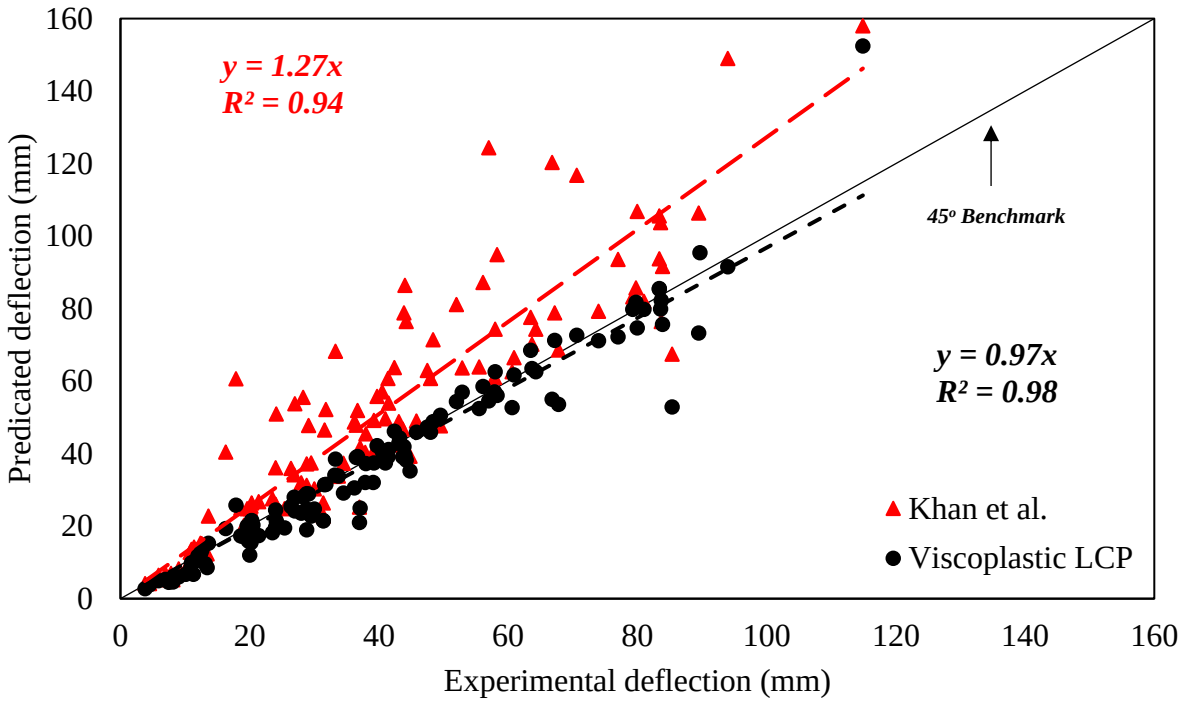

Figure 4. 6: Khan et al. vs viscoplastic LCP model prediction

4.3.2.2.4 Kishi and Mikami Model

The comparison of viscoplastic LCP with the Kishi and Mikami model is shown in Fig. 4.7. This model is valid to 76 tested beams data. Therefore, only that 76 data were used for LCP model as well. The R^2 of the LCP model becomes 0.98 with AAE equal to 9%. The average PER value becomes 0.97 with CoV equal to 13.7%. Similarly, the R^2 of the Kishi and Mikami model is 0.96 with AAE of 21.6%. The mean PER value is 1.02 with coefficient of variation of 32.9%.

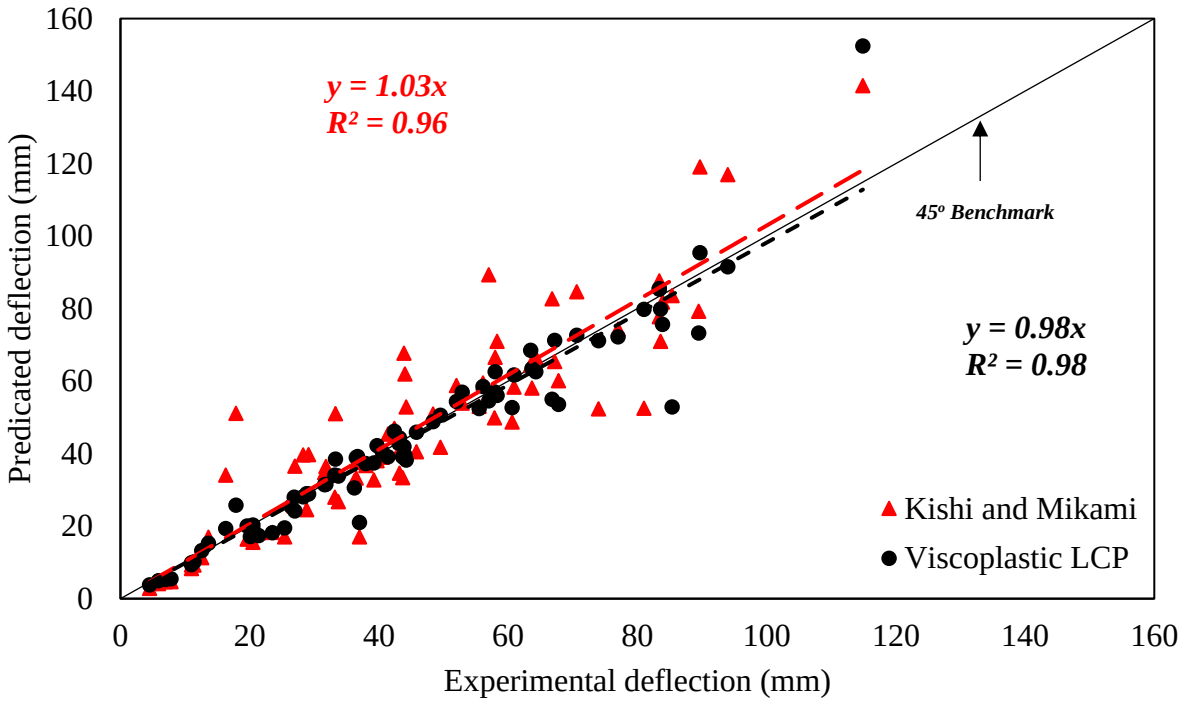

Figure 4. 7: Comparison of viscoplastic vs Kishi and Mikami model

4.3.2.2.5 Tachibana et al. Model

The comparison of viscoplastic LCP with the Tachibana et al. model is shown in Fig. 4.8. This model is valid to 47 tested beams data. Therefore, only that 47 data were used for LCP model as well. The R^2 of the LCP model becomes 0.97 with AAE equal to 12.1%. The average PER value becomes 0.95 with CoV equal to 17.1%. Similarly, the R^2 of the Tachibana et al. model is 0.93 with AAE of 28.7%. The mean PER value is 0.87 with coefficient of variation of 40.4%.

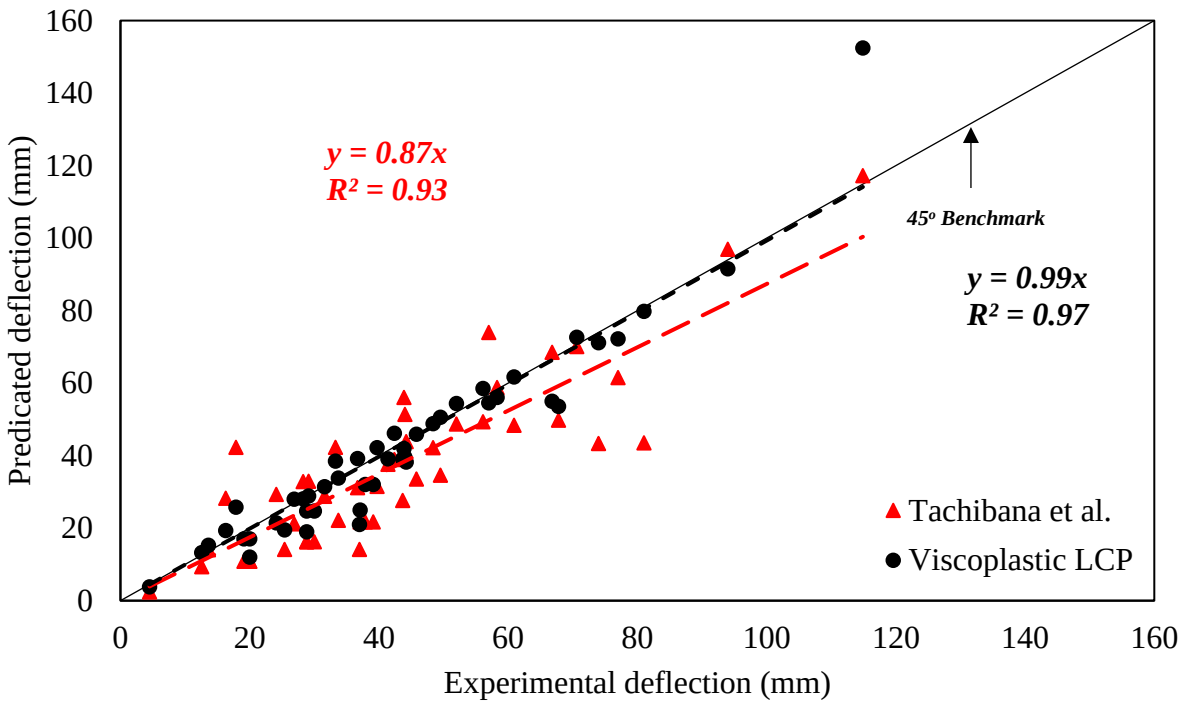

Figure 4. 8: Tachibana et al. vs viscoplastic LCP

Table 4. 1: Statistical analysis of maximum mid-span deflection prediction models of RC beams under Impact loading

Author	No of samples	Mean PER	Standard Deviation	CoV (%)	AAE (%)	R^2
Tachibana et al. [64]	47	0.87	0.35	40.4	28.7	0.93
Kishi and Mikami [18]	76	1.02	0.34	32.9	21.6	0.96
Khan et al. [8]	118	1.26	0.38	30.5	30.8	0.94
Adhikary et al. [110]	114	0.85	0.29	34.1	25.5	0.95
Zhao et al. [66]	118	1.07	0.32	30.2	26.9	0.96
Viscoplastic LCP Model	118	0.92	0.15	16.5	12.5	0.98

4.4 Bending shear LCP

4.4.1 Experimental Database

An extensive experimental database of 100 simply supported RC beams has been constructed from the literature [13,14,62,72,78,99,100,102] by employing a consistent set of inclusion criteria. Within the database, all beams are of rectangular cross-sections subjected to impact load at the midspan having either flat or spherical contact surface. Out of this dataset of 100 RC beams, the specimens failing in shear and bending-shear are included. Therefore, 54 specimens are removed from the data due to flexural failure, and the validation of the proposed LCP is carried out with the remaining 46 beams.

4.4.1.1 Distribution of key influence parameters

The important influence parameters of RC simply supported beam is examined herein. The influence parameters, such as the impacted drop velocity, and mass, geometric size of beam, concrete compressive stresses, longitudinal reinforcement, and shear reinforcement, are given in Fig. 4.9. It is visible from the figure that the velocity of the projectile ranges from 1-16 m/sec, whereas most of the data lie in 2-8 m/sec regime. Similarly, the impact mass M is in the range of 100-1800 kg, having many tested beams within 300-600 kg. Further, the net span of simply supported RC beams ranges from 1000 to 5000 mm, compressive strength lies within 15-50 Mpa, the width and height of RC beams lie within the range limit 100-250 mm and 150-500 mm, respectively, and the longitudinal tensile and shear reinforcement ratio falls in the range 0.75-2.85% and 0-0.5%, respectively.

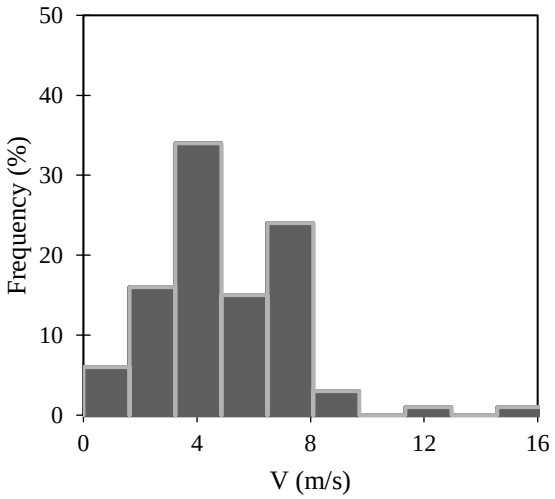
Frequency (%)
V (m/s)

(a)

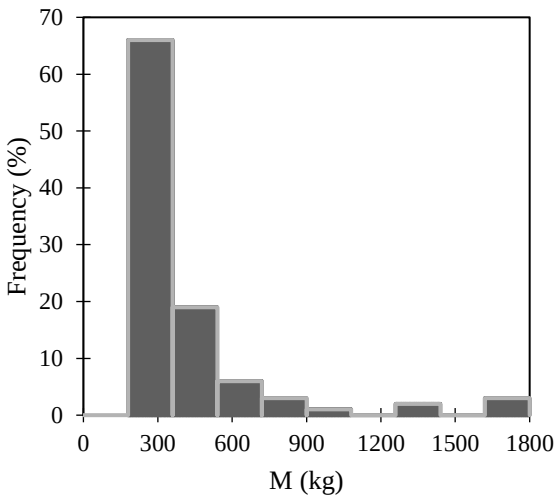
Frequency (%)
M (kg)

(b)

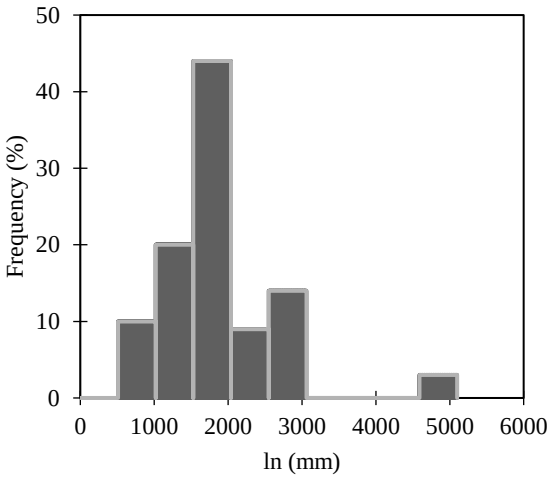
Frequency (%)
ln (mm)

(c)

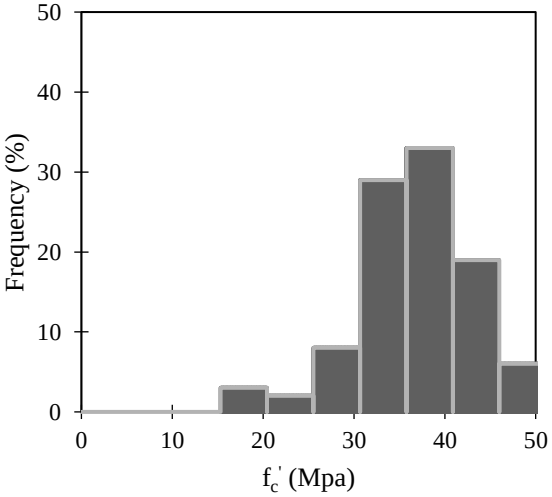
Frequency (%)
f'c (Mpa)

(d)

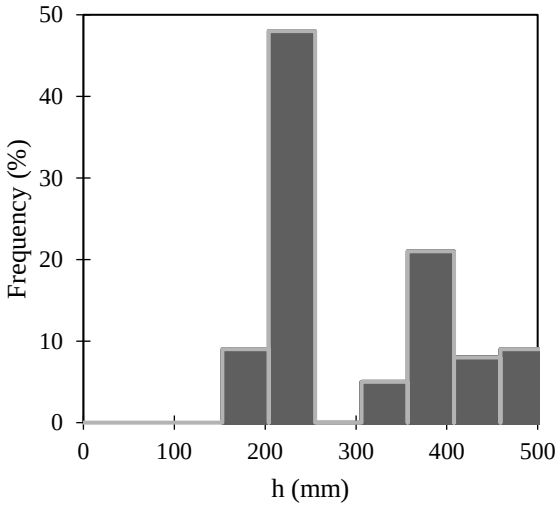
Frequency (%)
h (mm)

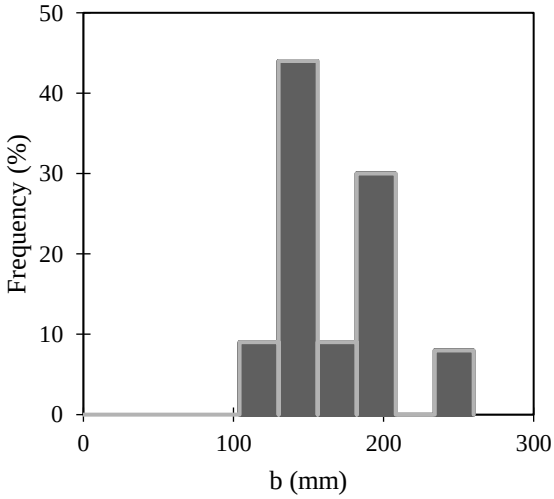
Frequency (%)
b (mm)

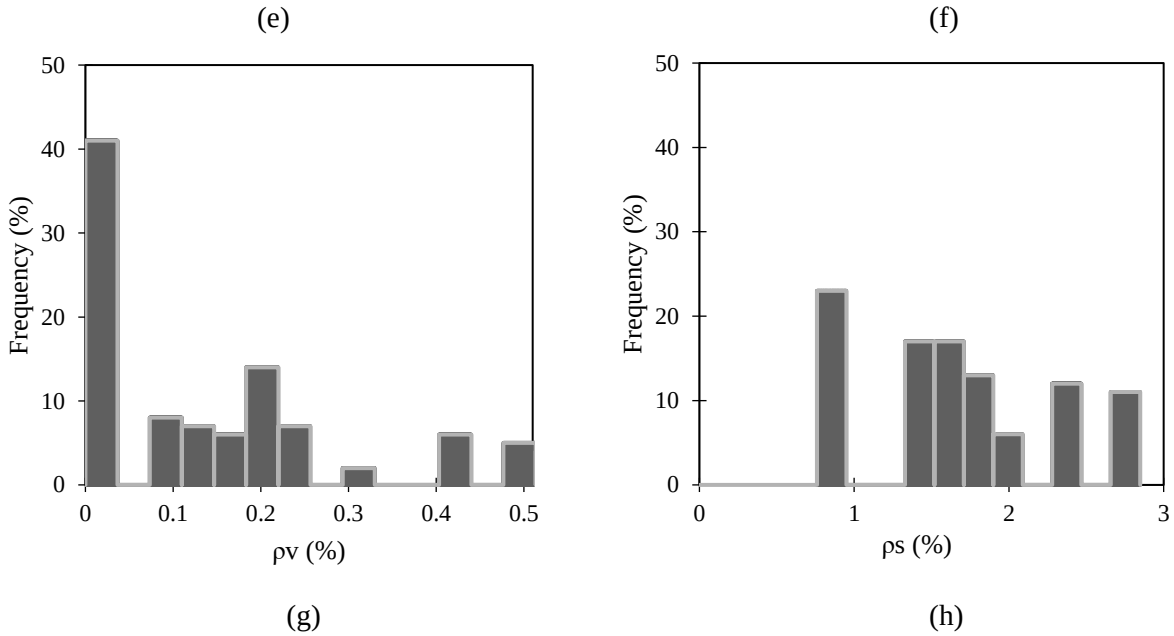

Figure 4. 9: Frequencies of different experimental tested beams parameters. (a) Drop mass velocity. (b) Impacted Mass. (c) Beam net length. (d) Compressive strength. (e) Beam depth. (f) Beam-width. (g) Shear reinforcement ratio. (h) Tensile reinforcement ratio.

4.4.2 Validation of midspan deflection

4.4.2.1 Validation with experimental tested data

A statistical comparison is undertaken between the developed bending-shear LCP model, and the experimental results, as shown in Fig. 4.10. To validate this LCP model with the collected dataset, the statistical presentation of midspan deflection is evaluated using the coefficient of determination (R^2). This is the variance-dependent coefficient whose value near 1 indicates best prediction. In this context, the correlation factor of the experimental and predicted results is $R^2 = 0.95$, indicating better prediction. Furthermore, the best-fit line for the predicted peak midspan deflection is $y = 1.05x$, which is closely aligned with the 45^o benchmark, suggesting a solid relation between the experimental and the predicted results.

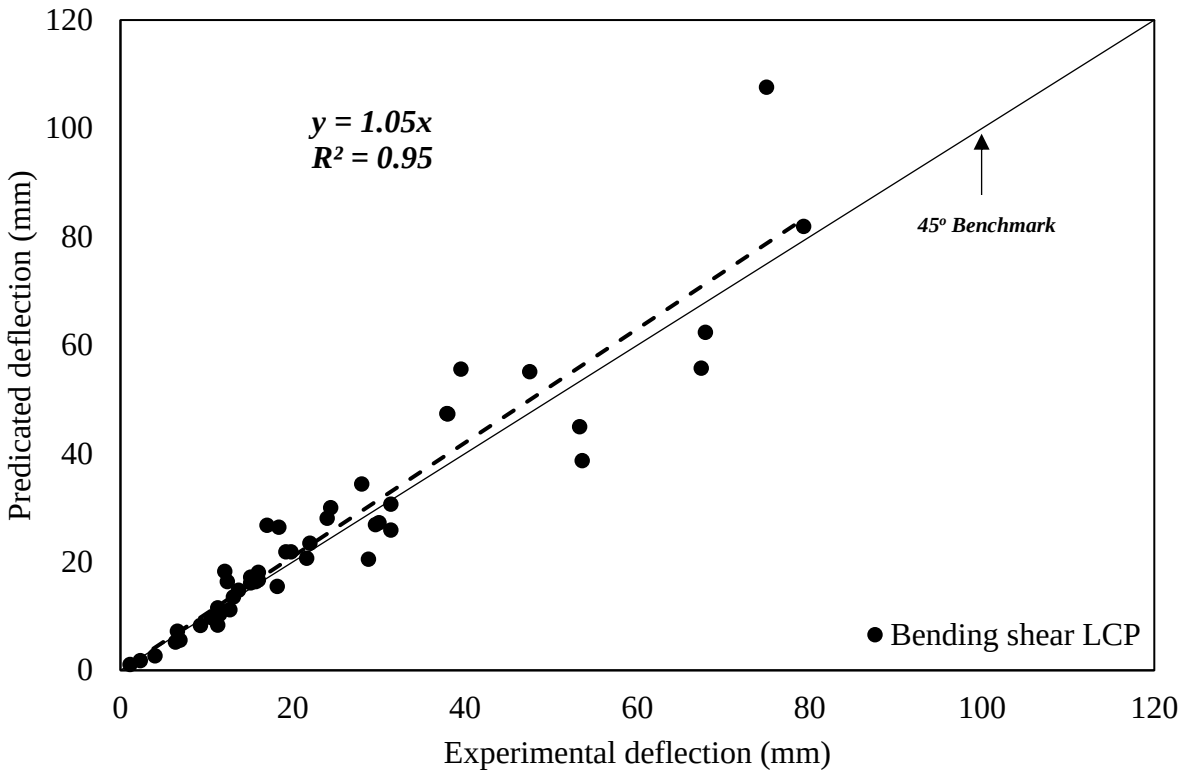

Figure 4. 10: Comparison of predicted and experimental results of midspan maximum deflection

Another statistical indicator is the predicted to the experimental deflection ratio (PER), whose value close to 1 specify better prediction. The average PER is 1.04, close to a benchmark value of 1, with a coefficient of variation (CoV) of 21.2%. Fig. 4.11 presents the sensitivity analysis of different parameters in the developed bending shear LCP model for predicting the maximum mid-span deflection. It is visible from Fig. 4.11(a), that the influence of the velocity on the model accuracy has a virtual average of 1.04 for maximum mid-span deflection within the interval (0.7-1.6). This clearly demonstrates that the proposed model has adequate performance for various ranges of velocity. The mid-span deflection predicted by the bending shear LCP model is compared with the experimental impact mass, as shown in Fig. 4.11(b). The accuracy and reliability of the developed formulation are still in the range of (0.7-1.6). Fig. 4.11(c) and (d) also confirm the satisfactory performance of the LCP model with experimental mass ratio and depth of the beam, respectively. Evidently, the proposed LCP method is predicting deflection with reasonable accuracy as PER ranges between 0.7-1.6. It can also be found that the overall deflection of PER is insignificantly

affected by changing the impact parameters, which means that this formulation can be well used for an extended spectrum of these impacted parameters.

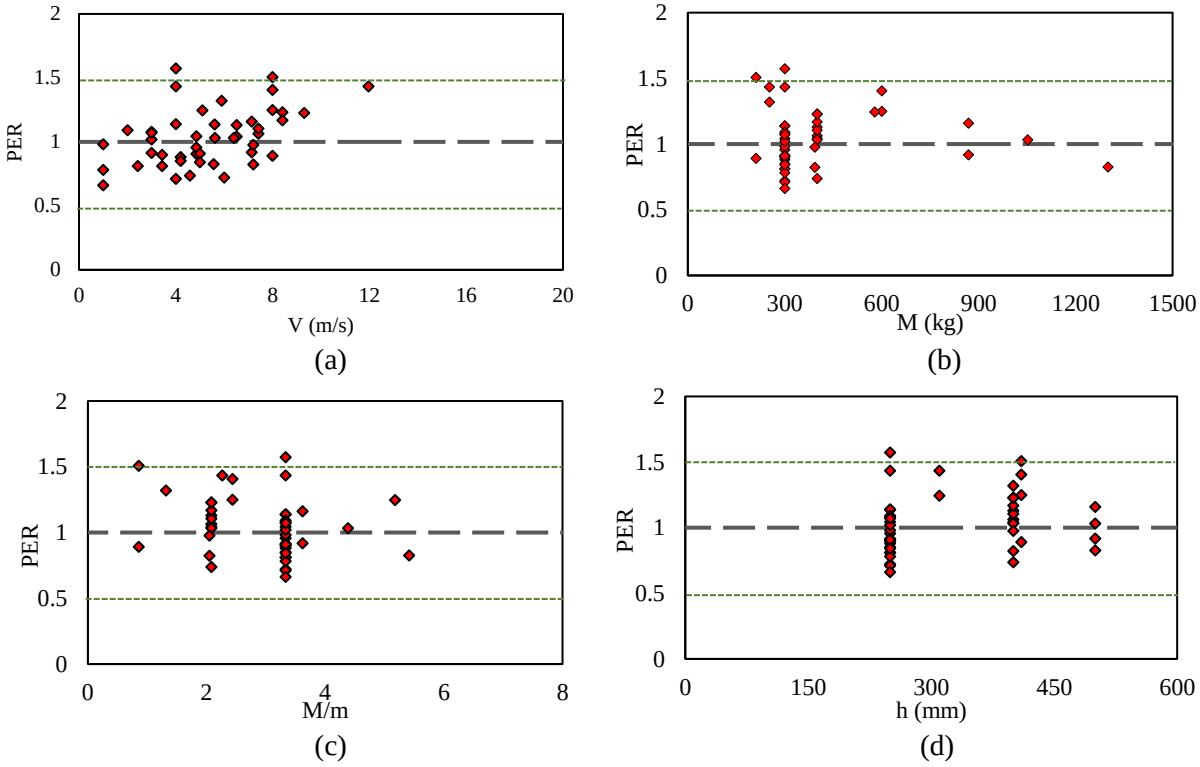

Figure 4. 11: Influence of parameters on the estimative performance of the developed formulation. (a) Projectile velocity. (b) Impacted mass. (c) Mass ratios (d) Beam depth

4.4.2.2 Validation with the available models

A comparison of various available models through statistical parameters is shown in Table 4.2. It is really important to note down the reliability of developed formulation is best than all other models because of higher value of R^2, and the resulting slope of the best-fit line (m) is closest to the slope of the benchmark line.

4.4.2.2.1 Khan et al. Model

The comparison of bending-shear LCP with the Khan et al. model is shown in Fig. 4.12. This model is valid to 46 tested beams data. The R^2 of the Khan et al. model is 0.93 with AAE of 22.7%. The mean PER value is 0.93 with coefficient of variation of 29.1%.

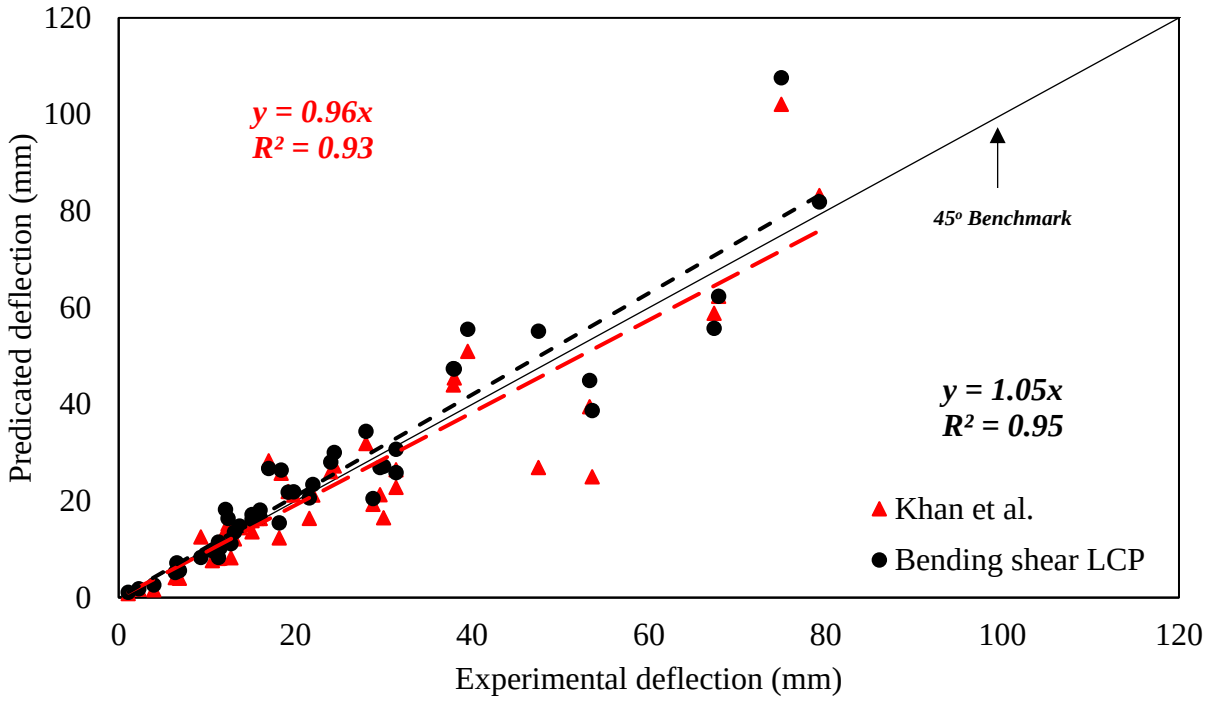

Figure 4. 12: Khan et al. vs bending-shear LCP

4.4.2.2.2 Adhikary et al. Model

The comparison of bending shear LCP with the Adhikary et al. model is shown in Fig. 4.13. This model is valid to 35 tested beams data. Therefore, only that 35 data were used for LCP model as well. The R^2 of the LCP model becomes 0.97 with AAE equal to 17.1%. The average PER value becomes 1.04 with CoV equal to 20.9%. Similarly, the R^2 of the Adhikary et al. model is 0.92 with AAE of 26.7%. The mean PER value is 1.09 with coefficient of variation of 37.1%.

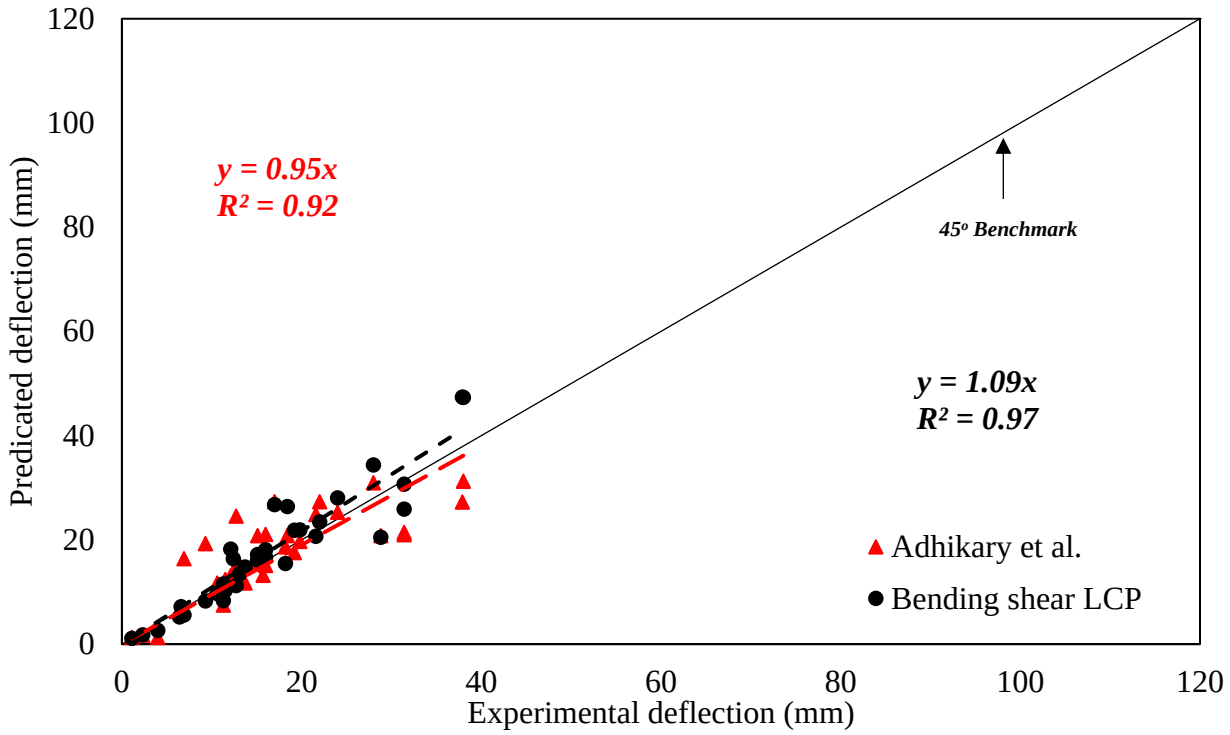

Figure 4. 13: Comparison of bending shear LCP with Adhikary et al. model

Table 4. 2: Statistical analysis of maximum midspan deflection prediction models of RC beams under Impact loading

Author	No of samples	Mean PER	Standard Deviation	CoV (%)	AAE (%)	R^2
Khan et al. [8]	46	0.93	0.27	29.1	22.7	0.93
Adhikary et al. [110]	35	1.09	0.40	37.1	26.7	0.92
Bending shear LCP Model	46	1.04	0.22	21.2	17.7	0.95

4.5 Peak Impact Force

4.5.1 Experimental Database

In ways to precisely predict the peak impacted force on RC beam from a dropweight, a collection of 126 experimental tests from previous studies is compiled into a database [18,59,62,64,72,98–102]. Within the database, all beams are of rectangular cross-sections subjected to impact load at the midspan having either

flat or spherical contact surface. For GEP analysis, only a randomly selected portion of 84 experiments is used to develop the model. The remaining 42 samples are employed for the model validation.

4.5.1.1 Distribution of key influence parameters

The important influence parameters of RC simply supported beam is examined herein. The influence parameters, such as the impact velocity, impact mass, geometrical size of the beams, concrete compressive stresses, longitudinal reinforcement, and shear reinforcement, are given in Table 4.3. It is clear from the table that the velocity of the projectile ranges from 1-16 m/sec, and the impact mass M is in the range of 33-1700 kg. Further, the net span of simply supported RC beams ranges from 1000 to 5000 mm, the width and height of RC beams lie within the range limit 100-300 mm and 120-500 mm, respectively, and the longitudinal tensile and shear reinforcement ratio falls in the range 0.29-3.1% and 0-1.4%, respectively.

Table 4. 3: Distribution of key influence parameters

Parameters	Ranges
Velocity	1-16 (m/s)
Mass	33-1700 (kg)
Compressive strength	20-42 (MPa)
Net span length	1000-5000 (mm)
Beam width	100-300 (mm)
Beam height	120-500 (mm)
Tensile reinforcement ratio	0.29-3.1 (%)
Shear reinforcement ratio	0-1.4 (%)

4.5.2 Validation with experimental tested data

A statistical comparison is undertaken between the developed GEP model, and the experimental results, as shown in Fig. 4.14. To validate this GEP model with the collected dataset, the statistical presentation of midspan deflection is evaluated using the coefficient of determination (R^2). This is the variance-dependent coefficient whose value near 1 indicates best prediction. In this context, the correlation factor of the experimental and predicted results is $R^2 = 0.98$, indicating better prediction. Furthermore, the best-fit line

for the predicted peak midspan deflection is y =0.96x, which is closely aligned with the 45º benchmark, suggesting a solid relation between the experimental and the predicted results.

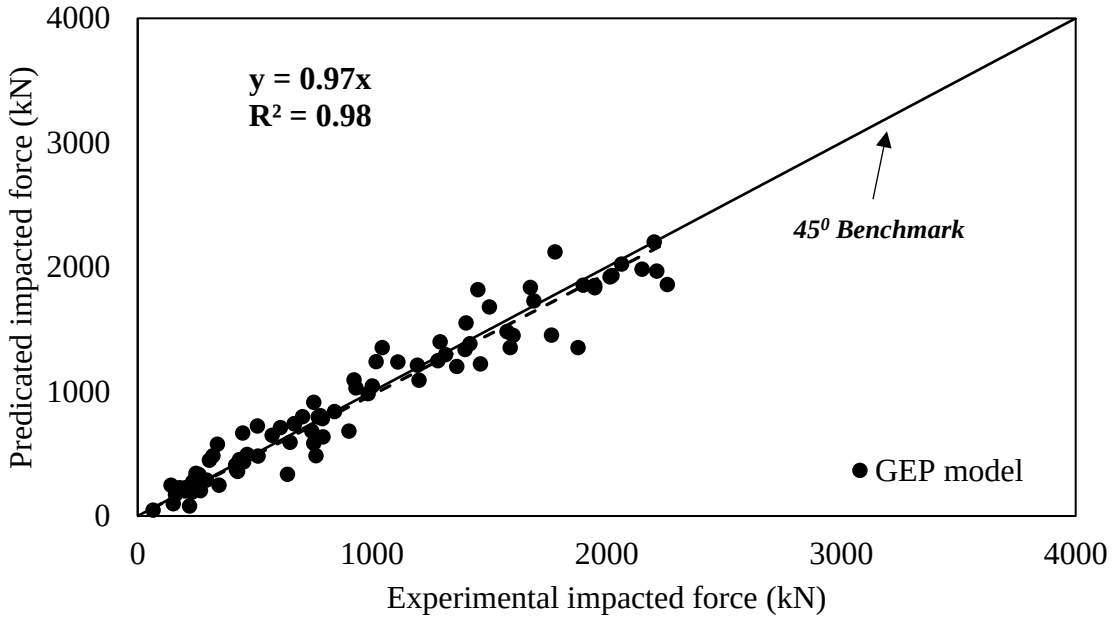

(a)

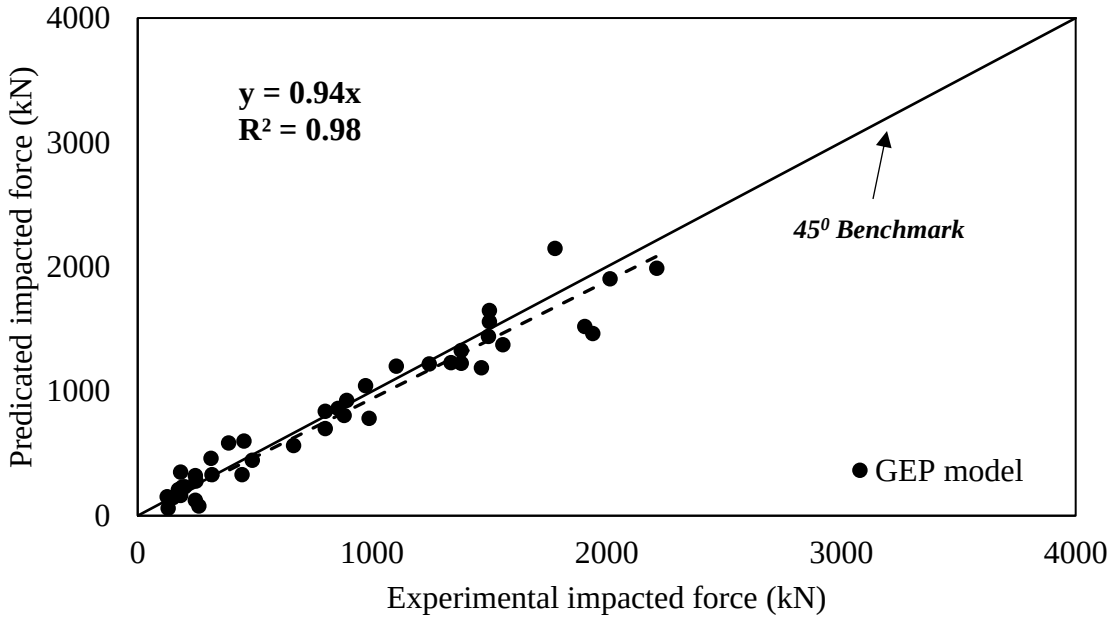

(b)

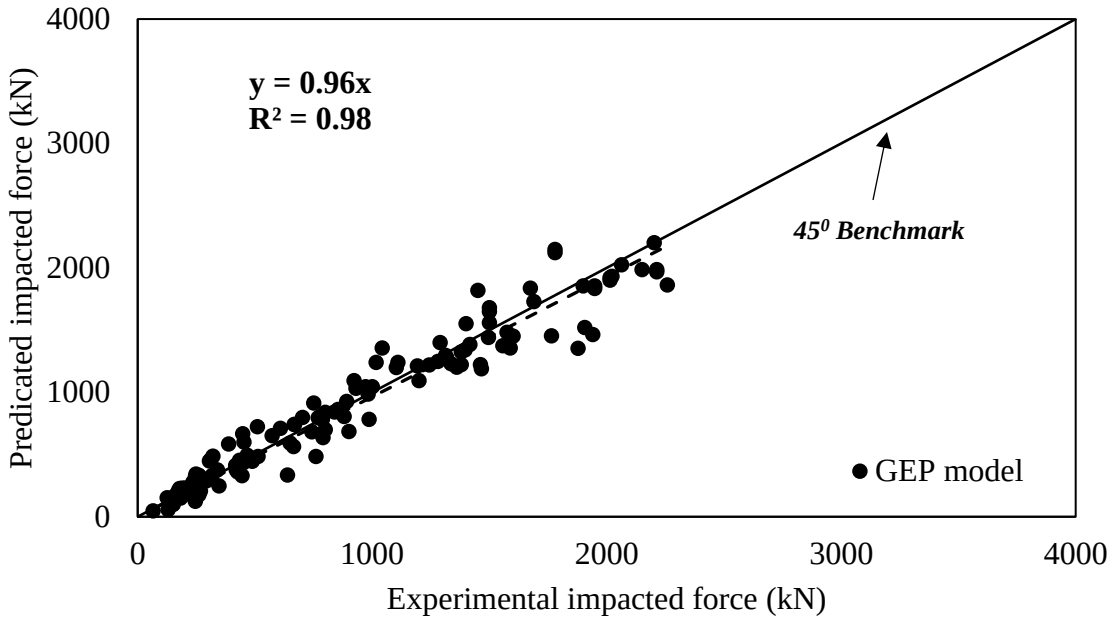

(c)

Figure 4. 14: Comparison of predicted and experimental results of peak impacted force (a) Training data (b) Validation data (c) All data

4.5.3 Sensitivity of the proposed model

The formulated GEP model has adequate capacity to incorporate the effect of all the controlling parameters that are already discussed in Section 3.4.1. From Fig. 4.15(a), and (b) it is worth to be noted that increasing the breadth, and depth of the beam increases the stiffness of the member, thereby attracting more impact force. Similarly, Fig. 4(c) shows that increasing the concrete strength in compression increases the modulus of elasticity and the stiffness of the RC member, thus attracting more impact force. On the contrary, the peak impacted force reduces as the span of the member increases, as shown in Fig. 4.15(d). The effect of tension force of longitudinal reinforcement follows the pattern akin to that of Fig. 4.15(a)-(c) Fig 4(e) because the ultimate bending moment capacity and the load-resisting capacity increases with the increase in longitudinal reinforcement. The influence of input kinetic energy on the impact force is featured in Fig. 4.15(f). It can be seen that the higher magnitude of the imparted kinetic energy results in a larger impact force.

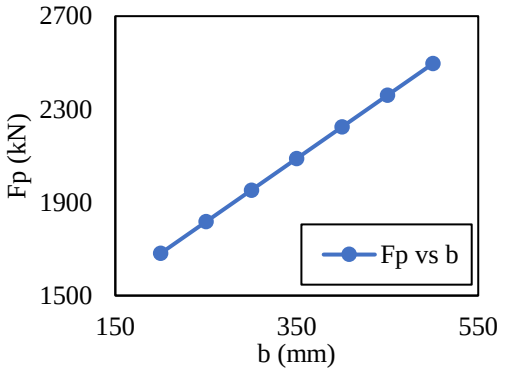

(a) Impacted force vs beam breadth

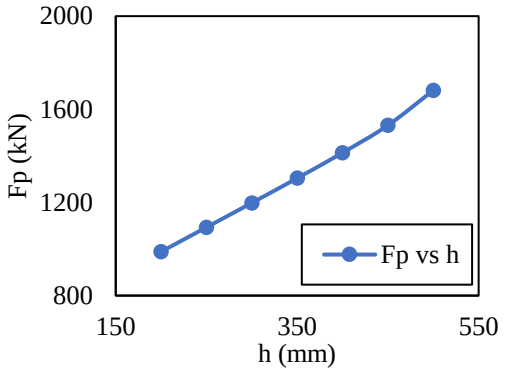

(b) Impacted force vs beam height

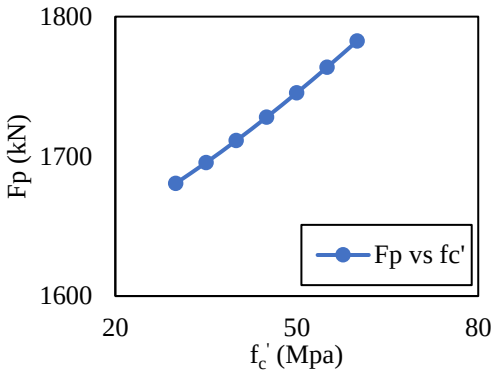

(b) Impacted force vs Compressive Strength

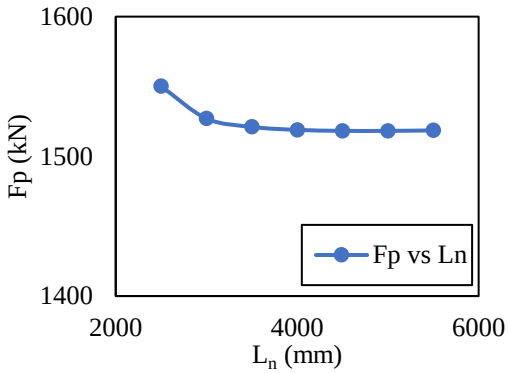

(d) Impacted force vs beam span

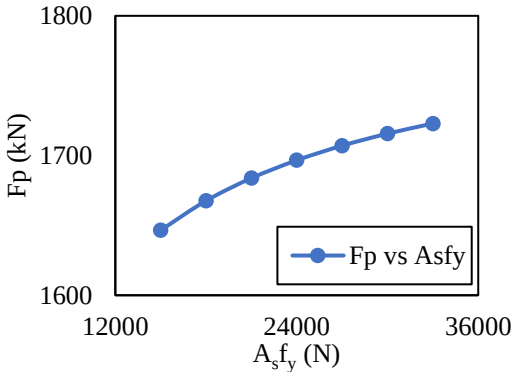

(e) Impacted force vs steel tension force

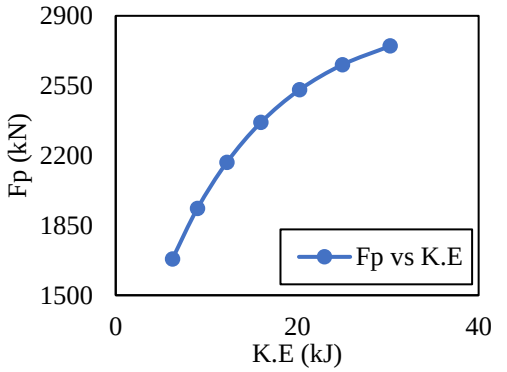

(f) Impacted force vs input kinetic energy

Figure 4. 15: Parametric study

Another statistical indicator is the predicted to experimental deflection ratio (PER), whose value close to 1 specify better prediction. The average PER is 1.01, very close to a benchmark value of 1, with a coefficient of variation (CoV) of 19.9%. Fig. 4.16 presents the sensitivity analysis of various key parameters in the formulated GEP model for predicting the peak impact force. It is clear from Fig. 4.16(a) that the influence

of the velocity on the model accuracy has a virtual average of 1.01 for peak impact force within the interval (0.45-1.5). This clearly demonstrates that the proposed model has adequate performance for various ranges of velocity. The impacted force predicted by the GEP model is compared with the experimental impact mass, as shown in Fig. 4.16(b). The accuracy and precision of the formulated model are still in the range of (0.45-1.5). Fig. 4.16(c) – (f) also confirm the satisfactory performance of the GEP model with experimental beam width, depth of the beam, f_c', and $\frac{A_s f_y}{f_c'}$ respectively. Evidently, the proposed GEP method is predicting deflection with reasonable accuracy as PER ranges between 0.45-1.5. It can also be found that the overall impact force of PER is insignificantly affected by changing the impacted parameters, which means that this procedure can be best and reliable for a wide spectrum of these impacted parameters.

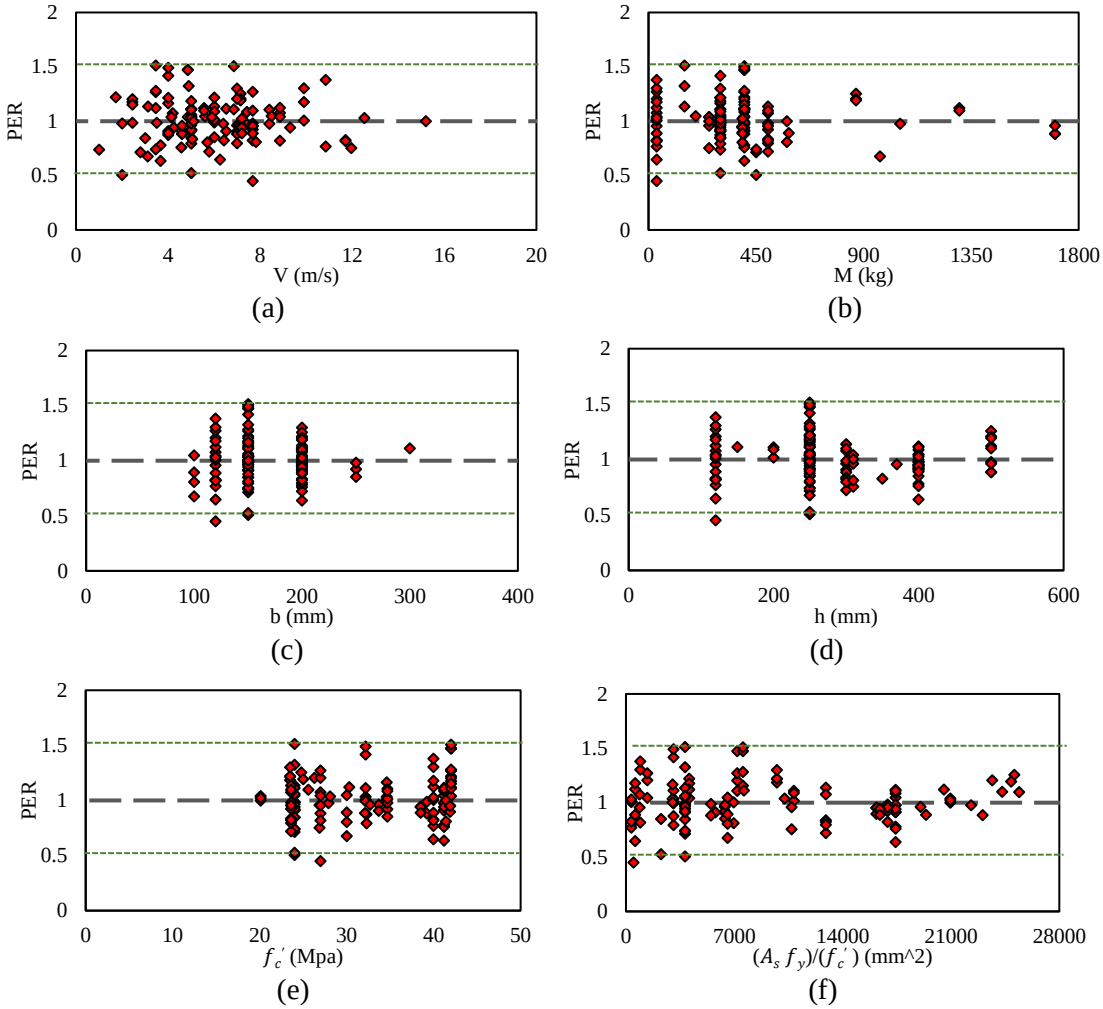

Figure 4. 16: The effect of main parameters on the precision of developed GEP

4.5.4 Comparison with numerical model

It is aimed in this section to compare the proposed empirical model with a numerical model developed using finite element (FE) code ABAQUS. Particular attention has been focused on the peak impacted force transferred to the beam.

4.5.4.1 Experimental program Bhatti

As per the experimental study reported by Bhatti [62], a series of 2,400 mm long beams were tested under impact loading of 400 Kg. The RC beam was of 41.2 MPa compressive strength having a square cross-section of 400 x 200 mm and 50 mm cover all around. Further, the longitudinal and transverse bars were of 35 and 6 mm diameters respectively, with the yield, and ultimate strength of 395 MPa, and 501 MPa, and the spacing of stirrups was 150 mm. Following Btatti's classification of tested specimens, the beam with stirrups spacing of 150 mm is named Type-A.

4.5.4.2 Response of RC beam predicted by ABAQUS

A 3-D finite element model, Fig. 4.17, is constructed to simulate the dynamic-response of RC beam. C3D8R brick elements are adopted for the beam, T3D2 wire elements are employed to model the steel in the beam, and isoparametric elements are used to model the striker weight. Interfacial elements are adopted to permit both the two bodies to be fully in contact along with small sliding without frictional resistance effects. The drop-weight striker has the same mass given as used in the experimental tests and is supposed elastic with Young's modulus property adapted to accommodate the stress-wave effect. The concrete has a prescribed density of $2400\ kg/m^3$, the Poisson's ratio of 0.19, and the Young modulus of 25.7 GPa. In the same way, the reinforcement has a mass-density of $7850\ kg/m^3$, the Poisson's ratio of 0.3, and the Young modulus of 206 GPa. The quantitative number of elements used in the dynamic analysis is 7371 for the beam, and 1771 for the impactor. The dynamic response is examined using the explicit time integration with an automatic time step control.

As per the experimental study, the support conditions are simulated as simply supported. It is considered that 3D effects are incorporated. The most excessive deformed location on a beam is near to the point of

impact because when a beam undergoes deformation, the striker Pearce through the beam surface. Convergence study is carried out to best optimize the size of mesh.

Mechanical properties of concrete are modeled using Concrete Damage Plasticity. True strain and true stress are employed as the strain and stress measurements, and geometrical nonlinearity is considered. Incremental portion elastic-plastic material properties without isotropic strain-hardening and strain-rate effect were used for reinforcing bars. The comparison is shown in Table 4.4.

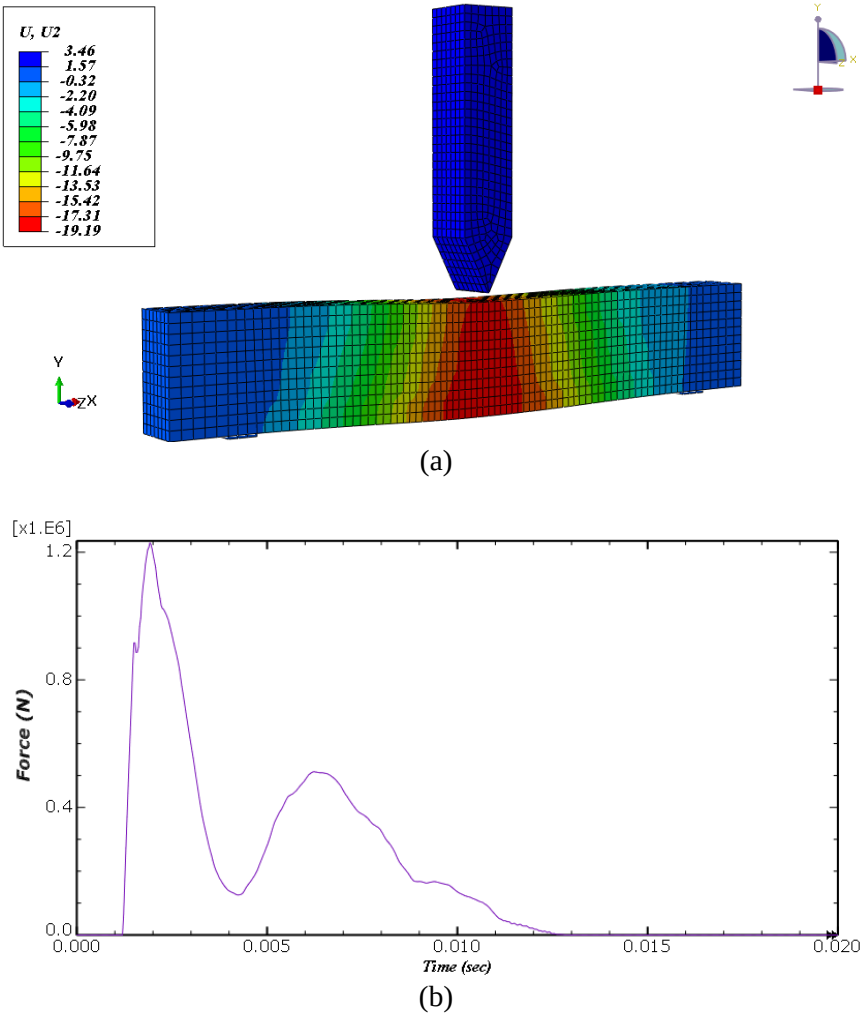

Figure 4. 17: Response of RC beam model in ABAQUS (a) Maximum midspan deflection (b) Peak impact force

Table 4. 4: Comparison of GEP result with Experimental result and ABAQUS solution

	Experimental Results	**ABAQUS Results**	**GEP Results**
Peak Impact force on the beam (kN)	1110	1229	1240

4.5.5 Comparison with the available model

A comparison of various available models through statistical parameters is shown in Table 4.5. It is really important to note down the reliability of developed formulation is best than all other models because of higher value of R^2, and the resulting slope of the best-fit line (m) is closest to the slope of the benchmark line.

4.5.5.1 Pham and Hao model [21]

The comparison of GEP proposed model with the Pham and Hao model is shown in Fig. 4.18. This model is valid to 126 tested beams data. The R^2 of the Pham and Hao model is 0.80 with AAE of 109.1%. The mean PER value is 1.96 with coefficient of variation of 116.3%.

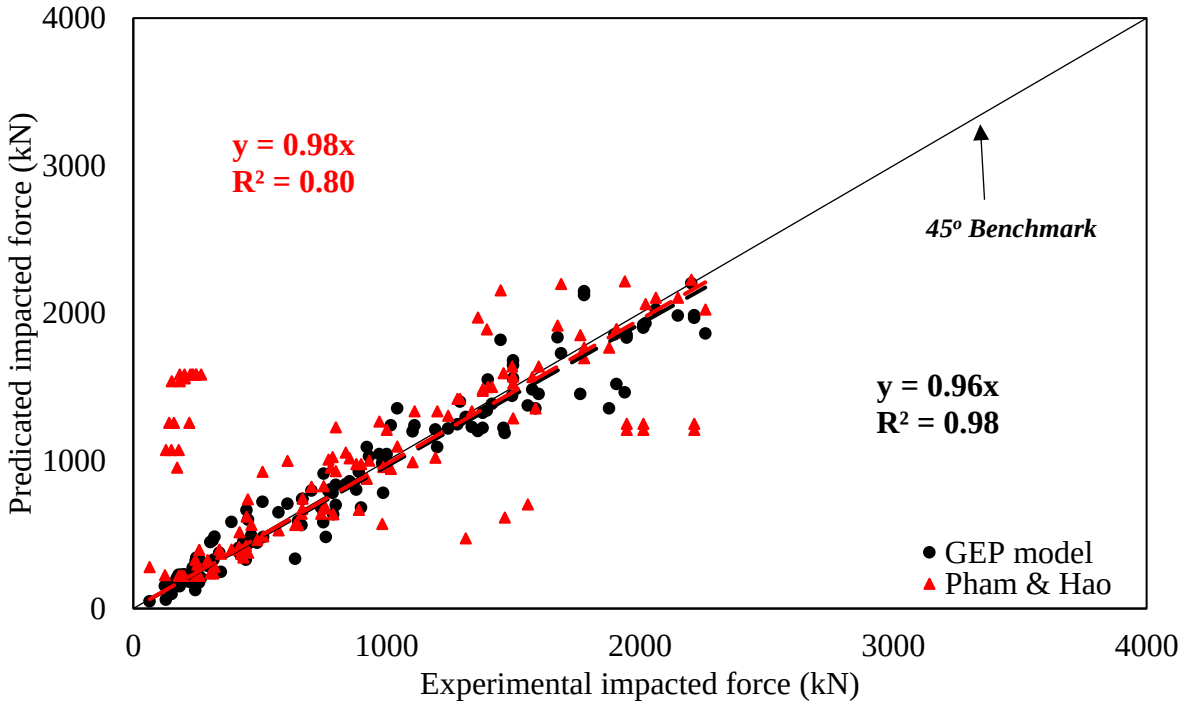

Figure 4. 18: Comparison of GEP with Pham and Hao model

4.5.5.2 **Zhao et al. model** [66]

The comparison of GEP proposed model with the Zhao et al. model is shown in Fig. 4.19. This model is valid to 126 tested beams data. The R^2 of the Zhao et al. model is 0.93 with AAE of 55.4%. The mean PER value is 1.43 with coefficient of variation of 41%.

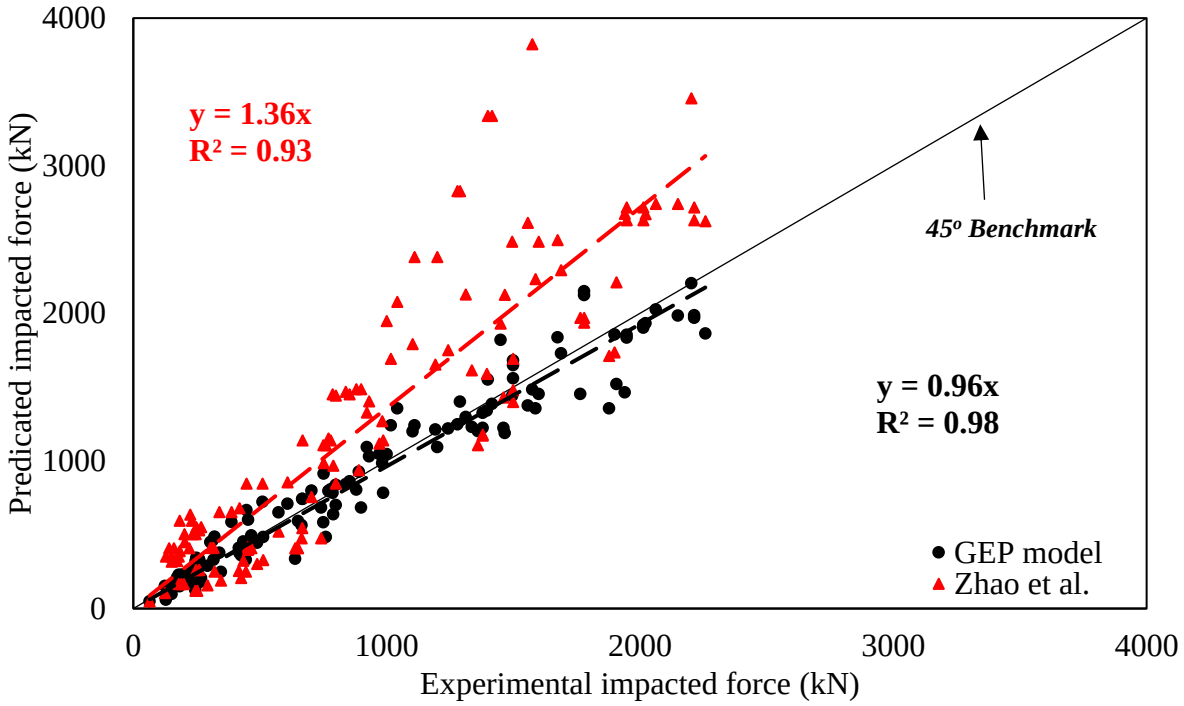

Figure 4. 19: GEP model vs Zhao et al. model

Table 4. 5: Comparison with available models

Author	No of samples	Mean PER	Standard Deviation	CoV (%)	AAE (%)	R^2
Pham & Hao	126	1.96	2.27	116.3	109.1	0.80
Zhao et al.	126	1.43	0.58	41.0	55.4	0.93
GEP Model	126	1.01	0.20	19.9	15.2	0.98

4.5.6 Remarks about shear force, and bending moment plots

In the preceding sections, empirical formulations have been derived for determining the peak impacted force on the RC beam from a dropweight. This force can then be used for deriving the shear forces and bending moment diagrams with the assumption of the linear distribution of inertial force between nodes.

A full procedure shown in Fig. 4.20 for generating this response is given by Pham et. al [12]. According to this procedure, these diagrams can be reasonably predicted provided the maximum impact force and the location of the plastic hinges are known. Having the maximum impact force determined from (3.65) and the hinge locations estimated from the model proposed by Pham et. al [12], the shear force, and bending moment diagrams can be easily generated.

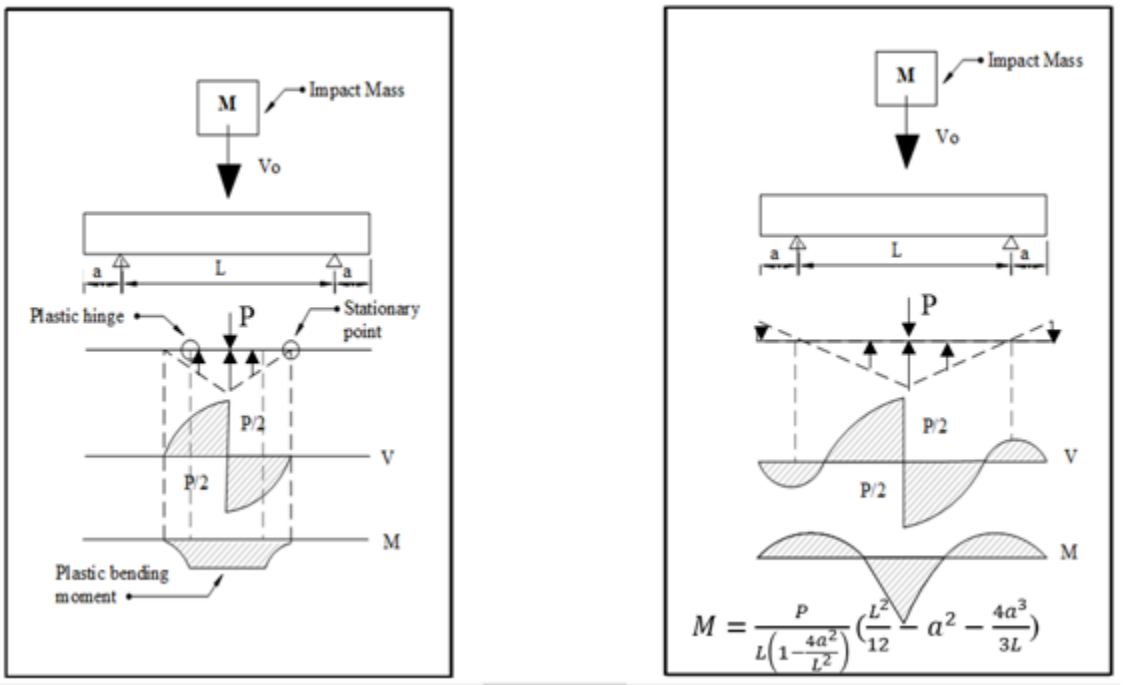

Figure 4. 20: Calculation of the shear force, and bending moment diagram

5 CONCLUSION AND RECOMMENDATION

Generally speaking, the rigid-plastic dynamic analysis is adequately expressive of the true response nature of the RC structures, provided that the total imparted input energy transmitted to the structure is significantly huge than the capacity of maximum stored elastic strain energy. In the context of incorporating this powerful theory into a systematic solution procedure, a robust formulation called a linear complementarity problem (LCP) can be established and applied with a substantial reward. With this intention, the kinetic, and kinematic laws in nodal description, governing the network of finite elements (FE) representing the actual structural system, are presented in the form of nodal velocities, while the rate-dependent materials causality relations are in the nature of nonholonomic piecewise linear plasticity laws. The effect of the strain-rate on the dynamic resulting deformation is incorporated via the Cowper-Symonds equation, which can be modified to result in rate-dependent plastic capacities. The material coefficients of the rate equation have been determined for the RC material. Finally, the approximating formulations of the viscoplastic LCP are developed by employing the Newmark integration scheme.

It is worthwhile to state that the uniqueness of the viscoplastic LCP acceleration fields cannot be guaranteed. The acceleration field of a finite element assembly can be partitioned into the master and the slave sets. Utilizing Cottle's theorem [82], it is established that the master acceleration components can be unique, whereas the uniqueness of slave acceleration cannot be guaranteed. For modeling in which the slave set is empty, the entire acceleration field is unique. Cottle's theorem also establishes that the independent member forces are not necessarily unique unless the structure is isostatic.

A comparative statistical study is illustrated to explore the underlying mechanics of a rigid-perfectly-plastic simply supported end conditions beam subjected to midspan impact. Therefore, an extensive experimental database of 118 RC simply supported beams under impact loading has been constructed by using a consistent set of criteria. It is seen that using only 10 lumped mass elements; the viscoplastic LCP formulation is able to offer an accurate prediction of midspan displacements than the existing formulations

developed by previous scholars. Precisely, the average absolute error (AAE) of the proposed LCP formulation is 12.5%. Similarly, less coefficient of variation CoV values of 16.5% indicates less scatteral variations of the output results estimated through the obtained formulation. The higher value of the coefficient of determination R^2, that is, 98% is compared to the previous formulations, which are less, makes the obtained formulation more precise, and reliable. The average performance factor for the LCP is found to be 0.92, which is close to the reference value.

Similarly, the rigid-perfectly-plastic dynamic analysis is adequately expressive of the true natural behavioral response of the RC structures, especially when brittle shear failures occur. Because of the complexity associated with these analyses, the design code of practices provides limited information and procedures. In this context of incorporating this simplified rigid-plastic theory into a systematic solution procedure, a robust formulation called a linear complementarity problem (LCP) can be established and applied with a substantial reward. With this intention, the kinetic, and kinematic laws in nodal description, governing the network of finite elements (FE) representing the actual structural system, is presented in the form of nodal velocities. In order to make more tractable the resulting LCP, the interaction relationship between the bending moment, and shear force is idealized as a rectangular yield criterion. Finally, the approximating formulations of this interaction-based LCP are developed by employing the Newmark integration scheme. This LCP formulation can efficiently predict the maximum deflections for RC beams' flexural and shear responses under impact loading.

A comparative statistical study is illustrated to explore the underlying mechanics of a rigid-perfectly-plastic simply supported beam subjected to midspan dropweight impact. Therefore, an extensive experimental database of 46 RC simply supported beams under impact loading has been constructed concerning shear and flexure-shear failures only. It is seen that using only 20 lumped mass elements; the LCP formulation can offer an accurate prediction of midspan displacements than the formulations developed by previous scholars. Precisely, the average absolute error (AAE) of the proposed LCP formulation is 17.7%. Similarly, less coefficient of variation CoV values of 21.2% indicates less scatteral variations of the output results

estimated through the developed formulations. The greater value of the coefficient of determination R^2, i.e., 95% is compared to the previous formulations, which are less, making the developed formulation more precise and reliable. The average value of the performance factor for the LCP is found to be 1.04, which is close to the reference value.

It is needless to say that the peak impacted force is the most important key parameter required to predict the dynamic response of impacted beams. This work actually adopts the previous experimental data to formulate peak impacted force predictive models for an impacted reinforced concrete (RC) beam using an algorithm known as Gene Expression Programming. The proposed formulation is intended to capture the response of RC beams under extreme dynamic loading with the desired range of impacted weight, impacted velocity, geometrical cross-section sizes, and provided reinforcement ratio. This GEP-based non-linear empirical formulation is developed incorporating the key important parameters that control the peak impacted force on RC beam from dropweight, i.e., strength of concrete in compression, steel bar tensile strength, longitudinal steel reinforcement ratio, geometrical properties of structural members, and input kinetic energy. The formulation actually produces a more precise prediction of the peak impacted force than the available existing models. Especially, the average absolute error *(AAE)* of the GEP formulation is 15.2%. Similarly, fewer CoV values of 19.9% show less scatteral variations of the output results estimated through the formulated model. Further, the greater value of the coefficient of determination, i.e., 98% for the impact value, are compared to existing developed formulations, which are less, making the developed GEP formulation more precise, and reliable. Finally, the performance factor i.e., predicted to the experimental ratio (PER) is found to be 1.01, which is close to the reference value 1.

For further verification of the impact force GEP model, FE-based simulation is developed based on one of the existing test results. The GEP model gives good agreement with the numerical results showing less than 1% error.

In the end, it can be confirmed with these findings and comparison, that the current model presents the best prediction of the peak impacted force on the RC beam from dropweight. Therefore, its application to the design of RC beams may be employed with greater confidence.

5.1 Recommendations

Following are some of the recommendations based on this study;

- Large displacement should be incorporated instead of small displacement in the mathematical formulation.
- Extend this 1D formulation to 2D that is for plates and shell objects.
- Strain rate should be also incorporated into bending shear interaction as well.
- More experimental data is required to further refine the GEP model.

References

[1] Symonds PS. Survey of methods of analysis for plastic deformation of structures under dynamic loading. Brown Univ Div Eng Rep 1967:1–67.

[2] Jones N. Structural Impact. 2nd ed. Cambridge university press; 2011.

[3] Symonds PS, Fleming WT. Parkes revisited: On rigid-plastic and elastic-plastic dynamic structural analysis. Int J Impact Eng 1984;2:1–36. https://doi.org/10.1016/0734-743X(84)90013-7.

[4] Yu TX. Elastic effects in the dynamic plastic response of structures. Struct Crashworthiness Fail 1993:295–332.

[5] Capurso M. A quadratic programming approach to the impulsive loading analysis of rigid plastic structures. Meccanica 1972;7:45–57. https://doi.org/10.1007/bf02128839.

[6] Lloyd Smith D, Sahlit CL. Dynamic response of pulse loaded structures as a linear complementarity problem. Eng Optim 1991;18:23–41.

[7] Sahlit CLDM. Mathematical programming methods for dynamically loaded rigid-plastic framed structures. Ph.D. thesis, Civil Engineering Department, Imperial College, University of London, 1992.

[8] Khan A, Smith DL, Izzuddin BA. Investigation of rigid-plastic beams subjected to impact using linear complementarity. Eng Struct 2013;50:137–48. https://doi.org/10.1016/j.engstruct.2012.12.005.

[9] Bischoff PH, Perry SH. Compressive Behavior of Concrete at High Strain Rates. Mater Struct 1991;24:425–50.

[10] Kulkarni SM, Shah SP. Response of reinforced concrete beams at high strain rates. ACI Struct J 1998;95:705–15. https://doi.org/10.14359/584.

[11] Takeda JI, Tachikawa H, Fujimoto K. Basic Concept of the Responses of Structural Members and Structures Under Impact or Impulsive Loadings. 1982:13–11.

[12] Pham TM, Hao H. Plastic hinges and inertia forces in RC beams under impact loads. Int J Impact Eng 2017;103:1–11. https://doi.org/10.1016/j.ijimpeng.2016.12.016.

[13] Saatci S, Vecchio FJ. Effects of shear mechanisms on impact behavior of reinforced concrete beams. ACI Struct J 2009;106:78–86. https://doi.org/10.14359/56286.

[14] Kishi N, Mikami H, Matsuoka KG, Ando T. Impact behavior of shear-failure-type RC beams without shear rebar. Int J Impact Eng 2002;27:955–68. https://doi.org/10.1016/S0734-743X(01)00149-X.

[15] Aashto. Aashto Lrfd Bridge Design Specifications. 8th ed. Washington, DC: American association of state highway and transportation officials; 2017.

[16] British Standards Institution. UK National Annex to Eurocode 1: Actions on structures. Part 2 Traffic Loads Bridg 2008;3.

[17] Cotsovos DM. A simplified approach for assessing the load-carrying capacity of reinforced concrete beams under concentrated load applied at high rates. Int J Impact Eng 2010;37:907–17. https://doi.org/10.1016/j.ijimpeng.2010.01.005.

[18] Kishi N, Mikami H. Empirical formulas for designing reinforced concrete beams under impact loading. ACI Struct J 2012;109:509–19. https://doi.org/10.14359/51683870.

[19] Adhikary S Das, Li B, Fujikake K. Dynamic behavior of reinforced concrete beams under varying rates of concentrated loading. Int J Impact Eng 2012;47:24–38. https://doi.org/10.1016/j.ijimpeng.2012.02.001.

[20] Qasrawi Y, Heffernan PJ, Fam A. Dynamic behaviour of concrete filled FRP tubes subjected to impact loading. Eng Struct 2015;100:212–25. https://doi.org/10.1016/j.engstruct.2015.06.012.

[21] Pham TM, Hao H. Prediction of the impact force on reinforced concrete beams from a drop weight. Adv Struct Eng 2016;19:1710–22. https://doi.org/10.1177/1369433216649384.

[22] Goldston M, Remennikov A, Sheikh MN. Experimental investigation of the behaviour of concrete beams reinforced with GFRP bars under static and impact loading. Eng Struct 2016;113:220–32. https://doi.org/10.1016/j.engstruct.2016.01.044.

[23] Pham TM, Hao H. Review of Concrete Structures Strengthened with FRP Against Impact Loading. Structures 2016;7:59–70. https://doi.org/10.1016/j.istruc.2016.05.003.

[24] Chen S, Li Q, Liu Y, Xia J, Xue Z. Dynamic elastoplastic analysis using the meshless local natural neighbor interpolation method. Int J Comput Methods 2011;8:463–81. https://doi.org/10.1142/S0219876211002629.

[25] Jones N. Plastic failure of ductile beams loaded dynamically. J Manuf Sci Eng Trans ASME 1976;98:131–6. https://doi.org/10.1115/1.3438805.

[26] Jones N. Some Comments on the Dynamic Plastic Behaviour of Structures.(Retroactive Coverage). Int Symp Intense Dyn Load Its Eff 1986:49–71.

[27] Cennamo C, Gesualdo A, Monaco M. Shear Plastic Constitutive Behavior for Near-Fault Ground Motion. J Eng Mech 2017;143:04017086. https://doi.org/10.1061/(asce)em.1943-7889.0001300.

[28] Taylor GI. The use of flat-ended projectiles for determining dynamic yield stress I. Theoretical considerations. Proc R Soc London Ser A 1948;194:289–99. https://doi.org/https://doi.org/10.1098/rspa.1948.0081.

[29] Lee EH, Symonds PS. Large plastic deformations of beams under transverse impact. J Appl Mech ASME 1952;19:308–14.

[30] Bleich HH, Shaw R. Dominance of shear stresses in early stages of impulsive motion of beams. J Appl Mech Trans ASME 1960;27:132–8. https://doi.org/10.1115/1.3643887.

[31] Jones N, Shen WQ. Criteria for the inelastic rupture of ductile metal beams subjected to large dynamic loads. Struct Crashworthiness Fail 1993:95–130.

[32] Ling Q, He Y, He Y, Pang C. Dynamic response of multibody structure subjected to blast loading. Eur J Mech A/Solids 2017;64:46–57. https://doi.org/10.1016/j.euromechsol.2017.01.010.

[33] Lowe WT, Al-Hassani STS, Johnson W. Impact Behaviour of Small Scale Model Motor Coaches. Proc Inst Mech Eng 1972;186:409–19. https://doi.org/10.1243/pime_proc_1972_186_042_02.

[34] Mehreganian N, Fallah AS, Louca LA. Plastic dynamic response of simply supported thick square plates subject to localised blast loading. Int J Impact Eng 2019;126:85–100. https://doi.org/10.1016/j.ijimpeng.2018.12.010.

[35] Menkes SB, Opat HJ. Broken beams. Exp Mech 1973;13:480–6.

https://doi.org/10.1007/bf02322734.

[36] Parkes EW. The permanent deformation of a cantilever struck transversely at its tip. Proc R Soc London Ser A Math Phys Sci 1955;228:462–76.

[37] Parkes EW. The permanent deformation of an encastré beam struck transversely at any point in its span. Proc Inst Civ Eng 1958;10:277–304.

[38] Symonds PS, Frye CWG. On the relation between rigid-plastic and elastic-plastic predictions of response to pulse loading. Int J Impact Eng 1988;7:139–49. https://doi.org/10.1016/0734-743X(88)90022-X.

[39] Mihashi H, Wittmann FH. Stochastic Approach To Study the Influence of Rate of Loading on Strength of Concrete. Heron 1980;25.

[40] Reinhardt HW, Weerheijm J. Tensile fracture of concrete at high loading rates taking account of inertia and crack velocity effects. Curr Trends Concr Fract Res 1991;51:31–42. https://doi.org/10.1007/978-94-011-3638-9_3.

[41] Bazant ZP, Adley MD, Carol I, Jirasek M, Akers SA, Rohani B, et al. Large-strain generalization of micro plane model for concrete and application. J Eng Mech 2000;126:971–80.

[42] Bazant ZP, Caner FC, Adley MD, Akers SA. Fracturing rate effects and creep in micro plane model for dynamics. J Eng Mech 2000;126:962–70.

[43] Ožbolt J, Rah KK, Meštrović D. Influence of loading rate on concrete cone failure. Int J Fract 2006;139:239–52.

[44] Wimal S, Surendra P S. Properties of Concrete Subjected To Impact. J Struct Eng 1983;109:1727–41.

[45] Zielinski AJ, Reinhardt HW. Stress strain behavior of concrete and mortar at high rates of tensile loading. Cem Concr Res 1982;12:309–19.

[46] Malvar LJ, Ross CA. Review of strain rate effects for concrete in tension. ACI Mater J 1998;95:735–9.

[47] Comite Euro-International du Beton. CEB-FIP Model Code 1990. Trowbridge, Wiltshire, UK: Redwood Books; 1993.

[48] Soroushian P, Choi KB, Alhamad A. Dynamic Constitutive Behavior of Concrete. J Am Concr Inst 1986;83:251–9. https://doi.org/10.14359/10423.

[49] Ross A, Tedesco JW, Kuennen ST. Effect of strain rate on concrete strength. ACI Mater J 1995;82:37–47.

[50] Ross CA, Jerome DM, Tedesco JW, Hughes ML. Moisture and strain rate effects on concrete strength. ACI Mater J 1996;93:293–300. https://doi.org/10.14359/9814.

[51] Tedesco JW, Ross CA. Strain-rate-dependent constitutive equations for concrete. J Press Vessel Technol Trans ASME 1998;120:398–405. https://doi.org/10.1115/1.2842350.

[52] Li QM, Meng H. About the dynamic strength enhancement of concrete-like materials in a split Hopkinson pressure bar test. Int J Solids Struct 2003;40:343–60. https://doi.org/10.1016/S0020-7683(02)00526-7.

[53] YAMAGUCHI H, FUJIMOTO K, NOMURA S. STRESS-STRAIN RELATIONSHIP FOR

CONCRETE UNDER HIGH TRIAXIAL COMPRESSION : Part 2 Rapid loading. J Struct Constr Eng (Transactions AIJ) 1989;396:50–9. https://doi.org/10.3130/aijsx.396.0_50.

[54] Fujikake K, Mori K, Uebayashi K, Ohno T, Mizuno J. Constitutive model for concrete materials with high-rates of loading under tri-axial compressive stress states. Proc, 3rd Int Conf Concr under Sev Cond 2001;1:636–43.

[55] Fu HC, Erki MA, Seckin M. Review of Effects of Loading Rate on Reinforced Concrete. J Struct Eng 1991;117:3660–79. https://doi.org/10.1061/(asce)0733-9445(1991)117:12(3660).

[56] Wakabayashi M, Nakamura T, Yoshida N, Iwai S, Watanabe Y. Dynamic Loading Effects on the Structural Performance of Concrete and Steel Materials and Beams. Proc Seventh World Conf Earthq Eng Istanbul, Turkey 1980;6:271–8.

[57] Soroushian P, Choi K. Steel Mechanical Properties at Different Strain Rates. J Struct Eng 1987;113:663–72. https://doi.org/10.1061/(asce)0733-9445(1987)113:4(663).

[58] Malvar LJ. Review of static and dynamic properties of steel reinforcing bars. ACI Mater J 1998;95:609–16. https://doi.org/10.14359/403.

[59] Fujikake K, Li B, Soeun S. Impact Response of Reinforced Concrete Beam and Its Analytical Evaluation. J Struct Eng 2009;135:938–50. https://doi.org/10.1061/(asce)st.1943-541x.0000039.

[60] Mylrea TD. Effect Of Impact On Reinforced Concrete Beams. ACI J Proc 1940;11. https://doi.org/10.14359/8539.

[61] Kishi N, Nakano O, Matsuoka KG, Ando T. Experimental Study on Ultimate Strength of Flexural-Failure-Type RC Beams under Impact Loading. Trans 16th Int Conf Struct Mech React Technol 2001:1525.

[62] Bhatti AQ, Kishi N, Mikami H, Ando T. Elasto-plastic impact response analysis of shear-failure-type RC beams with shear rebars. Mater Des 2009;30:502–10. https://doi.org/10.1016/j.matdes.2008.05.068.

[63] Chen Y, May IM. Reinforced concrete members under drop-weight impacts. Proc Inst Civ Eng Struct Build 2009;162:45–56. https://doi.org/10.1680/stbu.2009.162.1.45.

[64] Tachibana S, Masuya H, Nakamura S. Performance based design of reinforced concrete beams under impact. Nat Hazards Earth Syst Sci 2010;10:1069–78. https://doi.org/10.5194/nhess-10-1069-2010.

[65] Saatci S, Vecchio FJ. Nonlinear finite element modeling of reinforced concrete structures under impact loads. ACI Struct J 2009;106:717–25. https://doi.org/10.14359/51663112.

[66] Zhao W, Qian J, Jia P. Peak Response Prediction for RC Beams under Impact Loading. Shock Vib 2019;2019. https://doi.org/10.1155/2019/6813693.

[67] Gholipour G, Zhang C, Mousavi AA. Loading rate effects on the responses of simply supported RC beams subjected to the combination of impact and blast loads. Eng Struct 2019;201. https://doi.org/10.1016/j.engstruct.2019.109837.

[68] Adhikary S Das, Li B, Fujikake K. Effects of high loading rate on reinforced concrete beams. ACI Struct J 2014;111:651–60. https://doi.org/10.14359/51686579.

[69] FIB. fib Model Code for Concrete Structures 2010. Wiley; 2013. https://doi.org/10.1002/9783433604090.

[70] Cowper GR, Symonds PS. Strain-hardening and strain-rate effects in the impact loading of cantilever beams. Brown Univ Provid Ri 1957.

[71] Aspden RJ, Campbell JD. The effect of loading rate on the elasto-plastic flexure of steel beams. Proc R Soc London Ser A Math Phys Sci 1966;290:266–85. https://doi.org/10.1098/rspa.1966.0048.

[72] Zhao D-B, Yi W-J, Kunnath SK. Shear Mechanisms in Reinforced Concrete Beams under Impact Loading. J Struct Eng 2017;143:04017089. https://doi.org/10.1061/(asce)st.1943-541x.0001818.

[73] Symonds PS. Survey of methods of analysis for plastic deformation of structures under dynamic loading. Division of Engineering Report BU/NSRDC/; Brown University: Providence, RI, (1967) 1-148, 1967.

[74] Nonaka T. Shear and bending response of a rigid-plastic beam to blast-type loading. Ingenieur-Archiv 1977;46:35–52. https://doi.org/10.1007/BF00534958.

[75] Symonds PS. Plastic shear deformations in dynamic load problems. Eng Plast Cambridge Univ Press 1968:647–64.

[76] Li QM. Continuity conditions at bending and shearing interfaces of rigid, perfectly plastic structural elements. Int J Solids Struct 2000;37:3651–65. https://doi.org/10.1016/S0020-7683(98)00310-2.

[77] Li H, Chen W, Pham TM, Hao H. Analytical and numerical studies on impact force profile of RC beam under drop weight impact. Int J Impact Eng 2021;147. https://doi.org/10.1016/j.ijimpeng.2020.103743.

[78] Adhikary S, Li B, Fujikake K. Low Velocity impact response of reinforced concrete beams: Experimental and numerical investigation. Int J Prot Struct 2015;6:81–111. https://doi.org/10.1260/2041-4196.6.1.81.

[79] Zhang C, Gholipour G, Mousavi AA. Nonlinear dynamic behavior of simply-supported RC beams subjected to combined impact-blast loading. Eng Struct 2019;181:124–42. https://doi.org/10.1016/j.engstruct.2018.12.014.

[80] Li H, Chen W, Hao H. Influence of drop weight geometry and interlayer on impact behavior of RC beams. Int J Impact Eng 2019;131:222–37. https://doi.org/10.1016/j.ijimpeng.2019.04.028.

[81] Fan W, Liu B, Huang X, Sun Y. Efficient modeling of flexural and shear behaviors in reinforced concrete beams and columns subjected to low-velocity impact loading. Eng Struct 2019;195:22–50. https://doi.org/10.1016/j.engstruct.2019.05.082.

[82] Cottle RW. Symmetric dual quadratic programs. Q Appl Math 1963;21:237–43. https://doi.org/10.1090/qam/156707.

[83] Kostreva MM. Cycling in linear complementarity problems. Math Program 1979;16:127–30. https://doi.org/10.1007/BF01582098.

[84] Lemke CE. Bimatrix equilibrium points and mathematical programming. Manage Sci 1965;11:681–9.

[85] Smith DL, Sahlit CL. Rigid Plastic Dynamics. Math Program Methods Struct Plast 1990:293–313. https://doi.org/10.1007/978-3-7091-2618-9_15.

[86] Murty K, Yu VF. Linear complementarity, linear and nonlinear programming. Heldermann Verlag; 1988.

[87] Fujikake K, Senga T, Ueda N, Ohno T, Katagiri M. Study on impact response of reactive powder

concrete beam and its analytical model. J Adv Concr Technol 2006;4:99–108. https://doi.org/10.3151/jact.4.99.

[88] Maier G, Munro J. Mathematical Programming Applications To Engineering Plastic Analysis. Appl Mech Rev 1982;35:1631–43.

[89] Mattock AH. Discussion of "Rotational Capacity of Reinforced Concrete Beams." J Struct Div 1967;93:519–22. https://doi.org/10.1061/jsdeag.0001678.

[90] Tamuzh VP. On a minimum principle in dynamics of rigid-plastic bodies. J Appl Math Mech 1962;26:1067–77. https://doi.org/10.1016/0021-8928(62)90165-X.

[91] Martin JB. A note on the uniqueness of solutions for dynamically loaded rigid-plastic and rigid-viscoplastic continua 1966.

[92] Adhikary S Das, Li B, Fujikake K. Parametric study of RC beams under a wide range of loading rates. Proc Inst Civ Eng Struct Build 2015;168:729–46. https://doi.org/10.1680/stbu.15.00024.

[93] Adhikary S Das. DYNAMIC BEHAVIOR OF REINFORCED CONCRETE BEAMS UNDER VARYING RATES OF CONCENTRATED AND IMPACT LOADINGS. Nanyang Technological University, Singapore, 2014.

[94] Soleimani SM, Banthia N, Mindess S. Behavior of RC beams under impact loading: Some new findings. Proc 6th Int Conf Fract Mech Concr Concr Struct 2007;2:867–74.

[95] Hughes BP, Mahmood AT. Impact behaviour of prestressed concrete beams in flexure. Mag Concr Res 1984;36:157–64. https://doi.org/10.1680/macr.1984.36.128.157.

[96] Louw J, Maritz G, Loedolff M. The behaviour of RC columns under impact loading. Civ Eng South Africa 1992;34:371–8.

[97] May IM, Chen Y, Roger D, Owen J, Feng YT, Thiele PJ. Reinforced concrete beams under drop-weight impact loads. Comput Concr 2006;3:79–90. https://doi.org/10.12989/cac.2006.3.2_3.079.

[98] Zhan T, Wang Z, Ning J. Failure behaviors of reinforced concrete beams subjected to high impact loading. Eng Fail Anal 2015;56:233–43. https://doi.org/10.1016/j.engfailanal.2015.02.006.

[99] Jin L, Zhang R, Dou G, Xu J, Du X. Experimental and numerical study of reinforced concrete beams with steel fibers subjected to impact loading. Int J Damage Mech 2018;27:1058–83. https://doi.org/10.1177/1056789517721616.

[100] Xu B, Zeng X. Experimental study on the behaviors of reinforced concrete beams under impact loadings. Tumu Gongcheng Xuebao/China Civ Eng J 2014;47.

[101] Zhao DB, Yi WJ. Anti-impact behavior and design method for RC beams. Zhendong Yu Chongji/Journal Vib Shock 2015;34:139–45. https://doi.org/10.13465/j.cnki.jvs.2015.11.025.

[102] Dou G, Du X, Li L. Experimental study on the behavior of high strength reinforced concrete beams under impact load. Tianjin Daxue Xuebao (Ziran Kexue Yu Gongcheng Jishu Ban)/Journal Tianjin Univ Sci Technol 2014;47:1072–80. https://doi.org/10.11784/tdxbz201403083.

[103] Koza JR. Genetic programming as a means for programming computers by natural selection. Stat Comput 1994:87–112.

[104] Murad Y, Tarawneh A, Arar F, Al-Zu'bi A, Al-Ghwairi A, Al-Jaafreh A, et al. Flexural strength prediction for concrete beams reinforced with FRP bars using gene expression programming. Structures 2021;33:3163–72. https://doi.org/https://doi.org/10.1016/j.istruc.2021.06.045.

[105] Tariq M, Khan A, Shayanfar J, Hanif MU, Ullah A. A regression model for predicting the shear strength of RC knee joint subjected to opening and closing moment. J Build Eng 2021;41. https://doi.org/10.1016/j.jobe.2021.102727.

[106] Ilie I, Dittrich P, Carvalhais N, Jung M, Heinemeyer A, Migliavacca M, et al. Reverse engineering model structures for soil and ecosystem respiration: The potential of gene expression programming. Geosci Model Dev 2017;10:3519–45. https://doi.org/10.5194/gmd-10-3519-2017.

[107] Teodorescu L, Sherwood D. High Energy Physics event selection with Gene Expression Programming. Comput Phys Commun 2008;178:409–19. https://doi.org/10.1016/j.cpc.2007.10.003.

[108] Kose MM, Kayadelen C. Modeling of transfer length of prestressing strands using genetic programming and neuro-fuzzy. Adv Eng Softw 2010;41:315–22. https://doi.org/10.1016/j.advengsoft.2009.06.013.

[109] Zeng X, Xu B. Experimental study on the impact-resistant behavior of RC beams without shear-resistant rebar. Tumu Gongcheng Xuebao/China Civ Eng J 2012;45:63–73.

[110] Adhikary S Das, Li B, Fujikake K. State-of-the-art review on low-velocity impact response of reinforced concrete beams. Mag Concr Res 2016;68:701–23. https://doi.org/10.1680/jmacr.15.00084.